

Services for the Quantum Internet

by

Laszlo Gyongyosi

PhD

Submitted to the Section of Engineering Sciences
in partial fulfillment of the requirements for the degree of

Doctor of Science

at the

HUNGARIAN ACADEMY OF SCIENCES

April 2019

© Laszlo Gyongyosi, 2019.

The author hereby grants to MTA permission to reproduce and
to distribute copies of this thesis document in whole or in part.

Signature of Author

Section of Engineering Sciences

11 April 2019

Services for the Quantum Internet

by

Laszlo Gyongyosi

Submitted to the Section of Engineering Sciences
on 11 April 2019, in partial fulfillment of the
requirements for the degree of
Doctor of Science

Abstract

As traditional computer architectures reach their physical limits in the near future, we will transition into the age of quantum information. The quantum Internet utilizes the fundamental concepts of quantum mechanics for networking. The entangled quantum network structure of the quantum Internet characterizes a high-complexity network space with several advantages and challenges. The construction of efficient services for the quantum Internet is an emerging issue. This dissertation defines a routing service, an entanglement distribution and differentiation service, and an optimization service for the quantum Internet. The purpose of the proposed services is to increase the performance and decrease the resource requirements of the quantum Internet.

Acknowledgments

I would like to express my thank and gratitude to Prof. Sandor Imre for the support and advices.

I would like to thank Laszlo Bacsardi for the administrative support.

I acknowledge the support of the European Structural Fund - GOP-1.1.1-11-2012-0092 and COST Action MP1006, the European Research Council through the Advanced Fellow Grant, the Royal Society's Wolfson Research Merit Award, Engineering and Physical Sciences Research Council under Grant EP/L018659/1, the National Research Development and Innovation Office of Hungary (Project No. 2017-1.2.1-NKP-2017-00001), and the Hungarian Scientific Research Fund - OTKA K-112125 and the support from the BME Artificial Intelligence FIKP grant of EMMI (BME FIKP-MI/SC). I acknowledge the grant of the Hungarian Academy of Sciences and the University of Southampton.

I would like to thank my family for the support and assistance.

Finally, I would like to thank the editors and anonymous referees who helped and supported my work through the years.

Contents

| | | |
|----------|---|-----------|
| 1 | Introduction | 1 |
| 1.1 | Motivation | 3 |
| 1.2 | Dissertation | 5 |
| 1.2.1 | Results | 5 |
| 1.2.2 | Contents and Structure | 7 |
| 2 | Preliminaries | 8 |
| 2.1 | Basic Terms | 8 |
| 2.1.1 | Quantum Entanglement | 8 |
| 2.1.2 | Entanglement Fidelity | 10 |
| 2.1.3 | Relative Entropy of Entanglement | 11 |
| 2.2 | Operations in the Quantum Internet | 11 |
| 2.3 | Network Management in the Quantum Internet | 13 |
| 3 | Decentralized Routing Service for the Quantum Internet | 15 |
| 3.1 | Introduction | 15 |
| 3.1.1 | Results | 18 |
| 3.2 | System Model | 19 |
| 3.2.1 | Entanglement Levels | 19 |
| 3.2.2 | Problem Setting and Available Resources | 20 |
| 3.2.3 | Mapping the Structure of the Quantum Internet | 22 |

| | | |
|----------|---|-----------|
| 3.2.4 | Swapping by Quantum Teleportation | 25 |
| 3.2.5 | Next-Generation Repeaters | 28 |
| 3.2.6 | Classical Communications in the Quantum Network | 29 |
| 3.3 | Decentralized Routing | 29 |
| 3.3.1 | Routing Complexity | 31 |
| 3.3.2 | Implementation | 34 |
| 3.4 | Diameter Bounds | 35 |
| 3.5 | Conclusions | 37 |
| 4 | Entanglement Availability Differentiation Service for the Quantum Internet | 38 |
| 4.1 | Introduction | 39 |
| 4.1.1 | Results | 40 |
| 4.2 | System Model | 41 |
| 4.2.1 | Classical Transmission Phase | 41 |
| 4.2.2 | Quantum Transmission Phase | 43 |
| 4.2.3 | Entanglement Distribution via Hamiltonian Dynamics | 43 |
| 4.2.4 | Framework | 47 |
| 4.3 | Methods of Entanglement Availability Differentiation | 48 |
| 4.3.1 | Differentiation in the Amount of Entanglement | 49 |
| 4.3.2 | Differentiation in the Time Domain | 52 |
| 4.3.3 | Comparative Analysis | 54 |
| 4.4 | Conclusions | 54 |
| 5 | Multilayer Optimization Service for the Quantum Internet | 57 |
| 5.1 | Introduction | 57 |
| 5.1.1 | Results | 60 |
| 5.2 | System Model | 60 |
| 5.2.1 | Quantum Memory Scheduling | 63 |

| | | |
|----------|---|------------|
| 5.2.2 | Entanglement Throughput Tree | 64 |
| 5.2.3 | Entanglement Assignment Cycle | 67 |
| 5.3 | Quantum Layer Optimization | 70 |
| 5.4 | Classical Layer Optimization | 72 |
| 5.4.1 | Large-Constrained Optimization | 76 |
| 5.5 | Numerical Analysis | 79 |
| 5.5.1 | Quantum Layer Optimization | 79 |
| 5.5.2 | Classical Layer Optimization | 81 |
| 5.6 | Conclusions | 84 |
| 6 | Discussion | 86 |
| 6.1 | Future Work | 86 |
| | Bibliography | 88 |
| A | List of Papers | 101 |
| A.1 | Peer-Reviewed Journals | 101 |
| A.2 | Conference Papers | 105 |
| B | Extended Routing Services for the Quantum Internet | 114 |
| B.1 | Introduction | 114 |
| B.1.1 | Results | 115 |
| B.2 | System Model | 115 |
| B.2.1 | Quantum Memory Failures | 117 |
| B.3 | Shortest Replacement Paths in the Entangled Network | 122 |
| B.3.1 | Discussion | 123 |
| B.3.2 | Computational Complexity | 126 |
| B.4 | Performance Evaluation | 127 |

| | |
|---|------------|
| C EAD Service | 130 |
| C.1 Classical Correlations | 130 |
| D Multilayer Optimization Service | 133 |
| D.1 Cost Uncertainty of Large-Scaled Optimization | 133 |
| E Abbreviations | 135 |
| F Notations | 136 |

Thesis Groups

Thesis Group 1: Decentralized Routing Service for the Quantum Internet

Thesis 1.1 (Mapping the entangled network structure) *The quantum nodes and the entangled connections of the entangled quantum network N can be mapped into a k -dimensional, n -size base graph G^k .*

Thesis 1.2 (Stabilization of an entangled quantum network) *The stabilization procedure of the entangled quantum network N can be established by quantum teleportation between quantum nodes.*

Thesis 1.3 (Complexity of the routing service) *The complexity of the decentralized routing service is upper bounded by $\mathcal{O}(\log n)^2$ for any entangled quantum network N .*

Thesis Group 2: Entanglement Availability Differentiation Service for the Quantum Internet

Thesis 2.1 (Entanglement establishment via Hamiltonian dynamics) *Maximally entangled quantum systems can be established in the multiuser environment of the quantum Internet via Hamiltonian dynamics.*

Thesis 2.2 (Differentiation in the amount of entanglement) *The EAD service can be utilized for differentiation of the entanglement amount between the users of the quantum Internet in terms of relative entropy of entanglement.*

Thesis 2.3 (Differentiation in the time domain) *The EAD service can be utilized to differentiate in the amount of time required for the establishment of the maximally entangled systems between the users of the quantum Internet.*

Thesis Group 3: Multilayer Optimization Service for the Quantum Internet

Proposition 3.1 *The \mathcal{G}_m quantum memory utilization graph is a directed graph with abstract nodes and links to schedule the quantum memory usage mapped from the quantum repeater network.*

Thesis 3.1 (Entanglement throughput tree) *The \mathcal{G}_{et} entanglement throughput tree is a structure modeling the multi-objective optimization problem of the quantum Internet. The tree structure is derived from the \mathcal{G}_m quantum memory utilization graph.*

Lemma 3.1 *An entanglement assignment cycle can be determined by a weighted graph coloring method.*

Thesis 3.2 (Quantum layer optimization) *At a given \mathcal{G}_m , the quantum layer of an entangled quantum network N can be optimized by a procedure \mathcal{P}_Q that achieves a parallel minimization of the quantum memory usage time t_s , the maximization of entanglement throughput B_F , and the minimization of the number $|\mathcal{P}|$ of entangled connections between two arbitrary quantum nodes.*

Thesis 3.3 (Classical layer optimization) *The cost function of classical communications in a quantum Internet setting can be minimized by a procedure \mathcal{P}_C .*

List of Figures

- 2-1 Entanglement distribution in the doubling architecture. The aim is to generate long-distance entanglement between distant quantum nodes A and B through a chain of q intermediate R_i , $i = 1, \dots, q$, quantum repeaters. The architecture defines different l entanglement levels, $l = 1, 2, 3, 4$ in the current network situation with $q = 7$. First, the $l = 1$ level entangled connections are established between the quantum nodes. To double the spanned distance, entanglement swapping is applied in the quantum repeaters. The result of the entanglement swapping procedure is a higher-level entangled connection. The $l = 2$ level entangled connections are generated by quantum repeaters R_1, R_3, R_5 and R_7 . The $l = 3$ level entangled connections are generated by R_2 and R_6 , while the $l = 4$ level entangled connection between A and B is generated by R_4 12
- 3-1 Entangled overlay quantum network $N = (V, E)$ with heterogeneous entanglement levels. The network consists of single-hop entangled (gray) nodes with L_1 -level entanglement connection, and multi-hop entangled (blue, green) nodes with L_2 and L_3 -level entangled connections. An L_l -level, $l = 1, 2, 3$, entangled connection between nodes $x, y \in V$ is established with probability $\Pr_{L_l}(E(x, y))$. The overlay network consists of q quantum repeater nodes $R_i \in V$, $i = 1, \dots, q$ between the transmitter (A) and the receiver (B) nodes. The L_l -level entangled nodes consist of $d(x, y)_{L_l} - 1$ intermediate quantum nodes, as depicted by the dashed lines. 21

3-2 G^2 base-graph of an overlay entangled quantum network N , with entangled nodes $\phi(A), \phi(R_i), i = 1, 2, 3$, where $A \in V$ is a transmitter node in the overlay quantum network N , while $R_i \in V$ are quantum repeater nodes in N . In N , nodes A and R_1 are connected through L_1 -level entanglement with probability $\text{Pr}_{L_1}(A, R_1)$, nodes A and R_2 are connected via L_2 -level entanglement with probability $\text{Pr}_{L_2}(A, R_2)$, while A and R_3 have an L_3 -level entanglement connection with probability $\text{Pr}_{L_3}(A, R_3)$. The probability that nodes are connected in G^2 is $p(\phi(A), \phi(R_1)), p(\phi(A), \phi(R_2))$, and $p(\phi(A), \phi(R_3))$ 31

3-3 A tessellation of B_n of the base-graph G^2 of an overlay quantum network N onto n^γ side subsquare S_i , and n^{γ^2} side sub-subsquare S_{ik} , where $k/4 < \gamma < 1$. The nodes are connected through L_1, L_2 and L_3 -level entangled connections in the overlay network, with source node A and target node B . The points between $\phi(A)$ and $\phi(B)$ refer to the repeater quantum nodes. 36

4-1 Framework of the entanglement differentiation service in a multiuser quantum network. (a) Phase 1. Classical transmission. The \mathcal{E} encoder unit distributes the timing information for the legal transmit users U_1, \dots, U_K and receiver users B_1, \dots, B_K via a classical channel. (b) Phase 2. Quantum transmission. The users apply the core protocol for the entanglement establishment. Then, using the received timing information the transmit users U_1, \dots, U_K apply the local unitaries for time T_{U_1}, \dots, T_{U_K} 48

4-2 Entanglement differentiation service via Hamiltonian dynamics in a multiuser environment. (a) Protocol 1. Each user gives a different amount of entanglement $E(U_i : B_i) \leq 1$ at a global period of time T_π . The differentiation is made in the amount of entanglement (relative entropy of entanglement) by applying the local unitaries for time T_{U_i} for $U_i, i = 1, \dots, K$. User U_5 has the highest priority thus the user gets a maximally entangled system, user U_3 is the lowest priority user and associated with a low amount of entanglement. (b) Protocol 2. All users are assigned with a maximally entangled system, $E(U_i : B_i) = 1$, and the differentiation is made in the time domain. For users $U_i, B_i, i = 1, \dots, K$ a particular period of time $T_\pi(U_i : B_i)$ is assigned, and each local unitary is applied for $T_{U_i}(\pi/4) = T_\pi(U_i : B_i)/4$ time to achieve maximally entangled states between the parties. User U_5 has the highest priority thus the user associated with the shortest time period, user U_3 is the lowest priority user with a long time period for the generation of a maximally entangled system. . . . 55

5-1 The network model with a quantum switcher S and quantum repeater nodes $R_i, i = 1, \dots, 6$. The L_1, L_2 - and L_3 -level entangled connections of N are depicted by gray, blue and orange, respectively (additional nodes are not shown). (a) For a current shortest path $\mathcal{P}_1 = \{R_1, R_3, S, R_4, R_6\}$, the active repeater nodes selected by S are R_3 and R_4 . (b) Node S switches the entangled connections in the local quantum memory from R_3 to R_2 and from R_4 to R_6 . The switching operation defines a new shortest path $\mathcal{P}_2 = \{R_1, R_2, S, R_6\}$ 63

- 5-2 The \mathcal{G}_m graph of quantum memory utilization derived from the network setting in Fig. 1. The graph contains n abstracted transmitter nodes and n abstracted receiver nodes with directed entangled connections. An i -level entangled connect is depicted by L_i . The S quantum switcher has two states, S_1 and S_2 . The green circles represent quantum nodes operating on switcher mode S_1 . The yellow circles represent nodes operating on switcher mode S_2 65

- 5-3 The structure of a \mathcal{G}_{et} entanglement throughput tree. A quantum node has an ID identifier tag, $ID = \{A, B, \dots, L\}$, and all incoming and outgoing entangled connections are identified by the s_{ID} source neighbor node and the t_{ID} target neighbor node. Node A represents a source, while the destination nodes are J, K, L . The $B_F(E_{L_l}(x, y))$ entanglement throughput of all (x, y) node pairs are depicted above the directed lines; the link identifier $E_{L_l}(x, y)$ is depicted under the links. 68

- 5-4 The $D(X_{\mathcal{G}_{et},i}, X_{\mathcal{G}_{et}}^\infty)$ distance in function of N_{it} and χ . (a) The values of $D(X_{\mathcal{G}_{et},i}, X_{\mathcal{G}_{et}}^\infty)$ for $0 < N_{it} \leq 2 \cdot 10^3$ and $1 \leq \chi \leq 10$. (b) The values of $D(X_{\mathcal{G}_{et},i}, X_{\mathcal{G}_{et}}^\infty)$ for $0 < N_{it} \leq 2 \cdot 10^3$ and $11 \leq \chi \leq 20$ 81

- 5-5 The ratio $\zeta(X_{\mathcal{G}_{et}}(N_{it}), X_{\mathcal{G}_{et}}(N_{it} \rightarrow \infty))$ in function of N_{it} and χ . (a) The values of $\zeta(X_{\mathcal{G}_{et}}(N_{it}), X_{\mathcal{G}_{et}}(N_{it} \rightarrow \infty))$ for $0 < N_{it} \leq 2 \cdot 10^3$ and $1 \leq \chi \leq 10$. (b) The values of $\zeta(X_{\mathcal{G}_{et}}(N_{it}), X_{\mathcal{G}_{et}}(N_{it} \rightarrow \infty))$ for $0 < N_{it} \leq 2 \cdot 10^3$ and $11 \leq \chi \leq 20$ 82

- 5-6 (a) The $\phi_s(i)$ step-size function for $\phi_{\min} \in [0, 2 \cdot 10^{-3}]$, $\phi_{\max} = 500\phi_{\min}$ and $\kappa(j) \in [0, 10]$. (b) The $\phi_s(i)$ step-size function for $\phi_{\min} \in [0, 5 \cdot 10^{-1}]$, $\phi_{\max} = 2\phi_{\min}$ and $\kappa(j) \in [0, 40]$ 83

- 5-7 The J^* cost function values associated to the $\phi_s(i)$ step size function value, (a) $J_P = 1$ and $\omega = 1$, (b) $J_P = 1$ and $\omega = 100$ 84

B.1 A scenario of a quantum memory failure in an entangled overlay quantum network N . (a) The main path \mathcal{P} consists of a source node A and target node B , with several quantum repeater nodes $R_i, i = 1, \dots, q$ connected through multi-level entangled connections. The quantum nodes are referred to as single-hop entangled (L_1 -level, depicted by gray nodes) and multi-hop entangled (L_2 - and L_3 -level, depicted by blue and orange nodes). The actual shortest main path \mathcal{P} determined in the base-graph is depicted by the bold lines. The high-degree nodes (depicted by yellow) store the highest number of entangled states in their quantum memories and are not included in \mathcal{P} . (b) A quantum memory failure in repeater node R_{q-2} (depicted by red) destroys all entangled contacts of the given node. For seamless transmission, a node-disjoint shortest replacement path \mathcal{P}' is needed between source node R_2 and target node R_q , through high-degree repeater nodes $\tilde{R}_{q'-2}$ and $\tilde{R}_{q'-1}$. Path \mathcal{P}' between $\phi(R_2) \in G^k$ and $\phi(R_q) \in G^k$ is determined by a decentralized routing \mathcal{A} in the base-graph G^k 117

B.2 A $k = 2$ -dimensional base-graph G^2 of the overlay quantum repeater network N . (a) A reference source node $\phi(x)$ has entangled connections with $\phi(y), \phi(z),$ and $\phi(w)$. Each entangled connection is characterized by a given probability $p(\cdot)$ that depends on the level of entanglement. (b) Determination of a node-disjoint path \mathcal{P}'_j between a reference source node $\phi'(x)$ and the scaled positions $\phi'(y), \phi'(z),$ and $\phi'(w)$ for a given $M_{U_k, \rho}^{(\zeta)}$ in base-graph G'^2 , where $s(\zeta(E(\cdot))) \in [0, 1]$ is a scaled cost of the entangled connection. 127

- B.3 (a) The computational complexity (N_O refers to the number of operations) of the proposed method in function of ∂ and n , $\partial \in [0, 10]$, $n \in [0, 100]$ (b) The computational complexity of the KPI and KPA methods in function of ∂ and n , $\partial \in [0, 10]$, $n \in [0, 100]$. (c) The computational complexity of the KSP method in function of z and n , $z \in [0, 10]$, $n \in [0, 100]$ 129

List of Tables

| | | |
|-----|---|-----|
| 1.1 | Attributes and application scenarios of the quantum Internet. | 6 |
| F.1 | Summary of notations. | 136 |

Chapter 1

Introduction

According to Moore's Law [77], the physical limitations of classical semiconductor-based technologies could be reached within the next few years [3, 16, 17, 30, 44, 47, 76, 86, 115]. We will then step into the age of quantum information. The age of quantum information will not only reformulate our view of the nature of computation and communication, but will also open fundamentally new possibilities for realizing high-performance computer architecture and telecommunication networks [39, 40, 48, 55, 74, 108, 117–121]. Since our traditional data will no longer remain safe in the traditional Internet when quantum computers become available [1, 40, 47, 94, 117], there will be a need for a fundamentally different network structure: the *quantum Internet* [55, 74, 118, 121].

Available point-to-point communication link should be connected on one hand to cover large distances and on the other hand to reach huge number of users in the form of a network. Thus, the quantum Internet requires quantum repeaters and quantum switches/routers. Because of the consequences of the postulates of quantum mechanics, the construction of these network entities proves to be very hard [39].

The quantum Internet utilizes the fundamental concepts of quantum mechanics for networking [2, 7–11, 32–39, 49, 55, 59, 62, 74, 89, 91–93, 118–121]. The main attributes of the quantum Internet are unconditional security (quantum cryptographic protocols), advanced quantum phenomena and protocols (such as quantum superposition, quantum

entanglement, quantum teleportation and quantum coding) and an entangled network structure [4, 12, 13, 28, 41, 42, 57, 69–73, 75, 80, 105, 110, 129–131]. In contrast to traditional repeaters, quantum repeaters cannot apply the “receive-copy-retransmit” mechanism because of the so-called *no-cloning theorem* [39, 49, 118, 128]. This fundamental difference between the nature of classical and quantum information not just leads to fundamentally different networking mechanisms, but also requires the definition of novel networking services in a quantum Internet scenario [127]. In a quantum Internet setting, the main task is to distribute quantum entanglement from a source quantum node to a target quantum node through a set of intermediate quantum nodes called quantum repeaters [6, 20–23, 29, 31, 58, 65, 103, 107, 111, 114, 116, 133]. The entanglement distribution is realized in a step-by-step manner by the generation of short-distance entangled connections between quantum nodes. Next, the level of entanglement of the entangled connections is increased to generate longer-distance entangled connections. The entanglement level of an entangled connection determines the hop-distance (number of quantum nodes spanned by the particular entangled connection) between a source node and the target node of the given entangled connection. The level increment is realized by the so-called entanglement swapping (entanglement extension) procedure applied in the intermediate quantum repeaters. Specifically, the entanglement distribution is achieved within the framework of the so-called doubling architecture [118, 120, 121] (see also Section 2.2), where each increment of the level of entanglement doubles the hop-distance. At the end of the entanglement distribution procedure, the distant source node and the target node share a long-distance entangled connection.

A practical implementation of the quantum Internet integrates standard photonics devices [104, 127], quantum memories, optical cavities and fundamental physical devices [4, 12, 28, 32, 41–43, 45, 46, 69, 85, 92, 93, 100, 105, 129] required for practical quantum network communications [6, 19–21, 23, 29, 58, 65, 103, 107, 111, 114, 116, 133]. The quantum transmission and the auxiliary classical communications between the quantum nodes can be realized via standard links (e.g., optical fibers, wireless optical channels [26], satellite

communications [2, 5], etc) and by the utilization of the fundamental quantum protocols of quantum networks [118].

Experimental quantum Internet is currently in the development phase and exists on the level of physics laboratories and theoretical approaches. The engineering problems connected to the construction of the quantum Internet need to be discussed, and solutions must be found [127]. The main engineering issues cover the development of novel routing services for the heterogeneous network structure of the quantum Internet and the definition of connection establishment services, resource allocation services (such as services for entanglement distribution and entanglement allocation), and interoperability services (interoperability between different network layers and network components). This dissertation aims to address these main problems.

1.1 Motivation

Quantum communication networks can be classified into two main classes [49, 118, 121]: *unentangled* and *entangled* quantum networks. In an unentangled quantum network, the connections between the quantum nodes are formulated via unentangled quantum states. In an entangled quantum network, the connections between the quantum nodes are formulated via entangled states. The entangled states are stored within the internal quantum memories of the quantum nodes, such that the entangled connections span several hops and are established over long distances. The characteristics and aims of the two types of quantum network models are fundamentally different. While the main purpose in an unentangled quantum network is to implement a standard (unentangled) QKD (quantum key distribution) protocol [49, 118, 121] between the nodes in a point-by-point manner to ensure the security of the quantum communication (see also Section 3.2.5), the main task in an entangled quantum network is to distribute quantum entanglement over long distances. The services of unentangled and entangled quantum networks can be used as supplemental services for the tasks of traditional networks (to ensure stronger

encryption and security services via QKD—such as IPsec (Internet Protocol Security) with QKD [118] or TLS (Transport Layer Security) with QKD [118], to reduce the dependency on public key methods and on one-way functions, and to reduce the computational complexities of cryptographic methods, authentications, and privacy services). On the other hand, while unentangled quantum networks can provide only these supplemental services for traditional networks in short distances due to the point-by-point QKD-based quantum communication, the structure of entangled quantum networks allows us to construct a more complex network—called the quantum Internet. In a quantum Internet scenario, the core network is an entangled quantum network, and the main aim is to provide a general network structure for quantum computers (legal users) to establish reliable and secure long-distance quantum communications. A fundament of the quantum Internet concept is therefore quantum entanglement and quantum repeaters. Quantum repeaters serve as intermediate transmitter quantum nodes between a sender quantum node (Alice) and a receiver quantum node (Bob) in the entanglement distribution process. By utilizing quantum entanglement, communication distances can be extended to long distances (unlimited, by theory) via the entanglement distribution process.

The entangled connections of entangled quantum networks span multiple nodes (i.e., these connections are multi-hop connections). An entangled connection is created via the entanglement distribution process, that is, via many physical links. A given physical link (i.e., optical fiber, wireless optical link) serves only temporarily in the distribution process because a physical link can create entanglement only over short distances. This is the reason the entanglement distribution process is realized in a step-by-step manner via many physical links and by many short-distance entangled states. The end of the entanglement distribution process is an end-to-end entangled state between the distant sender and receiver. The end-to-end entangled state spans over the intermediate nodes and physical links used in the distribution process between the sender and the receiver.

In an unentangled quantum network, the achievable communication distances are limited because of the requirement of (primarily) point-by-point QKD between the quantum

nodes. In an entangled quantum network, the entanglement distribution procedure eliminates the requirement of point-by-point quantum communications and extends it to a multi-hop quantum communication.

Entangled quantum networks allow us to utilize all quantum protocols, such as QKD, and other quantum cryptographic primitives similar to untangled networks, but with the additional exploitation of the improved network structure, higher transmission reliability and transmission rates, and significantly longer achievable communication distances. As long-distance end-to-end entangled states are available, the entangled quantum network can be utilized as a QLAN (quantum local area network), a QMAN (quantum metropolitan area network), a QWAN (quantum wide area network), or a global quantum Internet network.

The main uses of the quantum Internet include the field of distributed computations [119] (quantum secret sharing [118], blind quantum computation [118, 119], client-server quantum communications [118, 119], system-area networks [118, 119]), distributed cryptographic functions (Byzantine agreement [113], leader election [118, 119], QKD [118, 119]), and the field of sensor technology [118] (interferometry, clocks, reference frames).

Since an entangled network architecture represents a core of the quantum Internet, our network model is also based on the entangled quantum network model.

The main attributes and application scenarios of the quantum Internet are summarized in Table 1.1.

1.2 Dissertation

1.2.1 Results

This dissertation defines novel services for the quantum Internet. The services consider the physical attributes of quantum transmission and the procedures of entanglement distribution. The proposed services utilize the fundamental architectural attributes of the quantum Internet, establish advanced services for the processes of entanglement

Table 1.1: Attributes and application scenarios of the quantum Internet.

| Network Structure | Application | Benefits over classical networks | Fundamental concept of the quantum Internet? |
|--------------------------|--|--|--|
| Entangled | Distributed cryptographic functions [107, 118, 119] | Reduced computational complexity, decreased use of one-way functions and public key methods | Yes |
| | Distributed computation [7, 10, 107, 113, 118, 119, 119, 127] | Unconditional security | Yes |
| | High precision sensor networks [55, 74, 118, 119, 127] | Improved precision | Yes |
| | Advanced quantum protocols [4, 6, 7, 10, 107, 118, 119, 127] | Unconditional security, advanced communications [49, 85, 118, 121] (quantum teleportation [85, 99], quantum encoding [39, 50, 75], etc.) | Yes |
| | Multi-hop QKD [49, 118, 121] | Unconditional security | Yes |
| | Multi-hop entanglement [6, 7, 10, 43, 45, 46, 100, 104, 107, 118–122, 127] | Quantum Internet [55, 74], long-distance quantum communications and QKD [118, 119], unconditional security over unlimited distances | Yes |
| | Extended secrecy for classical protocols [118, 119] | Unconditional security | Yes (strong multi-hop settings) |
| Unentangled | Point-to-point QKD [49, 118, 121] | Unconditional security | No (limited distances, expandable by free-space [2, 5, 26, 67] quantum channels) |
| | Extended secrecy for classical protocols [118, 119] | Unconditional security | No (weak multi-hop settings) |

distribution and differentiation, and define a network optimization framework.

The contributions of this dissertation are as follows:

- *A decentralized routing service is defined to perform a high-efficiency routing in the quantum Internet [33].*
- *A service is defined for the distribution and differentiation of quantum entanglement among the users of the quantum Internet [35].*
- *A service is defined for the optimization of the classical layer and the quantum layer of the quantum Internet [37].*

The novel contributions of the services are detailed and discussed separately in the chapters.

1.2.2 Contents and Structure

The structure of this dissertation is organized as follows. In Chapter 2, preliminaries are summarized. In Chapter 3, the routing service is proposed. Chapter 4 discusses the service for entanglement distribution and entanglement differentiation in the multiuser environment of the quantum Internet. Chapter 5 provides the multilayer optimization service for the quantum Internet. Finally, Chapter 6 concludes the results. Supplemental information with additional results is included in the Appendix.

The Appendix is organized as follows. In Appendix A, the list of papers is summarized. In Appendix B, additional results for the application of the proposed routing service are included. Supplemental results for the entanglement differentiation service, and the multilayer optimization service are found in Appendix C and Appendix D. Appendix E and Appendix F contain the list of abbreviations and the list of notations.

Chapter 2

Preliminaries

2.1 Basic Terms

2.1.1 Quantum Entanglement

A d -dimensional superposed quantum system $|\psi\rangle$ is a d -level system,

$$|\psi\rangle = \alpha_1|B_1\rangle + \dots + \alpha_d|B_d\rangle, \quad (2.1)$$

where the α_i -s are complex numbers, $|\alpha_1|^2 + \dots + |\alpha_d|^2 = 1$, while $|B_i\rangle$ is the i -th basis state, $i = 1, \dots, d$ [39, 49, 118]. For a qubit system, the dimension is $d = 2$, and (2.1) can be written as

$$|\psi\rangle = \alpha_1|0\rangle + \alpha_2|1\rangle, \quad (2.2)$$

with $|\alpha_1|^2 + |\alpha_2|^2 = 1$. A two qubit system formulates quantum state

$$|\psi\rangle = \alpha_1|00\rangle + \alpha_2|01\rangle + \alpha_3|10\rangle + \alpha_4|11\rangle, \quad (2.3)$$

where $\sum |\alpha_i|^2 = 1$. A separable two-qubit system $|\psi\rangle_s$ can be decomposed into a tensor product form as $|\psi\rangle_s = |\phi\rangle \otimes |\varphi\rangle$, where $|\phi\rangle$ and $|\varphi\rangle$ are one-qubit systems, while \otimes is the tensor product. An example for a $|\psi\rangle_s$ system is obtained at $\alpha_1 = \alpha_2 = \alpha_3 = \alpha_4 = \frac{1}{2}$

in (2.3). On the other hand, if $\alpha_1 = \alpha_4 = \frac{1}{\sqrt{2}}$ and $\alpha_2 = \alpha_3 = 0$, the two qubit system $|\psi\rangle$ in (2.3) cannot be decomposed, $|\psi\rangle \neq |\phi\rangle \otimes |\varphi\rangle$, and the qubits formulate an entangled system.

In an entangled system, operations performed on one half of the state affect the other, and the probabilities of the entangled qubits are not independent. The $d = 2$ dimensional twopartite entangled states are the so-called Bell states [39, 49, 118] (or EPR states, named after Einstein, Podolsky and Rosen [39, 49, 118]). The Bell states are given as

$$|\beta_{00}\rangle = \frac{1}{\sqrt{2}} (|00\rangle + |11\rangle), \quad (2.4)$$

$$|\beta_{01}\rangle = \frac{1}{\sqrt{2}} (|01\rangle + |10\rangle), \quad (2.5)$$

$$|\beta_{10}\rangle = \frac{1}{\sqrt{2}} (|00\rangle - |11\rangle) \quad (2.6)$$

and

$$|\beta_{11}\rangle = \frac{1}{\sqrt{2}} (|01\rangle - |10\rangle). \quad (2.7)$$

In the entanglement distribution process, we assume the use of the $|\beta_{00}\rangle$ state from (2.4).

A quantum system $|\psi\rangle$ can also be represented via a density matrix ρ . For an n -length, d -dimensional pure quantum system $|\psi\rangle$, ρ is a $d^n \times d^n$ size matrix, as

$$\rho = |\psi\rangle\langle\psi|, \quad (2.8)$$

such that $\text{Tr}(\rho) = 1$ for a general state, and for pure states $\text{Tr}(\rho^2) = 1$. For example, the density of $|\beta_{00}\rangle$ is

$$\rho = \frac{1}{2}|00\rangle\langle 00| + \frac{1}{2}|00\rangle\langle 11| + \frac{1}{2}|11\rangle\langle 00| + \frac{1}{2}|11\rangle\langle 11|. \quad (2.9)$$

2.1.2 Entanglement Fidelity

The fidelity of entanglement [52, 83, 106] is another critical parameter for entanglement distribution. In a quantum network with a chain of repeater nodes between a source and target nodes, for all pairs of entangled nodes (e.g., for nodes that share a common entanglement) a given lower bound in the fidelity of entanglement must be satisfied, otherwise the entanglement distribution fails [26, 118].

Let $|\beta_{00}\rangle$ from (2.4) be the target Bell state subject to be created at the end of the entanglement distribution procedure between a particular source node A and receiver node B . The entanglement fidelity F at an actually created noisy quantum system σ between A and B is

$$F(\sigma) = \langle \beta_{00} | \sigma | \beta_{00} \rangle, \quad (2.10)$$

where F is a value between 0 and 1, $F = 1$ for a perfect Bell state and $F < 1$ for an imperfect state. Without loss of generality, in an experimental quantum Internet setting, an aim is to reach $F \geq 0.98$ over long distances [118, 121].

Some properties of F are as follows [39]. The fidelity for two pure quantum states $|\varphi\rangle, |\psi\rangle$ is defined as

$$F(|\varphi\rangle, |\psi\rangle) = |\langle \varphi | \psi \rangle|^2. \quad (2.11)$$

The fidelity of quantum states can describe the relation of a pure state $|\psi\rangle$ and mixed quantum system $\sigma = \sum_{i=0}^{n-1} p_i \rho_i = \sum_{i=0}^{n-1} p_i |\psi_i\rangle \langle \psi_i|$, as

$$F(|\psi\rangle, \sigma) = \langle \psi | \sigma | \psi \rangle = \sum_{i=0}^{n-1} p_i |\langle \psi | \psi_i \rangle|^2. \quad (2.12)$$

Fidelity can also be defined for mixed states σ and ρ , as

$$F(\rho, \sigma) = (\text{Tr}(\sqrt{\sqrt{\sigma}\rho\sqrt{\sigma}}))^2 = \sum_i p_i (\text{Tr}(\sqrt{\sqrt{\sigma_i}\rho_i\sqrt{\sigma_i}}))^2. \quad (2.13)$$

2.1.3 Relative Entropy of Entanglement

The $E(\rho)$ relative entropy of entanglement [123–125] of a joint state ρ of subsystems A and B is defined by the $D(\cdot\|\cdot)$ quantum relative entropy function, without loss of generality as

$$E(\rho) = \min_{\rho_{AB}} D(\rho\|\rho_{AB}) = \min_{\rho_{AB}} \text{Tr}(\rho \log \rho) - \text{Tr}(\rho \log(\rho_{AB})), \quad (2.14)$$

where ρ_{AB} is the set of separable states $\rho_{AB} = \sum_{i=1}^n p_i \rho_{A,i} \otimes \rho_{B,i}$.

2.2 Operations in the Quantum Internet

In a quantum Internet scenario, quantum repeaters aim to create high-fidelity entangled systems over long distances. For practical reasons, let us assume that we are operating on $d = 2$ dimensional quantum systems. At a given target Bell state $|\beta_{00}\rangle$ subject to be created at the end of the entanglement distribution procedure, the entanglement fidelity at an actually created noisy quantum system σ is therefore evaluated as in (2.10).

The entangled system between two distant points A and B is distributed in a step-by-step manner through a set of intermediate quantum repeater nodes. In the first step, the neighboring quantum nodes create entanglement between each other. In the next step, particular quantum nodes apply a special operation called *entanglement swapping* [49, 118, 121] to double the number of spanned quantum nodes. The entanglement swapping operation splices two short-distance Bell states into a longer-distance Bell pair via unitary operations applied in the quantum node and via classical side information (i.e., a similar mechanism to quantum teleportation [49, 118, 121]). This type of entanglement distribution mechanism is referred to as *doubling architecture* [118]. The doubling architecture is depicted in Fig. 2-1.

An important problem connected to the entanglement distribution is the handling of the noise on the entangled states. Considering the noisy physical links and other effects

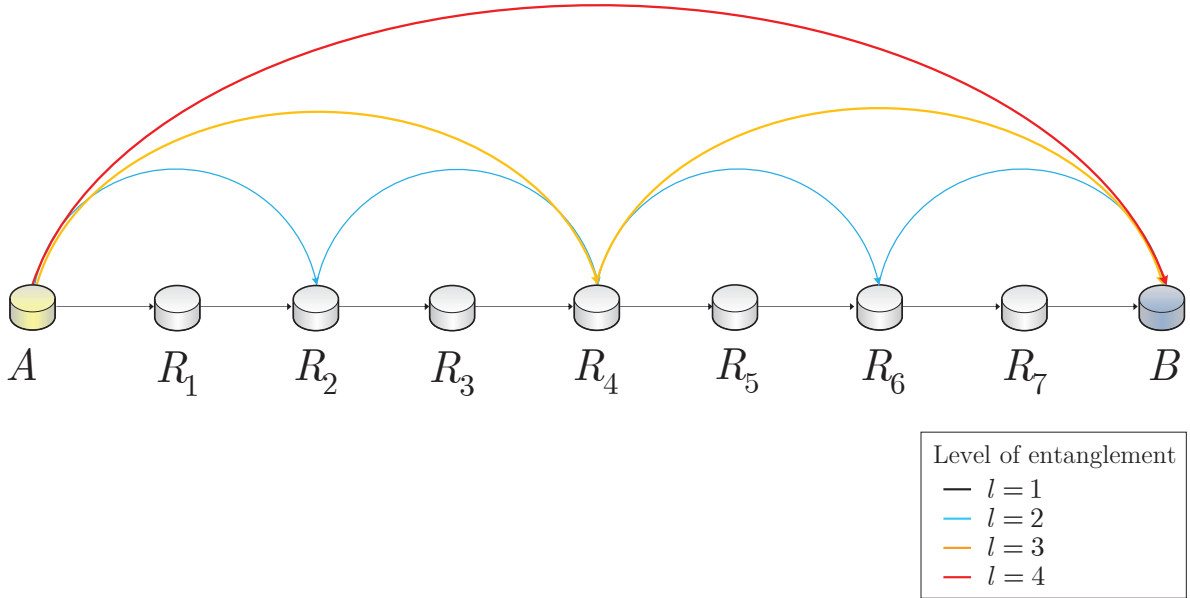


Figure 2-1: Entanglement distribution in the doubling architecture. The aim is to generate long-distance entanglement between distant quantum nodes A and B through a chain of q intermediate R_i , $i = 1, \dots, q$, quantum repeaters. The architecture defines different l entanglement levels, $l = 1, 2, 3, 4$ in the current network situation with $q = 7$. First, the $l = 1$ level entangled connections are established between the quantum nodes. To double the spanned distance, entanglement swapping is applied in the quantum repeaters. The result of the entanglement swapping procedure is a higher-level entangled connection. The $l = 2$ level entangled connections are generated by quantum repeaters R_1, R_3, R_5 and R_7 . The $l = 3$ level entangled connections are generated by R_2 and R_6 , while the $l = 4$ level entangled connection between A and B is generated by R_4 .

of the environment, the received quantum states are noisy. Particularly, the fidelity of the actually created entangled system σ is far from the target fidelity F . To handle the situation, the noisy states should be purified—this process is called *entanglement purification* [49, 118, 121]. The entanglement purification process takes two imperfect systems σ_1 and σ_2 with $F_0 < 1$, and outputs a higher-fidelity system ρ such that

$$F(\rho) > F_0. \quad (2.15)$$

The purification is a high-cost procedure since it requires a huge amount of resources (quantum systems, transmissions, and internal procedures in the nodes), causes delay in the transmission, and is probabilistic.

As follows, a network optimization is essential for a quantum Internet setting to reduce the purification steps. The problem is handled via our modeling scheme by determining optimal paths and via the application of entanglement switching nodes to switch between the entangled connections without the requirement of high-cost steps.

2.3 Network Management in the Quantum Internet

The quantum Internet requires the utilization of advanced network and service management. The main task in the physical layer of the quantum Internet is the reliable transmission of quantum states and the faithful internal storage of the received quantum systems in the quantum memories of the quantum nodes. The quantum transmission and quantum storage processes in the physical layer of the quantum Internet require a collaboration with network and service management services in a higher, logical layer. The logical layer utilizes classical side information available from the quantum network through traditional communication channels to provide feedback and adaption mechanism for the physical layer of the quantum network. The logical layer contains controlling and post-processing tasks, such as error correction, dynamic monitoring of the quantum links and quantum memories, controlling of the internal storage and error correction

mechanisms of the quantum nodes, network optimization, and advanced service management processes.

The field of the quantum Internet dynamically improves, and also challenges with several open questions. Since the structure and the processes of the quantum Internet are fundamentally different from the mechanisms of the traditional Internet, it requires the development of novel and advanced services. The main challenge regarding these services is to provide an optimal solution for the transmission of entangled systems, for the optimization of the network architecture, and for the development of the networking services connected to the entanglement distribution. The networking procedures of the quantum Internet should consider the fundamentals of quantum mechanics (such as superposition, quantum entanglement, and no-cloning theorem, among others) that require a significantly different network and service management compared with the networking services of the traditional Internet.

Chapter 3

Decentralized Routing Service for the Quantum Internet

Quantum repeater networks are a fundamental of any future quantum Internet and long-distance quantum communications. The entangled quantum nodes can communicate through several different levels of entanglement, leading to a heterogeneous, multi-level network structure. The level of entanglement between the quantum nodes determines the hop distance and the probability of the existence of an entangled connection in the network. In this chapter, we define a decentralized routing for entangled quantum networks. The proposed method allows an efficient routing to find the shortest paths in entangled quantum networks by using only local knowledge of the quantum nodes. We give bounds on the maximum value of the total number of entangled connections of a path. The scheme can be directly applied in practical quantum communications and quantum networking scenarios.

3.1 Introduction

In the quantum Internet [55, 74, 91, 118], the quantum nodes are connected with each other through entangled connections [39, 49, 55, 73, 74, 91, 118, 121] allowing one to perform

quantum communications beyond the fundamental limits of traditional sender-receiver communications [62, 92, 93]. The entangled quantum nodes can share several different levels of entanglement, leading to a heterogeneous, *multi-level entanglement* network structure [6, 20–23, 28, 29, 57, 59, 103, 111, 114, 116, 118, 121, 133]. The *level of entanglement* between the quantum nodes determines the achievable hop distance, the number of spanned intermediate nodes, and the probability of the existence of an entangled connection [2, 4, 12, 35, 36, 41, 42, 58, 62, 65, 70, 71, 87, 89, 105, 110, 123–125]. For an L_l -level entangled connection, the hop distance between quantum nodes x and y is 2^{l-1} , and each L_l -level entangled connection $E(x, y)$ can be established only with a given probability, $0 < \Pr_{L_l}(E(x, y)) \leq 1$, which depends on the properties of the actual overlay quantum network [12, 39, 41, 42, 49, 55, 57, 58, 65, 73, 74, 91, 105, 118, 121]. As the level of entanglement increases, the number of spanned nodes also increases, which decreases the probability of the existence of a higher-level entangled connection in the network [12, 21, 41, 42, 57–59, 65, 103, 105, 114, 118, 121]. Note that each quantum node can have an arbitrary number of entangled node contacts with an arbitrary level of entanglement between them. The intermediate nodes between x and y are referred to as quantum repeater nodes and participate only in the process of entanglement distribution from x to y .

In an entangled quantum network with heterogeneous entanglement levels, finding the shortest path between arbitrary quantum nodes for the level of entanglement is a crucial task to transmit a message between the nodes in as few steps as possible. Since in practical scenarios there is no global knowledge available about the nodes or about the properties of the entangled connections, the routing has to be performed in a *decentralized* manner. In particular, our decentralized routing uses only local knowledge about the nodes and their neighbors and their shared level of entanglement.

In this chapter, we show that the probability that a specific level of entanglement exists between the quantum nodes in the entangled overlay quantum network N is proportional to the L1 distance of the nodes in an n -sized base-graph. While most of the

currently available quantum routing methods [12, 41, 42, 57, 58, 65, 105, 118, 121] represent a variant of Dijkstra’s shortest path algorithm [19, 63, 64, 96, 97], the efficiency of these routing approaches is limited. We have found that the probability distribution of the entangled connections can be described by an inverse k -power distribution, where k is the dimension of the base-graph G^k , making it possible to achieve an $\mathcal{O}(\log n)^2$ decentralized routing in an entangled overlay quantum network. A k -dimensional base-graph contains all quantum nodes and entangled connections of the overlay quantum network via a set of nodes and edges such that each link preserves the level of entanglement and corresponding probabilities. Specifically, the construction of the base-graph of an entangled overlay network is a challenge, since in a practical decentralized networking scenario, there is no global knowledge about the exact local positions of the nodes or other coordinates. Particularly, mapping from the entangled overlay quantum network to a base-graph has to be achieved without revealing any routing-related information by security assumptions. It is necessary to embed the entangled overlay quantum network with the probabilistic entangled connections onto a simple base-graph if we want to achieve an efficient decentralized routing. Note, that the quantum links are assumed to be probabilistic, since in a quantum repeater network, both the entanglement purification and the entanglement swapping procedures are probabilistic processes [39, 49, 55, 73, 74, 91, 118, 121]. As follows, quantum entanglement between the distant points can exist only with a given probability, and this probability further decreased by the noise of the physical links used for the transmission.

As we show by utilizing sophisticated mathematical tools, the problem of embedding can be reduced to a statistical estimation task, and thus the base-graph can be prepared for the decentralized routing. Therefore, the shortest path in the heterogeneous entanglement levels of the quantum network can be determined by the L1 metric in the base-graph. Precisely, since the probability of a high-level entangled connection between the nodes is lower than the probability of a low-level entanglement, we can assign positions to the quantum nodes in the base-graph according to the *a posteriori* distribution

of the positions.

The system model allows the utilization of both bipartite and multipartite entangled states. It is because, while for a bipartite entangled system the entangled connection is directly formulated between the two quantum systems, in the case of a multipartite entangled system the entangled connections are formulated between the entangled partitions of the multipartite entangled state in the network model.

We show that the proposed method can be applied for an arbitrary-sized entangled quantum network, and by utilizing entangled connections, our decentralized routing does not require transmission of any routing-related information in the network. We also reveal the diameter bounds of a multi-level entangled quantum network, where the diameter refers to the maximum value of the shortest path (the total number of entangled connections in a path) between a source and a target quantum node.

3.1.1 Results

The novel contributions of the chapter are as follows:

1. *We define a decentralized routing for the quantum Internet. We construct a special graph, called base-graph, that contains all information about the quantum network to perform a high performance routing.*
2. *We show that the probability distribution of the entangled connections can be modeled by a specific distribution in a base-graph.*
3. *The proposed method allows us to perform efficient routing to find the shortest paths in entangled quantum networks by using only local knowledge of the quantum nodes.*
4. *We derive the computational complexity of the proposed routing scheme.*
5. *We give bounds on the maximum value of the total number of entangled connections of the path.*

This chapter is organized as follows. In Section 3.2, the proposed decentralized routing approach is discussed. Section 3.3 provides the computational complexity of the scheme. In Section 3.4 the diameter bounds are derived. Finally, Section 3.5 concludes the chapter. Supplemental material is included in Appendix B.

3.2 System Model

Let us formalize our statements in a strict mathematical manner. Let V refer to the nodes of an overlay entangled quantum network N , which consists of a transmitter node $A \in V$, a receiver node $B \in V$, and quantum repeater nodes $R_i \in V$, $i = 1, \dots, q$. Let $E = \{E_j\}$, $j = 1, \dots, m$ refer to a set of edges between the nodes of V , where each E_j identifies an L_l -level entanglement, $l = 1, \dots, r$, between quantum nodes x_j and y_j of edge E_j , respectively.

3.2.1 Entanglement Levels

An $N = (V, E)$ overlay quantum repeater network consists of several single-hop and multi-hop entangled nodes, such that the single-hop entangled nodes are directly connected through an L_1 -level entanglement, while the multi-hop entangled nodes communicate through L_l -level entanglement. According to the working mechanism of a doubling quantum repeater architecture [39, 74, 91, 118], the number of spanned nodes is doubled in each level $l_{sw} = l - 1$ of entanglement swapping. Therefore, the $d(x, y)_{L_l}$ hop distance in N for the L_l -level entangled nodes $x, y \in V$ is denoted by

$$d(x, y)_{L_l} = 2^{l-1}, \quad (3.1)$$

with $d(x, y)_{L_l} - 1$ intermediate nodes between the nodes x and y . Thus, $l = 1$ refers to a direct quantum link connection between two quantum nodes x and y without intermediate quantum repeaters. The probability that an L_l -level entangled connection $E(x, y)$ exists

between $x, y \in V$ is $\Pr_{L_i}(E(x, y))$, which depends on the actual network.

An entangled overlay quantum network N is illustrated in Fig. 3-1. The network consists of single-hop entangled nodes (depicted by gray nodes) and multi-hop entangled nodes (depicted by blue and green nodes) connected by edges. The single-hop entangled nodes are directly connected through an L_1 -level entanglement, while the multi-hop entangled nodes communicate with each other through L_2 and L_3 -level entanglement. Each entanglement level exists with a given probability.

3.2.2 Problem Setting and Available Resources

The proposed network model handles the quantum nodes and the quantum links in an abstract level. The quantum nodes are represented by nodes, while the quantum links are modeled by edges in a graph. The quantum links are formulated by bipartite or multipartite entangled states between the quantum nodes. The entangled quantum links are built-up by the physical layer procedures and resource allocation mechanisms of entanglement distribution [39,49,55,73,74,91,118,121], such as entanglement purification, entanglement swapping, and quantum error correction [6, 13, 20–23, 28, 29, 57, 59, 103, 107, 111, 114, 116, 129, 131, 133]. In the system model, if a new entangled connection is required to establish a shortest path, these physical layer procedures are called in the background. Note, that the quantum nodes also utilize classical links to perform some auxiliary communications (see Section 3.2.6) connected to the mechanisms of quantum layer such as entanglement distribution and node selection, distribution of measurement information and statistical information between the neighboring nodes, and other related information connected to the decentralized routing mechanism. The aim of the proposed system model is to handle these procedures in an abstracted background layer that allows us to focus only on the path selection problem.

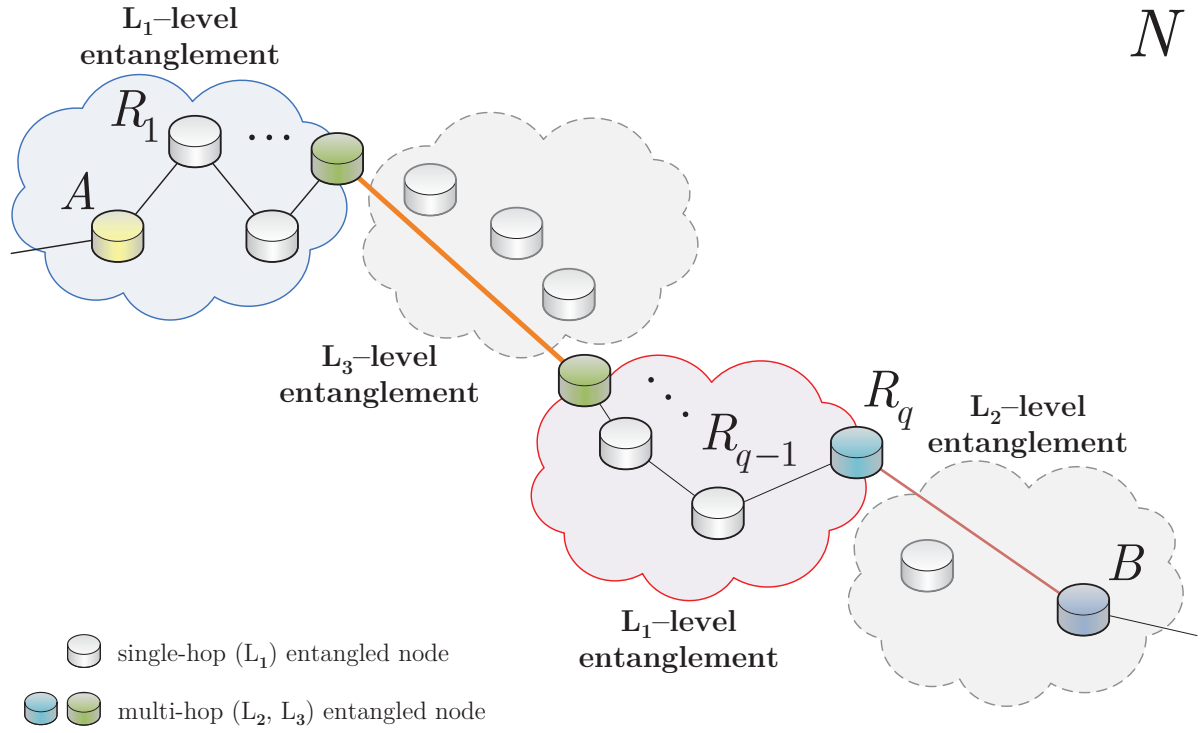


Figure 3-1: Entangled overlay quantum network $N = (V, E)$ with heterogeneous entanglement levels. The network consists of single-hop entangled (gray) nodes with L_1 -level entanglement connection, and multi-hop entangled (blue, green) nodes with L_2 and L_3 -level entangled connections. An L_l -level, $l = 1, 2, 3$, entangled connection between nodes $x, y \in V$ is established with probability $\Pr_{L_l}(E(x, y))$. The overlay network consists of q quantum repeater nodes $R_i \in V$, $i = 1, \dots, q$ between the transmitter (A) and the receiver (B) nodes. The L_l -level entangled nodes consist of $d(x, y)_{L_l} - 1$ intermediate quantum nodes, as depicted by the dashed lines.

Probability of Entanglement and Entanglement Fidelity

The F fidelity of entanglement [39, 49, 118, 123–125] at a particular density matrix σ between nodes x and y is defined as $F = \langle \Psi | \sigma | \Psi \rangle$, where $|\Psi\rangle$ refers to the entangled system subject to be established between x and y . Let's assume that σ is the density matrix associated with a particular link $E(x, y)$ as $\sigma = \sum_i p_i \rho_i = \sum_i p_i |\psi_i\rangle \langle \psi_i|$, thus the $F_{E(x,y)}$ entanglement fidelity between nodes x and y is as

$$F_{E(x,y)} = \langle \Psi | \sigma | \Psi \rangle = \sum_i p_i |\langle \Psi | \psi_i \rangle|^2. \quad (3.2)$$

Independent of the $\text{Pr}_{L_l}(E(x, y))$ probability of entanglement between the nodes, in the proposed routing method each $E(x, y)$ link can be also associated with a particular entanglement fidelity (see (3.2)). As a corollary, $F_{E(x,y)}$ can also be selected as a routing metric in our model to find the shortest path in the quantum network. However, the $\text{Pr}_{L_l}(E(x, y))$ probability of entanglement represents a more generalized metric that includes the effects of link noise, the effects of entanglement purification and entanglement swapping, error-correction, and disturbances of the physical environment.

Note that recent approaches to quantum networks employ quantum error correction in addition to, or instead of, entanglement purification [80]; therefore, in these networks the effect of entanglement purification on the entanglement probability is weighted by a particular weight coefficient ω , $\omega < 1$, or neglected, $\omega = 0$.

3.2.3 Mapping the Structure of the Quantum Internet

Thesis 1.1 (Mapping the entangled network structure) *The quantum nodes and the entangled connections of the entangled quantum network N can be mapped into a k -dimensional, n -size base graph G^k .*

Proof. The base-graph [24, 53, 56, 102] of an entangled quantum network N is determined as follows. Let V be the set of nodes of the overlay quantum network. Then let G^k be

the k -dimensional, n -sized finite square-lattice base-graph [27, 53, 56, 82, 102, 118], with position $\phi(x)$ assigned to an overlay quantum network node $x \in V$, where $\phi : V \rightarrow G^k$ is a mapping function which achieves the mapping from V onto G^k [102].

Specifically, for two network nodes $x, y \in V$, the L1 metric in G^k is denoted by $d(\phi(x), \phi(y))$, $\phi(x) = (j, k)$, $\phi(y) = (m, o)$ and is defined as

$$d((j, k), (m, o)) = |m - j| + |o - k|. \quad (3.3)$$

The G^k base-graph contains all entangled contacts of all $x \in V$. The probability that $\phi(x)$ and $\phi(y)$ are connected through an L_l -level entanglement in G^k is

$$p(\phi(x), \phi(y)) = \frac{d(\phi(x), \phi(y))^{-k}}{H_n} + c_{\phi(x), \phi(y)}, \quad (3.4)$$

where

$$H_n = \sum_z d(\phi(x), \phi(z)) \quad (3.5)$$

is a normalizing term [56, 102], which is taken over all entangled contacts of node $\phi(x)$ in G^k , while $c_{\phi(x), \phi(y)}$ is a constant defined as

$$c_{\phi(x), \phi(y)} = \text{Pr}_{L_l}(E(x, y)) - \frac{d(\phi(x), \phi(y))^{-k}}{H_n}, \quad (3.6)$$

where $\text{Pr}_{L_l}(E(x, y))$ is the probability that nodes $x, y \in V$ are connected through an L_l -level entanglement in the overlay quantum network N .

For an L_l -level entanglement between $\phi(x)$ and $\phi(y)$, $d(\phi(x), \phi(y))$ in G^k is evaluated as

$$d(\phi(x), \phi(y)) = 2^{l-1}. \quad (3.7)$$

Our idea is that the $\text{Pr}_{L_l}(E(x_i, y_i))$ probability of an L_l -level entanglement connection between nodes $x_i, y_i \in V$ in the entangled overlay quantum network N can be rephrased directly by the probability of $p(\phi(x_i), \phi(y_i))$ in the k -dimensional base-graph G^k via the

following distance connection:

$$d(\phi(x_i), \phi(y_i)) = d(x_i, y_i)_{L_i}. \quad (3.8)$$

Between the $\phi(\cdot)$ configuration of positions of the quantum nodes in G^k and the set E of the m edges of the overlay network V , the following conditional probability can be defined:

$$\Pr(E|\phi) = \prod_{E_i=1}^m \frac{d(\phi(x_i), \phi(y_i))^{-k}}{H_n} + c_{\phi(x_i), \phi(y_i)}, \quad (3.9)$$

where $x_i, y_i \in V$ are the quantum nodes connected via an entangled connection E_i in the overlay network N .

Thus, the mapping $V \rightarrow G^k$ holds the connectivity of V via the unique position configurations $\phi(x_i), \phi(y_i)$ of the overlay nodes such that the probability of an edge in G^k depends only on the distance $d(\phi(x_i), \phi(y_i))$ between $\phi(x_i), \phi(y_i)$ and the corresponding $\Pr_{L_i}(E(x_i, y_i))$ in N .

As follows from (3.9), to maximize $\Pr(E|\phi)$ we have to determine those base-graph $\phi(x_i) \in G^k$ assignments for all i of overlay nodes $x_i \in V$ that minimize the product of the $d(\cdot)$ distances in the base-graph G^k .

In particular, using stochastic optimization at a given set of m edges E of the overlay quantum network N , finding the positions $\phi(x_i), \phi(y_i), i = 1, \dots, m$ in G^k can be approached straightforwardly by the Bayes' rule as

$$\Pr(\phi|E) = \frac{\Pr(E|\phi) \Pr(\phi)}{\Pr(E)}, \quad (3.10)$$

which characterizes the a posteriori distribution of configuration ϕ at a given set E . Therefore, the $\phi : V \rightarrow G^k$ mapping function which maximizes $\Pr(\phi|E)$ can be determined via a statistical estimation.

For a candidate distribution $\Pr(\phi)$, $\Pr(\phi|E)$ can be rewritten without loss of gener-

ality as

$$\Pr(\phi|E) = \frac{\Pr(E|\phi)\Pr(\phi)}{\int_{\phi} \Pr(E|\phi)\Pr(\phi)d\phi}, \quad (3.11)$$

which clearly reveals that the determination of (3.11), specifically the computation

$$\int_{\phi} \Pr(E|\phi)\Pr(\phi)d\phi, \quad (3.12)$$

is also hard [24, 53, 102]. To solve the problem, Markov chain–based techniques [102] can be utilized, allowing us to generate samples of ϕ that conform to a given $\Pr(\phi)$ candidate distribution [102] (see also [33]); this is convenient since we can determine the denominator of (3.11). These techniques require the definition of a proposal density function to stabilize the resulting Markov chain. This stabilization is required to achieve (3.11) via the chain through a sequence of states. A proposal density function $q(r|s)$ proposes a next state s^* given a state s_i . ■

The stabilization procedure also requires the swapping of position information $\phi(x_i)$ and $\phi(y_i)$ between any two nodes $\phi(x_i), \phi(y_i) \in G^k$ subject to some constraints. The swapping operation between two nodes does not change the physical-level connections. However, assuming a classical channel for this purpose, the swapping would lead to security issues [53, 102].

3.2.4 Swapping by Quantum Teleportation

Thesis 1.2 (Stabilization of an entangled quantum network) *The stabilization procedure of the entangled quantum network N can be established by quantum teleportation between quantum nodes.*

Proof. By utilizing entangled connections between nodes, our solution requires no transmission of information $\phi(x_i)$ and $\phi(y_i)$ between the nodes $x_i, y_i \in V$ of the overlay network for stabilization. Particularly, our stabilization procedure uses quantum tele-

portation between nodes, which does not require transmission of any routing-related information in the network, as follows.

Let's assume that quantum nodes $x_i, y_i \in V$ are selected for swapping from the entangled overlay network N , associated with G^k position information $\phi(x_i)$ and $\phi(y_i)$. Let u_j refer to the j -th neighbor quantum node of x_i , $\{x_i, u_j\} \in E$ with position $\phi(u_j) \in G^k$, and let v_j identify the j -th neighbor quantum node of y_i , $\{y_i, v_j\} \in E$ with position $\phi(v_j) \in G^k$. In the first phase, all neighbor nodes of x_i, y_i locally prepare the quantum systems $|\phi(u_j)\rangle$ and $|\phi(v_j)\rangle$. Using the L_l -level entangled connections between u_j and x_i , v_j and y_i , all neighbor quantum nodes teleport their local quantum system to x_i and y_i . This is possible since all nodes of V are connected through an L_l -level entanglement in N , and therefore, an arbitrary neighbor node is at least connected through an L_1 -level (direct) entanglement.

Specifically, for $\forall j$, the neighbor node u_j teleports $|\phi(u_j)\rangle$ to x_i , while all v_j teleports $|\phi(v_j)\rangle$ to y_i , respectively. In the next step, for $\forall j$ the nodes x_i and y_i measure their states $|\phi(u_j)\rangle$ and $|\phi(v_j)\rangle$ via a local measurement M , which yields

$$M |\phi(u_j)\rangle = \phi(u_j) \quad (3.13)$$

and

$$M |\phi(v_j)\rangle = \phi(v_j). \quad (3.14)$$

Using the results of the local measurements, the two nodes x_i and y_i determine the following quantities:

$$\begin{aligned} & \zeta(x_i, y_i) \\ &= \prod_{\{x_i, u_j\} \in E} (\phi(x_i) - \phi(u_j)) \prod_{\{y_i, v_j\} \in E} (\phi(y_i) - \phi(v_j)), \end{aligned} \quad (3.15)$$

and

$$\begin{aligned} & \Phi(x_i, y_i) \\ &= \prod_{\{x_i, u_j\} \in E} (\phi(y_i) - \phi(u_j)) \prod_{\{y_i, v_j\} \in E} (\phi(x_i) - \phi(v_j)). \end{aligned} \quad (3.16)$$

In the final step, the two nodes x_i and y_i make a decision regarding their location information swapping.

Particularly, if

$$\zeta(x_i, y_i) \geq \Phi(x_i, y_i), \quad (3.17)$$

then nodes x_i, y_i perform the swapping operation, which yields

$$M |\phi(y_i)\rangle \equiv \phi(x_i) \quad (3.18)$$

at x_i , and

$$M |\phi(x_i)\rangle \equiv \phi(y_i) \quad (3.19)$$

at y_i , with unit probability

$$p_{\text{swap}}(\phi(x_i), \phi(y_i)) = 1. \quad (3.20)$$

If

$$\zeta(x_i, y_i) < \Phi(x_i, y_i), \quad (3.21)$$

then nodes x_i, y_i swap their position information only with probability

$$p_{\text{swap}}(\phi(x_i), \phi(y_i)) = \frac{\zeta(x_i, y_i)}{\Phi(x_i, y_i)}, \quad (3.22)$$

which is also a possible scenario if the nodes x_i, y_i are uniformly selected at random [24].

Applying the swapping procedure for all node pairs of V provably stabilizes the chain since it leads to the convergence of the $\phi(\cdot)$ positions to a state which allows us to perform efficient decentralized routing in the G^k base-graph, using the L1 metric.

The Markov chain for the base-graph construction is defined as follows. Let ϕ_2 be the x_i, y_i -swap of ϕ_1 , such that $\phi_1(x_i) = \phi_2(y_i)$, $\phi_1(y_i) = \phi_2(x_i)$, and $\phi_1(z_i) = \phi_2(z_i)$ for all $z_i \neq x_i, y_i$ [33]. Then let the Markov chain defined by transition matrix $T(\phi_1, \phi_2)$, as $T(\phi_1, \phi_2) = \Omega(\phi_1, \phi_2)\varepsilon(\phi_1, \phi_2)$, where $\phi_1 \neq \phi_2$. If ϕ_2 is the x_i, y_i -swap of ϕ_1 , then $\Omega(\phi_1, \phi_2) = 1/(n + \binom{n}{2})$, and $\Omega(\phi(x_i), \phi(y_i)) = 0$ otherwise [33]. The term $\varepsilon(\phi_1, \phi_2)$ is defined as

$$\begin{aligned} & \varepsilon(\phi_1, \phi_2) \\ &= \min \left(1, \prod_{E_i \in E(x \vee y)} \frac{d(\phi_1(x_i), \phi_1(y_i))^k + c_{\phi_1(x_i), \phi_1(y_i)}}{d(\phi_2(x_i), \phi_2(y_i))^k + c_{\phi_2(x_i), \phi_2(y_i)}} \right), \end{aligned} \quad (3.23)$$

where $E(x \vee y)$ refers to the edges connected to $x \in V$ or $y \in V$; therefore, $\varepsilon(\phi_1, \phi_2)$ can be determined via each node by only its local edge information.

As one can readily check, the chain with $T(\phi_1, \phi_2)$ has $\Pr(\phi | E)$ (see (3.10)) as its stationary distribution. ■

3.2.5 Next-Generation Repeaters

The result in (3.1) reflects the characteristic of the entanglement distribution mechanism of the doubling-architecture [55, 74, 118, 121]. On the other hand, the proposed routing method can also be extended to next-generation quantum repeater quantum networks [80] that do not necessarily involve the establishment of long-distance entangled connections. In this terminology, (3.1) identifies the $d(x, y)$ hop-distance between quantum nodes x and y in the network, without the utilization of entangled connections and the level characteristics of the doubling-architecture. As a corollary, for a next-generation quantum repeater network setting the level L_l of a $E(x, y)$ link refers directly to the hop-distance, i.e., l is set as

$$l = d(x, y). \quad (3.24)$$

Therefore, the proposed routing method remains directly applicable in next-generation quantum repeater networks, since the links between the quantum nodes can also be associated with a particular link probability $\text{Pr}_{L_l}(E(x, y))$. Note the swapping mechanism of Section 3.2.4 for these networking scenarios can be established via secure quantum communications.

3.2.6 Classical Communications in the Quantum Network

The proposed method also utilizes some classical communications to perform the decentralized routing to find a shortest path in the quantum network. Without loss of generality, a classical communication phase consists of the selection of the quantum nodes, local communications between the neighboring quantum nodes, distribution of measurement information between the neighboring nodes, and sharing of statistical information regarding the entangled connections. The locally distributed measurement information consists of the measurement results of the quantum teleportation procedure (see Section 3.2.4), and other measurements results connected to the entanglement distribution mechanism (e.g., entanglement purification, entanglement swapping, quantum error correction, etc) in the quantum network.

3.3 Decentralized Routing

The routing in the k -dimensional base-graph G^k is performed via a decentralized algorithm \mathcal{A} as follows. After we have determined the base-graph G^k of the entangled overlay quantum network N , we can apply the L1 metric to find the shortest paths. Since the probability that two arbitrary entangled nodes $\phi(x), \phi(y)$ are connected through an L_l -level entanglement is $p(\phi(x), \phi(y))$ (see (3.4)), this probability distribution associated with the entangled connectivity in G^k allows us to achieve efficient decentralized routing via \mathcal{A} in the base-graph.

Using the L1 distance function, a greedy routing (which always selects a neighbor node

closest to the destination node in terms of G^k distance function d and does not select the same node twice) can be straightforwardly performed in G^k to find the shortest path from any quantum node to any other quantum node, in

$$\mathcal{O}(\log n)^2 \tag{3.25}$$

steps on average (see Section 3.3.1), where n is the size of the network of G^k .

Note that the nodes know only their local links (neighbor nodes) and the target position. It also allows us to avoid dead-end nodes (where the routing would stop) by some constraints on the degrees of the nodes, which can be directly satisfied through the settings of the overlay quantum network.

The decentralized algorithm \mathcal{A} in the k -dimensional n -sized base-graph G^k is characterized by the following diameter bounds.

In our setting, the $D(G^k)$ diameter of G^k refers to the maximum value of the shortest path (total number of edges on a path) between any pair of mapped nodes in G^k .

Then, for the $D(\mathcal{A})$ minimal number of steps required by \mathcal{A} follows that

$$D(\mathcal{A}) \geq D(G^k). \tag{3.26}$$

We show that for any G^k with $p(\phi(x), \phi(y))$ (see (3.4)) probability for the entangled connections between an arbitrary $\phi(x), \phi(y) \in G^k$, the relation

$$D(\mathcal{A}) \leq \mathcal{O}(\log n)^2 \tag{3.27}$$

holds.

In Section 3.3.1 we prove that for any G^k , the relation of (3.27) holds.

In Fig. 3-2, a G^k , $k = 2$ dimensional base-graph is depicted with entangled nodes $\phi(A) \in G^2$, $\phi(R_i) \in G^2$, $i = 1, 2, 3$, where $A \in V$ is a transmitter node in the overlay quantum network V , while $R_i \in V$ are quantum repeater nodes in N . The

nodes are connected through an L_i -level entanglement in N with probability $\Pr_{L_i}(A, R_i)$. In the base-graph G^2 , the mapped nodes $\phi(A)$, $\phi(R_i)$ are connected with probability $p(\phi(A), \phi(R_i)) = \frac{d(\phi(A), \phi(R_i))^{-2}}{\sum_z d(\phi(A), \phi(R_z))^{-2}} + c_{\phi(A), \phi(R_i)}$, where $d(\phi(A), \phi(R_i)) = 2^{i-1}$.

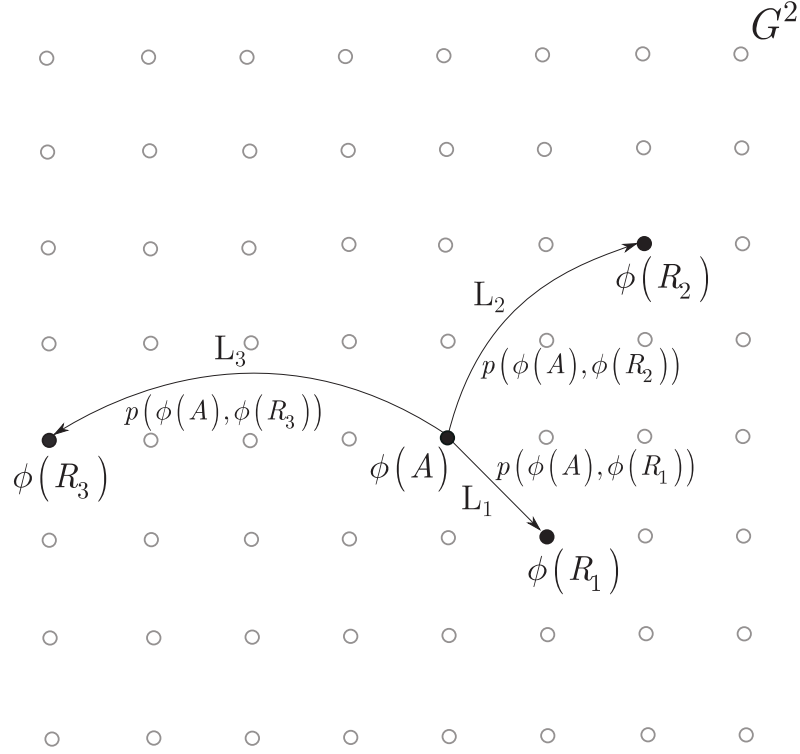


Figure 3-2: G^2 base-graph of an overlay entangled quantum network N , with entangled nodes $\phi(A)$, $\phi(R_i)$, $i = 1, 2, 3$, where $A \in V$ is a transmitter node in the overlay quantum network N , while $R_i \in V$ are quantum repeater nodes in N . In N , nodes A and R_1 are connected through L_1 -level entanglement with probability $\Pr_{L_1}(A, R_1)$, nodes A and R_2 are connected via L_2 -level entanglement with probability $\Pr_{L_2}(A, R_2)$, while A and R_3 have an L_3 -level entanglement connection with probability $\Pr_{L_3}(A, R_3)$. The probability that nodes are connected in G^2 is $p(\phi(A), \phi(R_1))$, $p(\phi(A), \phi(R_2))$, and $p(\phi(A), \phi(R_3))$.

3.3.1 Routing Complexity

Thesis 1.3 (Complexity of the routing service) *The complexity of the decentralized routing service is upper bounded by $\mathcal{O}(\log n)^2$ for any N .*

Proof. We prove that for our decentralized algorithm \mathcal{A} , for an arbitrary k -dimensional n -size base-graph G^k , the relation of

$$D(\mathcal{A}) \leq \mathcal{O}(\log n)^2 \quad (3.28)$$

holds.

Utilizing the tessellation of B_n for m times results in end squares with side length n^{γ^m} , for which situation m events, A_1, \dots, A_m , exist [27]. In this case, the resulting bound on the diameter is

$$D(G^2) \leq 2^{m+2} n^{\gamma^m}. \quad (3.29)$$

It can be verified that

$$m = (\log \log n - \log \log \log n + \log(4\gamma - k) - \log K) / \log \gamma^{-1}, \quad (3.30)$$

where K is a constant [24, 27, 102], and

$$\gamma^m = \frac{K \log \log n}{(4\gamma - k) \log n}, \quad (3.31)$$

therefore, the diameter bound is as

$$D(G^2) \leq (\log n)^C, \quad (3.32)$$

for some constant $C > 0$, which leads to

$$\lim_{n \rightarrow \infty} \Pr \left(D(G^2) \leq (\log n)^C \right) = 1. \quad (3.33)$$

Note, that the probability that an event A_i occurs (i.e., there is no edge between the n^{γ^i} side subsquares) is bounded by

$$\Pr(A_i) \leq n^4 e^{-Z n^{\gamma^{i-1}(4\gamma-k)}}, \quad (3.34)$$

where $Z > 0$ is a constant, while $n^{\gamma^{i-1}}$ refers to the large subsquare which is tessellated by the n^{γ^i} side sub-subsquares, respectively. Thus,

$$\Pr(A_1 \wedge \dots \wedge A_m) \leq mn^4 e^{-Zn^{\gamma^m} (4\gamma - k)}. \quad (3.35)$$

To verify the upper bound (3.28), we use the fact that for any $\phi(x) \in G^2$, by theory

$$\sum_{\phi(y) \in G^2, \phi(y) \neq \phi(x)} (d(\phi(x) - \phi(y)))^{-2} \leq 4 \log(6n) \quad (3.36)$$

from which the probability

$$\Pr(\phi(y) | \phi(x)) \quad (3.37)$$

that from node $\phi(x)$ a given $\phi(y)$ is selected is lower bounded by

$$\Pr(\phi(y) | \phi(x)) \geq \frac{d(\phi(x) - \phi(y))^{-2}}{4 \log(6n)}. \quad (3.38)$$

Then let e_j , be an event that from node $\phi(x)$ a set \mathcal{S}_j of nodes can be selected by \mathcal{A} , where

$$j \in [\log \log n, \log n], \quad (3.39)$$

such that \mathcal{S}_j are within L1 distance 2^j from the target node $\phi(B)$.

In set \mathcal{S}_j , each node is within the L1 distance

$$2^{j+1} + 2^j < 2^{j+2} \quad (3.40)$$

of $\phi(x)$. After some calculations [27, 56], the probability that an event e_j occurs is

$$\Pr(e_j) \geq \frac{1}{64 \log(6n)}. \quad (3.41)$$

Therefore, if the current node is $\phi(x)$, and

$$2^j < d(\phi(x), \phi(B)) \leq 2^{j+1} \quad (3.42)$$

holds for the L1 distance, then the number of steps are upper bounded by the mean $E(X_j)$ of an geometric random variable X_j ,

$$E(X_j) = \frac{1}{\Pr(e_j)} = \mathcal{O}(\log n). \quad (3.43)$$

Since the number of such events is maximized in $\log n$, it immediately follows that the total number of steps in G^2 is on average at most $\mathcal{O}(\log n)^2$, thus

$$D(\mathcal{A}) \leq \log n \frac{1}{\Pr(e_j)} = \mathcal{O}(\log n)^2, \quad (3.44)$$

which holds for an arbitrary, k -dimensional n -size base-graph G^k . ■

3.3.2 Implementation

Since the proposed method requires no additional physical apparatus in an experimental quantum networking scenario, the algorithm in a stationary quantum node can be implemented by standard photonics devices, quantum memories, optical cavities and other fundamental physical devices currently in practical use in experimental quantum networking [6, 20–23, 28, 29, 59, 103, 111, 114, 116, 133].

Practical Benefits

The practical benefits of the method in the context of an actual quantum network are as follows. Since the proposed routing has a low-complexity, it allows resource savings in the quantum nodes. Both the overall storage time of the quantum states in the local quantum memories of the quantum nodes, and the number of auxiliary communications and internal computational steps related to the path determination in the nodes can be

minimized. As a corollary, the proposed decentralized routing method has a minimal overall delay in the quantum network that has a crucial significance in an experimental quantum network setting.

3.4 Diameter Bounds

Here we derive the diameter bounds for a $k = 2$ dimensional n -size base-graph G^2 . The results can be extended for arbitrary dimensions.

Let B_n be a box of size $n \times n$ that contains G^2 . Let S_i be a subsquare of B_n of side length n^γ , where

$$k/4 < \gamma < 1, \quad (3.45)$$

and let us subdivide each S_i into smaller sub-subsquares S_{ik} of side length n^{γ^2} [27].

Let A_1 be the event that there exists at least two subsquares S_i and S_j in B_n such that there is no edge between them. Similarly, let A_2 identify the event that exists at one S_i in B_n such that there are two sub-subsquares S_{ik} in S_i which are not connected by edge. In particular, assuming a G^2 for which A_1 is violated means that subsquares S_i and S_j are connected by at least one edge, thus without loss of generality,

$$D(G^2) \leq 2D_{max}(S_i) + 1, \quad (3.46)$$

where $D_{max}(S_i)$ identifies the largest diameter of the subsquares of side length n^γ . By similar assumptions, if A_2 is violated then there exists an edge between at least two sub-subsquares S_{ik} of any S_i ; therefore,

$$D(G^2) \leq 4D_{max}(S_{ik}) + 3, \quad (3.47)$$

where $D_{max}(S_{ik})$ is the largest diameter of the sub-subsquares of side length n^{γ^2} , respec-

tively. As follows, in this case there exists a path of length

$$D(G^2) \leq 4D_{max}(S_{ik}) + 3 \tag{3.48}$$

in B_n which connects any two mapped nodes $\phi(x), \phi(y)$ in G^2 .

Tessellation of a base-graph G^2 of an overlay quantum network N for which these events are violated is illustrated in Fig. 3-3. The B_n box contains G^2 , with subsquares S_i , and sub-sub-squares S_{ik} . The nodes are connected through L_1, L_2 and L_3 -level entanglement in N .

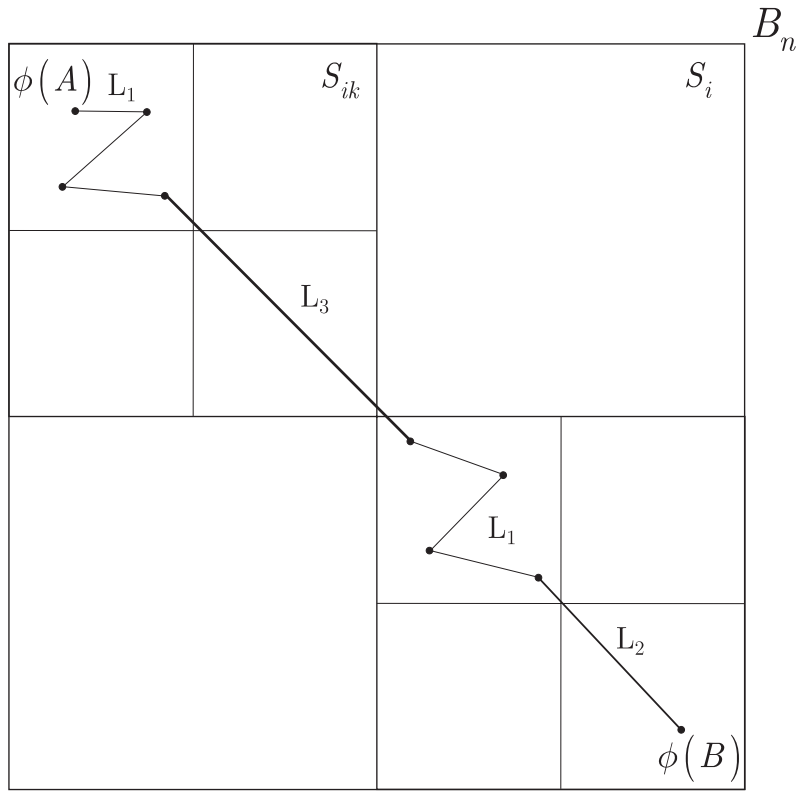


Figure 3-3: A tessellation of B_n of the base-graph G^2 of an overlay quantum network N onto n^γ side subsquare S_i , and n^{γ^2} side sub-sub-square S_{ik} , where $k/4 < \gamma < 1$. The nodes are connected through L_1, L_2 and L_3 -level entangled connections in the overlay network, with source node A and target node B . The points between $\phi(A)$ and $\phi(B)$ refer to the repeater quantum nodes.

3.5 Conclusions

This chapter proposed a method to perform efficient decentralized routing in the entangled networks of the quantum Internet. The solution allows us to find the shortest path in multi-level entangled quantum networks of the quantum Internet, using only local knowledge of the nodes. We showed that the entangled network structure can be embedded onto a base-graph, keeping the probability distribution of the entangled connections and allowing us to construct efficient decentralized routing. The results can be directly applied in the experimental quantum Internet and quantum networking scenarios.

Chapter 4

Entanglement Availability Differentiation Service for the Quantum Internet

A fundamental concept of the quantum Internet is quantum entanglement. In a quantum Internet scenario where the legal users of the network have different priority levels or where a differentiation of entanglement availability between the users is a necessity, an entanglement availability service is essential. In this chapter, we define the entanglement availability differentiation (EAD) service for the quantum Internet. In the proposed EAD framework, the differentiation is either made in the amount of entanglement with respect to the relative entropy of entanglement associated with the legal users, or in the time domain with respect to the amount of time that is required to establish a maximally entangled system between the legal parties. The framework provides an efficient and easily-implementable solution for the differentiation of entanglement availability in experimental quantum networking scenarios.

4.1 Introduction

In the quantum Internet [55, 74], one of the most important tasks is to establish entanglement [36, 39, 49, 60, 74, 79, 91, 118, 120, 121] between the legal parties [14, 15, 54, 88, 112] so as to allow quantum communication beyond the fundamental limits of point-to-point connections [62, 92, 93]. For the problem of entanglement distribution in quantum repeater networks several methods [14, 15, 54, 60, 79, 88, 112], and physical approaches have been introduced [2, 4–6, 20–23, 28, 29, 50, 55, 59, 61, 70, 71, 73, 89, 103, 107, 110, 111, 114, 116, 129, 131, 133]. The current results are mainly focusing on the physical layer of the quantum transmission [36, 49, 79, 120, 121], implementations of entanglement swapping and purification, or on the optimization of quantum memories and quantum error correction in the repeater nodes [4, 6, 20–23, 28, 29, 50, 55, 59, 70, 71, 73, 89, 103, 107, 110, 111, 114, 116, 129, 131, 133]. However, if the legal users of the quantum network are associated with different priority levels, or if a differentiation of entanglement availability between the users is a necessity in a multiuser quantum network, then an efficient and easily implementable entanglement availability service is essential.

In this chapter, we define the *entanglement availability differentiation* (EAD) service for the quantum Internet. We introduce differentiation methods, Protocols 1 and 2, within the EAD framework. In Protocol 1, the differentiation is made in the amount of entanglement associated with the legal users. The metric used for the quantization of entanglement is the relative entropy of entanglement function [123–125]. In Protocol 2, the differentiation is made in the amount of time that is required to establish a maximally entangled system between the legal parties.

The EAD framework contains a classical phase (Phase 1) for the distribution of timing information between the users of the quantum network. Phase 2 consists of all quantum transmission and unitary operations. In Phase 2, the entanglement establishment is also performed between the parties according to the selected differentiation method.

The entanglement distribution phase of EAD utilizes Hamiltonian dynamics, which allows very efficient practical implementation for both the entanglement establishment

and the differentiation of entanglement availability. Using the Hamiltonian dynamics approach as a core protocol of Step 2 of the EAD framework, the entanglement differentiation method requires only unitary operations at the transmitter and requires no entanglement transmission. The application time of the unitaries can be selected as arbitrarily small in the transmitter to achieve an efficient practical realization. The proposed EAD framework is particularly convenient for experimental quantum networking scenarios, quantum communication networks, and future quantum internet.

4.1.1 Results

The novel contributions of the chapter are as follows:

1. *We define the entanglement availability differentiation (EAD) service for the quantum Internet.*
2. *The entanglement availability differentiation is achieved via Hamiltonian dynamics between the users of the quantum network.*
3. *The EAD framework can differentiate in the amount of entanglement with respect to the relative entropy of entanglement associated to the legal users (Protocol 1), and also in the time domain with respect to the amount of time that is required to establish a maximally entangled system (Protocol 2) between the legal parties.*
4. *The framework provides an efficient and easily-implementable solution for the differentiation of entanglement availability in experimental quantum networking scenarios.*

This chapter is organized as follows. Section 4.2 defines the framework for the proposed entanglement differentiation methods. Section 4.3 discusses the entanglement differentiation schemes. Finally, Section 4.4 concludes the results. Supplemental information is included in Appendix C.

4.2 System Model

The proposed EAD service allows differentiation in the amount of entanglement shared between the users or the amount of time required for the establishment of maximally entangled states between the users. The defined service requires no entanglement transmission to generate entanglement between the legal parties. The differentiation service consists of two phases: a classical transmission phase (Phase 1) to distribute side information for the entanglement differentiation and a quantum transmission phase (Phase 2), which covers the transmission of unentangled systems between the users and the application of local unitary operations to generate entanglement between the parties.

The proposed entanglement availability differentiation methods are detailed in Protocol 1 and Protocol 2. The protocols are based on a core protocol (Protocol 0) that utilizes Hamiltonian dynamics for entanglement distribution in quantum communication networks (see Section 4.2.3). The aim of the proposed entanglement differentiation protocols (Protocol 1 and Protocol 2) is different from the aim of the core protocol, since Protocol 0 serves only the purpose of entanglement distribution, and allows no entanglement differentiation in a multiuser quantum network. Protocol 0 is used only in the quantum transmission phase and has no any relation with a classical communication phase.

4.2.1 Classical Transmission Phase

In the classical transmission phase (Phase 1), the timing information of the local Hamiltonian operators are distributed among the legal parties by an \mathcal{E} encoder unit. The content of the timing information depends on the type of entanglement differentiation method. The Hamiltonian operators will be applied in the quantum transmission phase (Phase 2) to generate entangled systems between the users. Since each types of entanglement differentiation requires the distribution of different timing information between the users, the distribution of classical timing information will be discussed in detail in Section 4.3.

Protocol 0 Core protocol

Step 1. Alice (transmitter node) and Bob (receiver node) agree on a time t , in which they want to establish entanglement between subsystems A and B . Alice generates a separable initial system AB , with no entanglement between A and B as

$$\rho_{AB} = \frac{1}{2} |\psi_+\rangle \langle \psi_+| + \frac{1}{2} |\phi_+\rangle \langle \phi_+|, \quad (4.1)$$

where $|\psi_+\rangle = \frac{1}{\sqrt{2}} (|01\rangle + |10\rangle)$, $|\phi_+\rangle = \frac{1}{\sqrt{2}} (|00\rangle + |11\rangle)$. Alice encodes subsystem B , $|\varphi_B\rangle = \alpha |0\rangle + \beta |1\rangle$ via an (m, n) redundant quantum parity code as

$$|\delta_B\rangle^{(m,n)} = \alpha |\chi_+\rangle_1^{(m)} \dots |\chi_+\rangle_n^{(m)} + \beta |\chi_-\rangle_1^{(m)} \dots |\chi_-\rangle_n^{(m)}, \quad (4.2)$$

where $|\chi_\pm\rangle^{(m)} = |0\rangle^{\otimes m} \pm |1\rangle^{\otimes m}$, and sends subsystem B to Bob through the network of n intermediate transfer nodes. Each intermediate transfer nodes $\mathcal{N}_{1\dots n}$ receives and retransmits $|\delta_B\rangle^{(m,n)}$. Bob receives $|\delta_B\rangle^{(m,n)}$ and decodes it.

Step 2. Alice prepares a system C , denoted by density $\rho_C = \frac{1}{2} (I + s\sigma^x)$ which is completely uncorrelated from ρ_{AB} , where I is the identity operator, σ^x is the Pauli X matrix, while s is a constant. Alice applies a unitary U'_{AC} on A and C , which produces the initial system ABC with no entanglement between A and B as

$$\rho_{ABC} = U'_{AC} \rho_{AB} \rho_C (U'_{AC})^\dagger = \frac{1}{2} |\psi_+\rangle \langle \psi_+| |+\rangle \langle +| + \frac{1}{2} |\phi_+\rangle \langle \phi_+| |-\rangle \langle -|, \quad (4.3)$$

where $|\pm\rangle = \frac{1}{\sqrt{2}} (|0\rangle \pm |1\rangle)$.

Step 3. Alice applies the unitary U_{AC} on subsystem AC for a time t , as

$$U_{AC} = \exp(-iH_{AC}t) = \cos(t) I - i \sin(t) \sigma_A^x \sigma_C^x, \quad (4.4)$$

where

$$H_{AC} = \sigma_A^x \sigma_C^x \quad (4.5)$$

is the Hamiltonian with energy E_{AC}

$$E_{AC} = \frac{1}{2} \hbar 2\pi \left(\frac{1}{4t}\right), \quad (4.6)$$

where \hbar is the reduced Planck constant, which results in the maximally entangled AB system with probability $p = 1$ as

$$\sigma_{AB} = \frac{1}{2} (|\psi_+\rangle - i|\phi_+\rangle) (\langle \psi_+| + i\langle \phi_+|). \quad (4.7)$$

4.2.2 Quantum Transmission Phase

The quantum transmission phase (Phase 2) utilizes a core protocol for the entanglement distribution protocol of the EAD framework. The core protocol requires no entanglement transmission for the entanglement generation, only the transmission of an unentangled quantum system (i.e., separable state [14, 15, 54, 60, 88, 112]) and the application of a unitary operation for a well-defined time in the transmit user. The core protocol of the quantum transmission phase for a user-pair is summarized in Protocol 0. It assumes the use of redundant quantum parity code [79] for the encoding¹.

4.2.3 Entanglement Distribution via Hamiltonian Dynamics

Thesis 2.1 (Entanglement establishment via Hamiltonian dynamics) *Maximally entangled quantum systems can be established in the multiuser environment of the quantum Internet via Hamiltonian dynamics.*

Proof. The proof of the Core Protocol (Protocol 0) is as follows.

In Step 1, the input system AB (4.1) is an even mixture of the Bell states which contains no entanglement. It is also the situation in Step 2 (on the selection of U'_{AC} , see [54]) for the subsystem AB of ρ_{ABC} (4.3), thus the relative entropy of entanglement for ρ_{AB} is zero, $E(A : B) = 0$. The initial ρ_{AB} in (4.1) and (4.3), is the unentangled, Bell-diagonal state

$$\rho_{AB} = \frac{1}{4} \begin{pmatrix} 1 & 0 & 0 & 1 \\ 0 & 1 & 1 & 0 \\ 0 & 1 & 1 & 0 \\ 1 & 0 & 0 & 1 \end{pmatrix} \quad (4.8)$$

with eigenvalues $v_+ = \frac{1}{2}, v_- = 0, u_+ = \frac{1}{2}, u_- = 0$.

In Step 3, dynamics generated by local Hamiltonian $H_{AC} = \sigma_A^x \sigma_C^x$ with energy E_{AC} will lead to entanglement oscillations in AB . Thus, if U_{AC} is applied exactly only for a

¹Actual coding scheme can be different.

well determined time t , the local unitary will lead to maximally entangled AB with a unit probability.

As a result, for subsystem AB , the entanglement $E(A : B)$ oscillates [60] with the application time t of the unitary. In particular, the entanglement oscillation in AB generated by the energy E_{AC} (4.6) of the Hamiltonian H_{AC} (4.5). This oscillation has a period time T_π , which exactly equals to $4t$, thus

$$T_\pi = 4t, \quad (4.9)$$

where t is determined by Alice and Bob. In other words, time t identifies $\pi/4$, where π is the oscillation period.

Therefore, after Step 3, the density σ_{ABC} of the final ABC state is as

$$\begin{aligned} \sigma_{ABC} &= |\varphi(t)\rangle\langle\varphi(t)|_{ABC} = U\rho_0U^\dagger \\ &= \frac{1}{2} \left(U_{AC} |\psi_+\rangle\langle\psi_+| |+\rangle\langle+| U_{AC}^\dagger \right) + \frac{1}{2} \left(U_{AC} |\phi_+\rangle\langle\phi_+| |-\rangle\langle-| U_{AC}^\dagger \right), \end{aligned} \quad (4.10)$$

where $|\varphi(t)\rangle_{ABC}$ at t is evaluated as

$$\begin{aligned} &|\varphi(t)\rangle_{ABC} \\ &= \frac{1}{\sqrt{2}} (U_{AC} (|\psi_+\rangle |+\rangle) + U_{AC} (|\phi_+\rangle |-\rangle)) \\ &= \frac{1}{\sqrt{2}} (\cos(t) \left(\frac{1}{2} (|010\rangle + |011\rangle + |100\rangle + |101\rangle) \right) \\ &\quad + \cos(t) \left(\frac{1}{2} (|000\rangle - |001\rangle + |110\rangle - |111\rangle) \right) \\ &\quad - i \sin(t) \left(\frac{1}{2} (|111\rangle + |110\rangle + |001\rangle + |000\rangle) \right) \\ &\quad + i \sin(t) \left(\frac{1}{2} (|101\rangle - |100\rangle + |011\rangle - |010\rangle) \right)) \end{aligned} \quad (4.11)$$

that can be rewritten as

$$\begin{aligned}
& \frac{1}{\sqrt{2}} (\cos(t) (|\psi_+\rangle |+\rangle + |\phi_+\rangle |-\rangle) - i \sin(t) (|\phi_+\rangle |+\rangle - |\psi_+\rangle |-\rangle)) \\
&= \frac{1}{\sqrt{2}} ((\cos(t) (|\psi_+\rangle) - i \sin(t) (|\phi_+\rangle)) |+\rangle + (\cos(t) (|\phi_+\rangle) + i \sin(t) (|\psi_+\rangle)) |-\rangle),
\end{aligned} \tag{4.12}$$

where the sign change on $U_{AC} (|\phi_+\rangle |-\rangle)$ is due to the $|-\rangle$ eigenstate on C .

Thus, at $t = \pi/4$,

$$\begin{aligned}
|\varphi(\pi/4)\rangle_{ABC} &= \frac{1}{\sqrt{2}} (\cos(\pi/4) (|\psi_+\rangle |+\rangle + |\phi_+\rangle |-\rangle) - i \sin(\pi/4) (|\phi_+\rangle |+\rangle - |\psi_+\rangle |-\rangle)) \\
&= \frac{1}{\sqrt{2}} \left(\frac{1}{\sqrt{2}} (|\psi_+\rangle |+\rangle + |\phi_+\rangle |-\rangle) - i \frac{1}{\sqrt{2}} (|\phi_+\rangle |+\rangle - |\psi_+\rangle |-\rangle) \right) \\
&= \frac{1}{\sqrt{2}} \left(\begin{aligned} & \left(\frac{1}{\sqrt{2}} (|\psi_+\rangle) - i \frac{1}{\sqrt{2}} (|\phi_+\rangle) \right) |+\rangle \\ & + \left(\frac{1}{\sqrt{2}} (|\phi_+\rangle) + i \frac{1}{\sqrt{2}} (|\psi_+\rangle) \right) |-\rangle \end{aligned} \right),
\end{aligned} \tag{4.13}$$

where

$$\frac{1}{\sqrt{2}} (|\phi_+\rangle + i |\psi_+\rangle) = i \left(\frac{1}{\sqrt{2}} (|\psi_+\rangle - i |\phi_+\rangle) \right); \tag{4.14}$$

i.e., up to the global phase both states are the same.

Therefore the $|\varphi(\pi/4)\rangle_{ABC}$ system state of ABC at $t = \pi/4$ is yielded as

$$|\varphi(\pi/4)\rangle_{ABC} = \frac{1}{\sqrt{2}} \left(\frac{1}{\sqrt{2}} (|\psi_+\rangle - i |\phi_+\rangle) \right) |+\rangle + \frac{1}{\sqrt{2}} \left(\frac{1}{\sqrt{2}} (|\psi_+\rangle - i |\phi_+\rangle) \right) |-\rangle, \tag{4.15}$$

while the density matrix σ_{ABC} of the final ABC system in matrix form is as

$$\sigma_{ABC} = \frac{1}{8} \begin{pmatrix} 1 & 0 & -i & 0 & -i & 0 & 1 & 0 \\ 0 & 1 & 0 & -i & 0 & -i & 0 & 1 \\ i & 0 & 1 & 0 & 1 & 0 & i & 0 \\ 0 & i & 0 & 1 & 0 & 1 & 0 & i \\ i & 0 & 1 & 0 & 1 & 0 & i & 0 \\ 0 & i & 0 & 1 & 0 & 1 & 0 & i \\ 1 & 0 & -i & 0 & -i & 0 & 1 & 0 \\ 0 & 1 & 0 & -i & 0 & -i & 0 & 1 \end{pmatrix}. \quad (4.16)$$

As one can verify, the resulting AB state $|\xi(\pi/4)\rangle_{AB}$ at $t = \pi/4$ is pure and maximally entangled,

$$|\xi(\pi/4)\rangle_{AB} = \frac{1}{\sqrt{2}} (|\psi_+\rangle - i|\phi_+\rangle), \quad (4.17)$$

yielding relative entropy of entanglement

$$E(A : B) = 1 \quad (4.18)$$

with unit probability.

The σ_{AB} density matrix of the final AB state is

$$\begin{aligned} \sigma_{AB} &= |\xi(\pi/4)\rangle \langle \xi(\pi/4)|_{AB} \\ &= \frac{1}{2} (|\psi_+\rangle - i|\phi_+\rangle) (\langle \psi_+| + i\langle \phi_+|) \\ &= \frac{1}{2} (|\psi_+\rangle \langle \psi_+| + i|\psi_+\rangle \langle \phi_+| - i|\phi_+\rangle \langle \psi_+| + |\phi_+\rangle \langle \phi_+|), \end{aligned} \quad (4.19)$$

which in matrix form is as

$$\sigma_{AB} = \frac{1}{4} \begin{pmatrix} 1 & -i & -i & 1 \\ i & 1 & 1 & i \\ i & 1 & 1 & i \\ 1 & -i & -i & 1 \end{pmatrix}. \quad (4.20)$$

The negativity for the $\sigma_{AB}^{T_B}$ partial transpose of σ_{AB} yields

$$N(\sigma_{AB}^{T_B}) = \frac{\|\sigma_{AB}^{T_B}\|_{-1}}{2} = \frac{\text{Tr}\left(\sqrt{(\sigma_{AB}^{T_B})^\dagger \sigma_{AB}^{T_B}}\right)^{-1}}{2} = \frac{i}{2}, \quad (4.21)$$

which also immediately proves that AB is maximally entangled. For a comparison, for the density matrix of initial AB , (4.1), is $N(\rho_{AB}^{T_B}) = 0$.

Note that subsystem C requires no further storage in a quantum memory, since the output density σ_{ABC} can be rewritten as

$$\begin{aligned} \sigma_{ABC} &= \frac{1}{2} (|\xi(\pi/4)\rangle_{AB} |+\rangle) (\langle\xi(\pi/4)|_{AB} \langle+| + \frac{1}{2} (|\xi(\pi/4)\rangle_{AB} |-\rangle) (\langle\xi(\pi/4)|_{AB} \langle-|) \\ &= |\xi(\pi/4)\rangle \langle\xi(\pi/4)|_{AB} (|+\rangle \langle+| + |-\rangle \langle-|) \\ &= (|\xi(\pi/4)\rangle \langle\xi(\pi/4)|_{AB}) I, \end{aligned} \quad (4.22)$$

where I is the identity operator. ■

4.2.4 Framework

In our multiuser framework, the quantum transmission phase is realized by the core protocol of Phase 2; however, time t of the Hamiltonian operator is selected in a different way among the users, according to the selected type of differentiation. For an i -th user U_i , the application time of the local unitary is referred to as T_{U_i} . Without loss of generality, the i -th transmit user is referred to as U_i , and the i -th receiver user is B_i .

In the system model, the user pairs can use the same physical quantum link, therefore in the physical layer the users can communicate over the same quantum channel. On the other hand, in a logical layer representation of the protocols, the communication between the user pairs formulate logically independent channels.

The method of entanglement differentiation service is summarized in Fig. 4-1. The basic model consists of two phases: distribution of timing information over classical links (Fig. 4-1(a)) and the transmission of quantum systems and the application of local unitary operations (Fig. 4-1(b)).

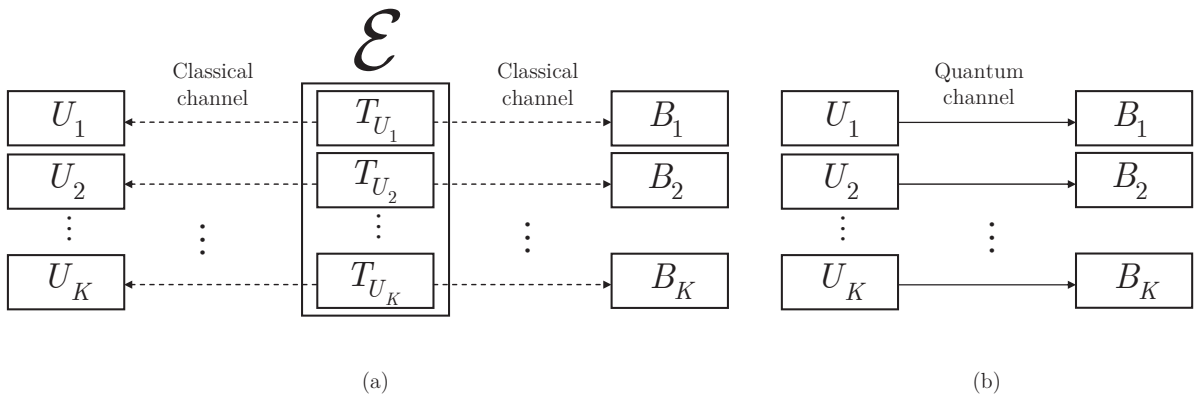


Figure 4-1: Framework of the entanglement differentiation service in a multiuser quantum network. (a) Phase 1. Classical transmission. The \mathcal{E} encoder unit distributes the timing information for the legal transmit users U_1, \dots, U_K and receiver users B_1, \dots, B_K via a classical channel. (b) Phase 2. Quantum transmission. The users apply the core protocol for the entanglement establishment. Then, using the received timing information the transmit users U_1, \dots, U_K apply the local unitaries for time T_{U_1}, \dots, T_{U_K} .

4.3 Methods of Entanglement Availability Differentiation

The EAD service defines different types of differentiation. The differentiation can be achieved in the amount of entanglement in terms of the relative entropy of entanglement between the users (*Protocol 1*: differentiation in the amount of entanglement). In this

method, all users have knowledge of a global oscillation period [60] of time for the application of their local unitaries, but the users will get different amounts of entanglement as a result.

The differentiation is also possible in the amount of time that is required to establish a maximally entangled system between the users (*Protocol 2*: differentiation in the time domain). In this method, all users get a maximally entangled system as a result; however, the time that is required for the entanglement establishment is variable for the users, and there is also no global oscillation period of time.

4.3.1 Differentiation in the Amount of Entanglement

Thesis 2.2 (Differentiation in the amount of entanglement) *The EAD service can be utilized for differentiation of the entanglement amount between the users of the quantum Internet in terms of relative entropy of entanglement.*

Proof. Using the timing information distributed in Phase 1 between the K transmit users U_1, \dots, U_K

$$T_{U_i} = x_{U_i} + (\pi/4), i = 1, \dots, K, \quad (4.23)$$

where

$$x_{U_i} \in [-(\pi/4), (\pi/4)], \quad (4.24)$$

for an i -th transmit user U_i , the protocol generates an initial system ABC , transmits separable B to receiver B_i , and applies the local unitary U_{AC} on subsystem AC for time T_{U_i} (using the core protocol of Phase 2). Depending on the selected T_{U_i} , the resulting AB subsystem between users U_i and B_i contains the selected amount of entanglement,

$$E^{(T_{U_i})}(U_i : B_i) \leq 1. \quad (4.25)$$

In the proposed service framework, the amount of entanglement is quantified by the $E(\cdot)$ relative entropy of entanglement function, see (2.14).

The Phases 1 and 2 of the method of entanglement amount differentiation (Protocol 1) are as included in Protocol 1.

Protocol 1 Differentiation in the amount of entanglement

Step 1. Let $U_i, i = 1, \dots, K$ be the set of transmit users, and $B_i, i = 1, \dots, K$ are the receiver users. Distribute the $T_{U_i} = x_{U_i} + (\pi/4), i = 1, \dots, K$, where $x_{U_i} \in [-(\pi/4), (\pi/4)]$, timing information via an encoder unit \mathcal{E} between all transmit users using a classical authenticated channel (Phase 1).

Step 2. In the transmit user U_i , generate the initial system ABC , transmit separable B to receiver B_i , and apply the local unitary U_{AC} on subsystem AC for time T_{U_i} (Core protocol of Phase 2 between the users).

Step 3. The resulting AB subsystem after total time $T = T_{U_i}$ between users U_i and B_i contains entanglement $E^{(T_{U_i})}(U_i : B_i) = \sin^2(2(\frac{\pi}{4} + x_{U_i}))$.

The steps are detailed as follows. In the quantum transmission phase, the entanglement oscillation in AB is generated by the energy E of the Hamiltonian H [60]. This oscillation has a period of time T_π , which exactly equals to $4t$,

$$T_\pi = 4t, \quad (4.26)$$

where t is determined by Alice and Bob. In other words, time t identifies $\pi/4$, where π is the oscillation period. Therefore, in Protocol 1, the density σ_{ABC} of the final ABC state is as

$$\begin{aligned} \sigma_{ABC} &= |\varphi(t)\rangle\langle\varphi(t)|_{ABC} = U\rho_0U^\dagger \\ &= \frac{1}{2}\left(U_{AC}|\psi_+\rangle\langle\psi_+||+\rangle\langle+|U_{AC}^\dagger\right) + \frac{1}{2}\left(U_{AC}|\phi_+\rangle\langle\phi_+||-\rangle\langle-|U_{AC}^\dagger\right), \end{aligned} \quad (4.27)$$

where $|\varphi(t)\rangle_{ABC}$ at time t is evaluated as

$$\begin{aligned}
& |\varphi(t)\rangle_{ABC} \\
&= \frac{1}{\sqrt{2}} (\cos(t) (|\psi_+\rangle |+\rangle) - i \sin(t) (|\phi_+\rangle |+\rangle)) + \frac{1}{\sqrt{2}} (\cos(t) (|\phi_+\rangle |-\rangle) + i \sin(t) (|\psi_+\rangle |-\rangle)) \\
&= \frac{1}{\sqrt{2}} (\cos(t) (|\psi_+\rangle) - i \sin(t) (|\phi_+\rangle)) |+\rangle + \frac{1}{\sqrt{2}} (\cos(t) (|\phi_+\rangle) + i \sin(t) (|\psi_+\rangle)) |-\rangle
\end{aligned} \tag{4.28}$$

which at T_{U_i} (see (4.23)) of user U_i , for a given x_{U_i} is evaluated as

$$\begin{aligned}
& |\varphi(T_{U_i})\rangle_{ABC} \\
&= \frac{1}{\sqrt{2}} \left(\cos\left(\frac{\pi}{4} + x_{U_i}\right) (|\psi_+\rangle) - i \sin\left(\frac{\pi}{4} + x_{U_i}\right) (|\phi_+\rangle) \right) |+\rangle \\
&\quad + \frac{1}{\sqrt{2}} \left(\cos\left(\frac{\pi}{4} + x_{U_i}\right) (|\phi_+\rangle) + i \sin\left(\frac{\pi}{4} + x_{U_i}\right) (|\psi_+\rangle) \right) |-\rangle \\
&= \frac{1}{\sqrt{2}} \left(\begin{array}{l} \left(\frac{1}{\sqrt{2}} (\cos(x_{U_i})) - \frac{1}{\sqrt{2}} (\sin(x_{U_i})) \right) (|\psi_+\rangle) \\ -i \left(\frac{1}{\sqrt{2}} (\cos(x_{U_i})) + \frac{1}{\sqrt{2}} (\sin(x_{U_i})) \right) (|\phi_+\rangle) \end{array} \right) |+\rangle \\
&\quad + \frac{1}{\sqrt{2}} \left(\begin{array}{l} \left(\frac{1}{\sqrt{2}} (\cos(x_{U_i})) - \frac{1}{\sqrt{2}} (\sin(x_{U_i})) \right) (|\phi_+\rangle) \\ +i \left(\frac{1}{\sqrt{2}} (\cos(x_{U_i})) + \frac{1}{\sqrt{2}} (\sin(x_{U_i})) \right) (|\psi_+\rangle) \end{array} \right) |-\rangle,
\end{aligned} \tag{4.29}$$

where the sign change on $U_{AC} (|\phi_+\rangle |-\rangle)$ is due to the $|-\rangle$ eigenstate on C , and where

$$\begin{aligned}
& \frac{1}{\sqrt{2}} (\cos(x_{U_i})) - \frac{1}{\sqrt{2}} (\sin(x_{U_i})) (|\phi_+\rangle) + i \left(\frac{1}{\sqrt{2}} (\cos(x_{U_i})) + \frac{1}{\sqrt{2}} (\sin(x_{U_i})) \right) (|\psi_+\rangle) \\
&= i \left(\left(\frac{1}{\sqrt{2}} (\cos(x_{U_i})) + \frac{1}{\sqrt{2}} (\sin(x_{U_i})) \right) (|\psi_+\rangle) - i \left(\frac{1}{\sqrt{2}} (\cos(x_{U_i})) - \frac{1}{\sqrt{2}} (\sin(x_{U_i})) \right) (|\phi_+\rangle) \right).
\end{aligned} \tag{4.30}$$

Thus, up to the global phase, both states are the same.

Therefore, the $|\varphi(T_{U_i})\rangle_{ABC}$ system state of ABC at T_{U_i} is yielded as

$$|\varphi(T_{U_i})\rangle_{ABC} = \frac{1}{\sqrt{2}} |\xi(T_{U_i})\rangle_{AB} |+\rangle + \frac{1}{\sqrt{2}} |\xi(T_{U_i})\rangle_{AB} |-\rangle, \tag{4.31}$$

therefore, the resulting time AB state at $t = T_{U_i} = x_{U_i} + (\pi/4)$ and $x_{U_i} \neq 0$, $|\xi(T_{U_i})\rangle_{AB}$ is a non-maximally entangled system

$$\begin{aligned} |\xi(T_{U_i})\rangle_{AB} = & \frac{1}{\sqrt{2}}(\cos(x_{U_i})) + \frac{1}{\sqrt{2}}(\sin(x_{U_i}))(|\psi_+\rangle) \\ & -i\left(\frac{1}{\sqrt{2}}(\cos(x_{U_i})) - \frac{1}{\sqrt{2}}(\sin(x_{U_i}))\right)(|\phi_+\rangle), \end{aligned} \quad (4.32)$$

with entanglement between user U_i and B_i as

$$E^{(T_{U_i})}(U_i : B_i) = \sin^2\left(2\left(\frac{\pi}{4} + x_{U_i}\right)\right). \quad (4.33)$$

■

4.3.2 Differentiation in the Time Domain

Thesis 2.3 (Differentiation in the time domain) *The EAD service can be utilized to differentiate in the amount of time required for the establishment of the maximally entangled systems between the users of the quantum Internet.*

Proof. In the time domain differentiation service, a transmit user U_i generates the initial system ABC , transmits separable B to receiver B_i , and applies the local unitary U_{AC} on subsystem AC for time $T_{U_i}(\pi/4)$ (using the core protocol of Phase 2). Using the oscillation period $T_\pi(U_i : B_i)$ distributed in Phase 1, the resulting AB subsystem after total time

$$T = T_{U_i}(\pi/4) = T_\pi(U_i : B_i)/4 \quad (4.34)$$

between users U_i and B_i , $i = 1, \dots, K$ is a maximally entangled system, $E^{(T_\pi)}(U_i : B_i) = 1$, for all i .

The Phases 1 and 2 of the time domain differentiation method (Protocol 2) are as included in Protocol 2.

The steps of the protocol are as follows. Let us focus on a particular ABC of users U_i and B_i . The same results apply for all users of the network.

Protocol 2 Differentiation in time domain

Step 1. Let $U_i, i = 1, \dots, K$ be the set of transmit users, and $B_i, i = 1, \dots, K$ are the receiver users. Let $T_\pi(U_i : B_i)$ be the oscillation time selected for user pairs U_i and B_i , and let $T_{U_i}(\pi/4)$ be defined as

$$T_{U_i}\left(\frac{\pi}{4}\right) = \frac{T_\pi(U_i : B_i)}{4}. \quad (4.35)$$

For all i , distribute the oscillation period of time $T_\pi(U_i : B_i)$ information via an encoder unit \mathcal{E} between U_i and B_i (Phase 1).

Step 2. In the transmit user U_i , generate the initial system ABC , transmit separable B to receiver B_i , and apply the local unitary U_{AC} on subsystem AC for time $T_{U_i}(\pi/4)$ (Core protocol of Phase 2 between the users).

Step 3. The resulting AB subsystem after total time $T = T_{U_i}(\pi/4) = T_\pi(U_i : B_i)/4$ between users U_i and B_i is a maximally entangled system, $E^{(T_\pi)}(U_i : B_i) = 1$, for all i .

After the steps of Protocol 2, the density σ_{ABC} of the final ABC state is as

$$\begin{aligned} \sigma_{ABC} &= |\varphi(t)\rangle\langle\varphi(t)|_{ABC} = U\rho_0U^\dagger \\ &= \frac{1}{2}\left(U_{AC}|\psi_+\rangle\langle\psi_+||+\rangle\langle+|U_{AC}^\dagger\right) + \frac{1}{2}\left(U_{AC}|\phi_+\rangle\langle\phi_+||-\rangle\langle-|U_{AC}^\dagger\right), \end{aligned} \quad (4.36)$$

where $|\varphi(t)\rangle_{ABC}$ at t is evaluated as

$$\begin{aligned} &|\varphi(t)\rangle_{ABC} \\ &= \frac{1}{\sqrt{2}}(U_{AC}(|\psi_+\rangle|+\rangle) + U_{AC}(|\phi_+\rangle|-\rangle)) \\ &= \frac{1}{\sqrt{2}}(\cos(t)\left(\frac{1}{2}(|010\rangle + |011\rangle + |100\rangle + |101\rangle)\right) + \cos(t)\left(\frac{1}{2}(|000\rangle - |001\rangle + |110\rangle - |111\rangle)\right) \\ &\quad - i\sin(t)\left(\frac{1}{2}(|111\rangle + |110\rangle + |001\rangle + |000\rangle)\right) + i\sin(t)\left(\frac{1}{2}(|101\rangle - |100\rangle + |011\rangle - |010\rangle)\right)) \\ &= \frac{1}{\sqrt{2}}(\cos(t)(|\psi_+\rangle|+\rangle + |\phi_+\rangle|-\rangle) - i\sin(t)(|\phi_+\rangle|+\rangle - |\psi_+\rangle|-\rangle)) \\ &= \frac{1}{\sqrt{2}}(((\cos(t)(|\psi_+\rangle) - i\sin(t)(|\phi_+\rangle))|+\rangle + (\cos(t)(|\phi_+\rangle) + i\sin(t)(|\psi_+\rangle))|-\rangle)), \end{aligned} \quad (4.37)$$

where the sign change on $U_{AC}(|\phi_+\rangle|-\rangle)$ is due to the $|-\rangle$ eigenstate on C .

Thus, at $t = \pi/4 = T_{U_i}(\pi/4)$, the system state is

$$\begin{aligned}
& |\varphi(T_{U_i}(\pi/4))\rangle_{ABC} \\
&= \frac{1}{\sqrt{2}} (\cos(\pi/4) (|\psi_+\rangle|+\rangle + |\phi_+\rangle|-\rangle) - i \sin(\pi/4) (|\phi_+\rangle|+\rangle - |\psi_+\rangle|-\rangle)) \\
&= \frac{1}{\sqrt{2}} \left(\frac{1}{\sqrt{2}} (|\psi_+\rangle|+\rangle + |\phi_+\rangle|-\rangle) - i \frac{1}{\sqrt{2}} (|\phi_+\rangle|+\rangle - |\psi_+\rangle|-\rangle) \right) \\
&= \frac{1}{\sqrt{2}} \left(\begin{array}{l} \left(\frac{1}{\sqrt{2}} (|\psi_+\rangle) - i \frac{1}{\sqrt{2}} (|\phi_+\rangle) \right) |+\rangle \\ + \left(\frac{1}{\sqrt{2}} (|\phi_+\rangle) + i \frac{1}{\sqrt{2}} (|\psi_+\rangle) \right) |-\rangle \end{array} \right),
\end{aligned} \tag{4.38}$$

where

$$\frac{1}{\sqrt{2}} (|\phi_+\rangle + i|\psi_+\rangle) = i \left(\frac{1}{\sqrt{2}} (|\psi_+\rangle - i|\phi_+\rangle) \right); \tag{4.39}$$

Thus, up to the global phase both states are the same yielding relative entropy of entanglement between users U_i and B_i as

$$E^{(T_\pi)}(U_i : B_i) = 1 \tag{4.40}$$

with unit probability. ■

4.3.3 Comparative Analysis

The results of the proposed differentiation methods, Protocols 1 and 2, are compared in Fig. 4-2. Fig. 4-2(a) illustrates the results of a differentiation in the entanglement quantity, while Fig. 4-2(b) depicts the results of the time-domain differentiation method.

4.4 Conclusions

Entanglement differentiation is an important problem in quantum networks where the legal users have different priorities or where differentiation is a necessity for an arbitrary

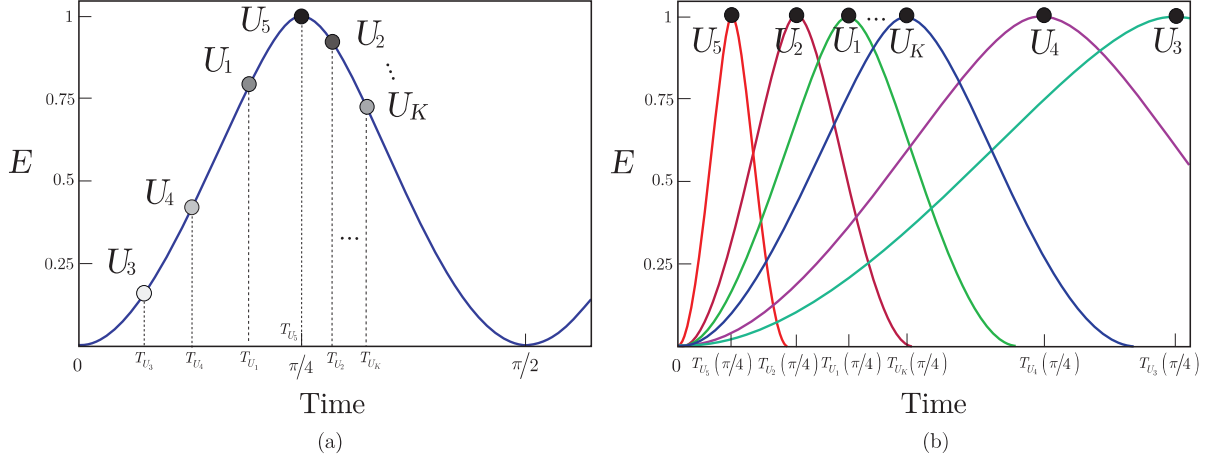


Figure 4-2: Entanglement differentiation service via Hamiltonian dynamics in a multi-user environment. (a) Protocol 1. Each user gives a different amount of entanglement $E(U_i : B_i) \leq 1$ at a global period of time T_π . The differentiation is made in the amount of entanglement (relative entropy of entanglement) by applying the local unitaries for time T_{U_i} for $U_i, i = 1, \dots, K$. User U_5 has the highest priority thus the user gets a maximally entangled system, user U_3 is the lowest priority user and associated with a low amount of entanglement. (b) Protocol 2. All users are assigned with a maximally entangled system, $E(U_i : B_i) = 1$, and the differentiation is made in the time domain. For users $U_i, B_i, i = 1, \dots, K$ a particular period of time $T_\pi(U_i : B_i)$ is assigned, and each local unitary is applied for $T_{U_i}(\pi/4) = T_\pi(U_i : B_i)/4$ time to achieve maximally entangled states between the parties. User U_5 has the highest priority thus the user associated with the shortest time period, user U_3 is the lowest priority user with a long time period for the generation of a maximally entangled system.

reason. In this chapter, we defined the EAD service for the availability of entanglement in quantum Internet. In EAD, the differentiation is either made in the amount of entanglement associated with a legal user or in the amount of time that is required to establish a maximally entangled system. The EAD method requires a classical phase for the distribution of timing information between the users. The entanglement establishment is based on Hamiltonian dynamics, which allows the efficient implementation of the entanglement differentiation methods via local unitary operations. The method requires no entanglement transmission between the parties, and the application time of the unitaries can be selected as arbitrarily small via the determination of the oscillation periods to

achieve an efficient practical realization. The EAD method is particularly convenient for practical quantum networking scenarios, quantum communication networks, and future quantum Internet.

Chapter 5

Multilayer Optimization Service for the Quantum Internet

This chapter defines a multilayer optimization method for the quantum Internet. Multilayer optimization integrates separate procedures for the optimization of the quantum layer and the classical layer of the quantum Internet. The multilayer optimization procedure defines advanced techniques for the optimization of the layers. The optimization of the quantum layer covers the minimization of total usage time of quantum memories in the quantum nodes, the maximization of the entanglement throughput over the entangled connections, and the reduction of the number of entangled connections between the arbitrary source and target quantum nodes. The objective of the optimization of the classical layer is the cost minimization of any auxiliary classical communications. The multilayer optimization framework provides a practically implementable tool for quantum network communications, or long-distance quantum communications.

5.1 Introduction

Quantum Internet is a communication network with quantum nodes and quantum links [8–11, 35, 36, 39, 49, 55, 74, 91, 118, 121] that allows to the parties to perform efficient

quantum communications [62, 92, 93]. The aim of quantum Internet [55, 74] and quantum repeater networks [2, 62, 89, 92, 93, 118, 124, 125] is to distribute quantum entanglement between distant nodes through a chain of intermediate quantum repeater nodes [4, 13, 28, 59, 70, 72, 73, 107, 110, 130]. In the quantum Internet, the quantum nodes share entangled connections that formulate entangled connections [36, 39, 49, 74, 91, 118]. The quantum nodes store the quantum states in their local quantum memory for path selection and path recovery purposes [4, 13, 28, 39, 55, 59, 70, 72, 73, 91, 107, 110, 118, 130]. Since several attributes must be optimized in parallel in an arbitrary quantum network, the optimization problem formulates a multi-objective procedure. Formally, multi-objective optimization covers the minimization of quantum memory usage time (storage time), the maximization of entanglement throughput (number of transmitted entangled states per second of a particular fidelity) of entangled connections [36, 39, 49, 74, 91, 118], and the reduction of the number of entangled connections between a source and a target quantum node [4, 13, 28, 55, 59, 70, 72, 73, 107, 110, 130]. However, the problem does not end here since a quantum repeater network can be approached on the quantum transmission (quantum layer) level and on the auxiliary classical communication (classical layer) level that is required for the dynamic functioning of the quantum layer. Therefore, the problem is not just a multi-objective optimization problem in the quantum layer but also a multilayer optimization issue that covers the development of both the quantum and classical layers of a quantum repeater network.

In this chapter, we define a multilayer optimization method for quantum repeater networks. This covers both the quantum layer and the classical layer of a quantum repeater network. By utilizing the tools of quantum Shannon theory [35, 36, 39, 49, 74, 91, 118], the optimization of the quantum layer includes minimizing the usage of quantum memories in the nodes to reduce the storage time of entangled states, the maximization of entanglement throughput of the entangled connections, and also these conditions have to be satisfied for the shortest path between a given source node and target quantum node (i.e., a multi-objective optimization of the quantum layer). The aim of classical layer optimiza-

tion is to curtail the cost of auxiliary classical communications, which is required for such optimization. The cost of the classical communication covers all communication costs required to achieve the optimal quantum network state including the classical communication steps for overall quantum storage time minimization, entanglement throughput maximization, and the selection of a shortest path.

The multilayer optimization employs advanced methods to solve the multi-objective optimization of the quantum layer. We define the structures of the quantum memory utilization graph and the entanglement throughput tree for the multi-objective optimization of the quantum layer of a quantum repeater network. The quantum memory utilization graph models the quantum memory usage for entanglement storage. The entanglement throughput tree shows the entanglement throughput of entangled connections with respect to the number of transmittable entangled states at a particular fidelity. Using these advanced constructions, we also define a method for the optimal assignment of entangled states in the repeater nodes. The input of the quantum layer optimization procedure is the quantum memory utilization graph, while the output of the method is a set of entanglement throughput trees. The output identifies the optimal states of the quantum network with respect to the multi-objective optimization function.

Classical layer optimization focuses on the minimization of the total cost of classical communications by utilizing swarm intelligence [18, 25, 78, 81, 101]. This also defines a multi-objective problem since the cost has to be reduced with respect to the classical communication cost required for the minimization of quantum memory usage, the classical cost of entanglement throughput maximization of entangled connections, and for the selection of the shortest path in the quantum layer. Classical layer optimization uses some fundamentals of bacteria foraging models [66, 68, 78, 81, 84, 98, 132] and probabilistic multi-objective uncertainty characterization [51, 68, 78, 90, 98, 126].

The optimization framework requires no changes in the physical layer, so the framework is directly implementable by the current physical devices [36, 39, 49, 62, 74, 91–93, 118] and quantum networking elements [4, 13, 28, 55, 59, 70, 72, 73, 107, 110, 130]. The method

is useful in quantum networking environments with diverse physical attributes (different quantum memory characteristics, quantum error correction, physical quantum nodes attributes, and transmission capabilities of noisy quantum links).

5.1.1 Results

The novel contributions of the chapter are as follows:

1. *We conceive a complex optimization framework for the quantum Internet. It integrates the development of the quantum and classical layers of the quantum Internet.*
2. *Quantum layer optimization utilizes the attributes of physical layer quantum transmissions, quantum memory usage, and entanglement distribution via the framework of quantum Shannon theory.*
3. *Classical layer optimization focuses on minimizing any auxiliary communications related to the quantum layer and optimization.*
4. *Multilayer optimization is applicable by current physical devices and quantum networking elements providing a solution for the optimization of arbitrary quantum networking scenarios with diverse physical attributes and environments.*

This chapter is organized as follows. In Section 5.2, the system model is proposed. In Section 5.3, the optimization procedure of the quantum layer of quantum repeater networks is defined. Section 5.4 studies the optimization of the classical layer. Section 5.5 provides a performance evaluation. Finally, Section 5.6 concludes the chapter. Supplemental information is included in Appendix D.

5.2 System Model

Our model assumes that the quantum repeater network consists of a source and target node with intermediate repeater nodes and a quantum switcher node. A quantum

switcher node S operates as follows. Node S is a quantum repeater node capable of switching between the entangled connections stored in its local quantum memory and a permit of applying entanglement swapping on the selected connections. While an i -th quantum repeater node establishes only the entangled connections with the neighbor quantum repeater nodes, a switcher node is equipped with an extended knowledge about the quantum network to select between the entangled connections. A general repeater node is not allowed to perform any link selection, since it is assumed in the model that a quantum repeater node has only local knowledge about the network. A switcher node based on its network knowledge can also send entanglement swapping commands to the quantum repeater nodes to define new paths in the network.

Let N be a quantum network, $N = (V, \mathcal{S})$, where V is a set of nodes, \mathcal{S} is a set of entangled connections. Without loss of generality, the level L_l of an entangled connection $E(x, y)$ is defined as follows. For an L_l -level entangled connection, the hop distance between quantum nodes x and y is [33, 118]

$$d(x, y)_{L_l} = 2^{l-1}, \quad (5.1)$$

with $d(x, y)_{L_l} - 1$ intermediate nodes between the nodes x and y . The probability that an L_l -level entangled connection $E(x, y)$ exists between nodes x, y is $\Pr_{L_l}(E(x, y))$, which depends on the actual network.

The S quantum switcher is modeled as a quantum node with the following attributes and permissions:

- *knowledge about the physical attributes of distant quantum repeater nodes and the entangled connections of N (e.g., entanglement fidelity, quantum memory status, link noise, etc),*
- *internal quantum memory for the storage of entangled states,*
- *quantum functionality:*

- *permission to set new entangled connections between its local quantum system and a selected quantum node of the quantum network,*
- *permission to switch between the stored entangled states to construct new paths,*
- *classical functionality:*
 - *permission to command distant quantum nodes of N via classical links (to construct new entangled connections in the network, to perform entanglement swapping between the selected nodes, other).*

The network model is illustrated in Fig. 5-1. The example network in Fig. 5-1(a) consists of six quantum repeater nodes R_i , $i = 1, \dots, 6$, and a quantum switcher S that switches between the entangled connections using its local quantum memory. The switcher also can perform entanglement swapping in the network. The switcher node S has knowledge about the physical attributes (e.g., entanglement fidelity, quantum memory status, etc) of quantum repeater nodes to make a decision on a path. The knowledge about the repeater nodes can be transmitted over a classical link to the quantum switcher (classical links are not depicted). As it is depicted in Fig. 5-1(b), the switcher node has a permission to set new entangled connections via its local quantum state with a selected quantum node. The S switcher node decided to set a new entangled connection between its local quantum system and repeater node R_2 . A standard quantum repeater is not allowed to perform these operations (except with the direct neighbors in the entanglement distribution phase) without a dedicated command from the switcher.

Note, path \mathcal{P}_1 in Fig. 5-1(a) provides a shortest path at a particular network situation at an initial network time T_1 . Since the quantum network N evolves in time (quality of the entangled connections, the status of the nodes, internal quantum memories, etc), at a given time T_2 , by utilizing the functions of the switcher node, the switcher node determined a new shortest path, \mathcal{P}_2 , as depicted in Fig. 5-1(b).

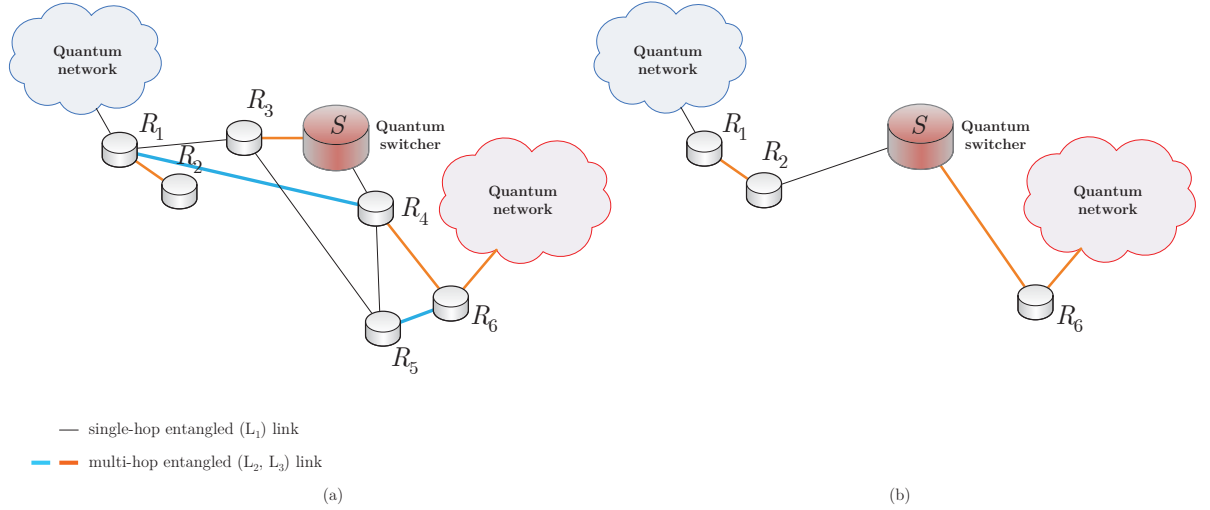


Figure 5-1: The network model with a quantum switcher S and quantum repeater nodes R_i , $i = 1, \dots, 6$. The L_1 , L_2 - and L_3 -level entangled connections of N are depicted by gray, blue and orange, respectively (additional nodes are not shown). (a) For a current shortest path $\mathcal{P}_1 = \{R_1, R_3, S, R_4, R_6\}$, the active repeater nodes selected by S are R_3 and R_4 . (b) Node S switches the entangled connections in the local quantum memory from R_3 to R_2 and from R_4 to R_6 . The switching operation defines a new shortest path $\mathcal{P}_2 = \{R_1, R_2, S, R_6\}$.

5.2.1 Quantum Memory Scheduling

In this section, we define a structure for scheduling quantum memory usage of the quantum nodes called the quantum memory utilization graph \mathcal{G}_m . This is a directed graph mapped from the network model, with several abstracted nodes and links.

Proposition 3.1 *The \mathcal{G}_m quantum memory utilization graph is a directed graph with abstract nodes and links to schedule the quantum memory usage mapped from the quantum repeater network.*

The \mathcal{G}_m graph of quantum memory utilization is constructed as follows. Assuming n quantum nodes (excluding the S switcher node) in the network, the graph contains n abstracted transmitter nodes and n abstracted receiver nodes with directed connections. Note if the quantum switcher S is modeled as the n -th node and $n_S = 1$, where n_S is the number of quantum switchers in N , the \mathcal{G}_m graph also can be constructed via

$(n - 1)$ transmitter and $(n - 1)$ receiver quantum nodes. A given N with an arbitrary number of quantum switcher nodes defines a particular \mathcal{G}_m , therefore the \mathcal{G}_m graph is a combination of all other possible switcher modes. The \mathcal{G}_m graph contains directed edges between quantum node pairs $(V_x|V_y)$ and $(V_y|V_z)$ of a particular switcher mode S_i , $i = 1, \dots, N_S$, where N_S is the total number of switcher modes, depicted via nodes labeled as $(x|y)$ and $(y|z)$.

Let us assume that N has a single switcher node S , and it has two states, S_1 and S_2 . In both modes S_1 and S_2 , repeater node R_1 serves as a transmitter node for node R_2 .

In switcher mode S_1 , the shared entangled connection defines the following relations. Repeater node R_1 serves as a transmitter node for nodes R_3 and R_4 . Node R_3 serves as a transmitter node for nodes R_4 and R_5 . Node R_4 serves as a transmitter node for nodes R_5 and R_6 . Node R_5 serves as a transmitter node for node R_6 .

In switcher mode S_2 , the shared entangled connection defines the following relation. Repeater node R_2 serves as a transmitter node for node R_6 .

The \mathcal{G}_m graph of quantum memory utilization derived from the quantum network setting of Fig. 5-1. is illustrated in Fig. 5-2.

5.2.2 Entanglement Throughput Tree

In this section, we define the structure of the entanglement throughput tree, which aims to extract information from the quantum memory utilization graph. The entanglement throughput tree is also the output format of the multi-objective optimization procedure of the quantum layer.

Thesis 3.1 (Entanglement throughput tree) *The \mathcal{G}_{et} entanglement throughput tree is a structure modeling the multi-objective optimization problem of the quantum Internet. The tree structure is derived from the \mathcal{G}_m quantum memory utilization graph.*

Proof. As a given source node is selected, the next nodes are added to the path with a given probability.

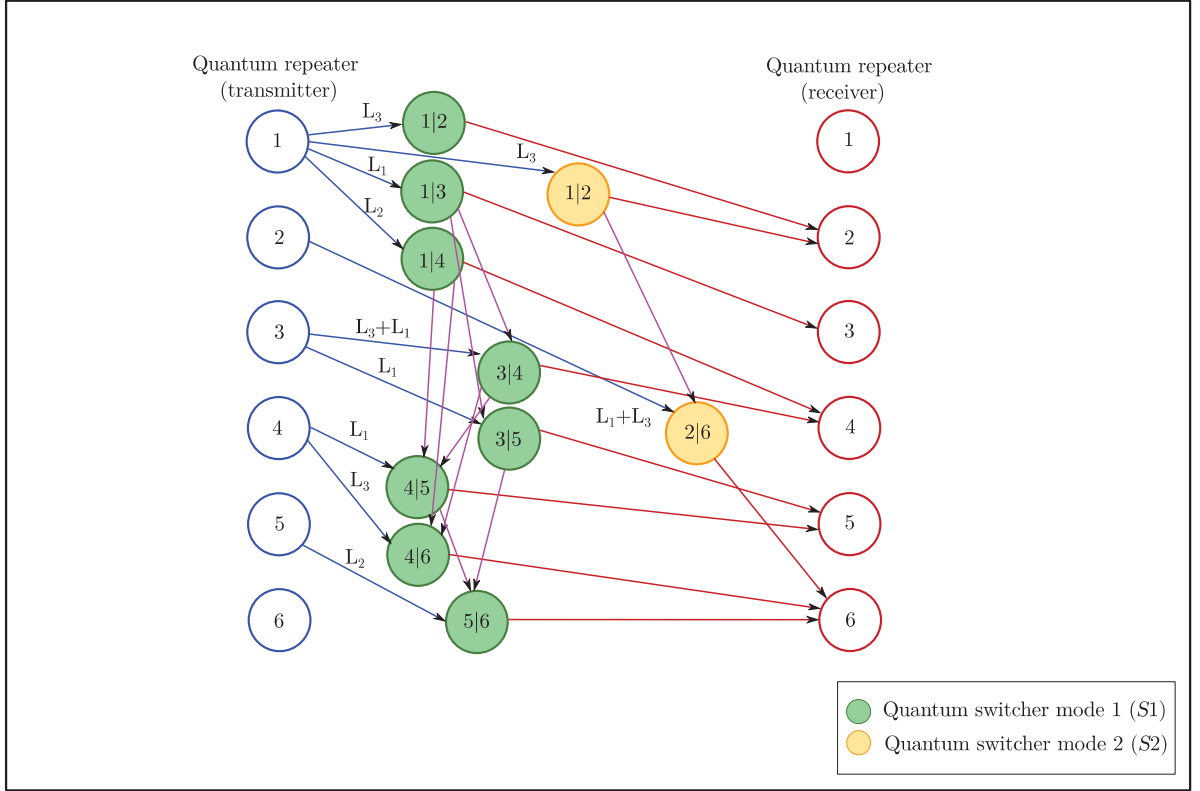


Figure 5-2: The \mathcal{G}_m graph of quantum memory utilization derived from the network setting in Fig. 1. The graph contains n abstracted transmitter nodes and n abstracted receiver nodes with directed entangled connections. An i -level entangled connect is depicted by L_i . The S quantum switcher has two states, S_1 and S_2 . The green circles represent quantum nodes operating on switcher mode S_1 . The yellow circles represent nodes operating on switcher mode S_2 .

Let us assume that \mathcal{G}_m is determined. Let us index the nodes by an ID identifier tag, $ID = \{A, B, \dots\}$, and let S_I be the set of unvisited neighbor nodes of a node I .

Let $B_F(E_{L_i}(I, J))$ refer to the entanglement throughput of a given L_i -level entangled connection $E_{L_i}(I, J)$ between nodes (I, J) measured in the number entangled states per second at a particular fidelity F [36, 91, 118].

Further, let J be a neighbor node of I with entangled connection $E_{L_i}(I, J)$ and with entanglement throughput $B_F(E_{L_i}(I, J))$.

A cost function, $\Omega(I, J)$, between nodes (I, J) is defined as

$$\Omega(I, J) = \frac{1}{C(E_{L_l}(I, J)) + \zeta_J}, \quad (5.2)$$

where $C(E_{L_l}(I, J))$ is the cost of entangled connection $E_{L_l}(I, J)$ defined as

$$C(E_{L_l}(I, J)) = \frac{1}{B_F(E_{L_l}(I, J))}, \quad (5.3)$$

while ζ_J is the cost of quantum storage in node J .

Let $\lambda_{E_{L_l}(I, J)}$ be the entanglement utility coefficient of entangled connection $E_{L_l}(I, J)$ between nodes I and J , initialized as $\lambda_{E_{L_l}(I, J)} \geq 0$. This amount is equivalent to the utility of the entangled connection $E_{L_l}(I, J)$ that it has taken to arrive at the current node J from I .

At a given $B_F(E_{L_l}(I, J))$, the initial $\lambda_{E_{L_l}(I, J)}$ entanglement utility [36] of link $E_{L_l}(I, J)$ is updated to $\lambda'_{E_{L_l}(I, J)}$ as

$$\begin{aligned} \lambda'_{E_{L_l}(I, J)} &= \left(\frac{1}{\lambda_{E_{L_l}(I, J)}} + B_F(E_{L_l}(I, J)) \right)^{-1} \\ &= \frac{\lambda_{E_{L_l}(I, J)}}{1 + B_F(E_{L_l}(I, J)) \lambda_{E_{L_l}(I, J)}}. \end{aligned} \quad (5.4)$$

Using these cost functions, the $\Pr(I, J)$ probability that from node I a node J is selected is as follows:

$$\Pr(I, J) = \begin{cases} \frac{\left(\lambda'_{E_{L_l}(I, J)}\right)^{\omega^*} (\Omega(I, J))^\delta}{\sum_{\forall X \in S_I} \left(\lambda'_{E_{L_l}(I, X)}\right)^{\omega^*} (\Omega(I, X))^\delta}, & \text{if } J \in S_I \\ 0, & \text{otherwise} \end{cases}, \quad (5.5)$$

where ω^* and δ are weighting coefficients [36].

Using (5.2), (5.3), and (5.5) for all node pairs, the \mathcal{M} method to build a random \mathcal{G}_{et} entanglement throughput tree using a \mathcal{G}_m graph is as follows [51, 90].

Let S' refer to the set of already reached destination nodes, and let \mathcal{I} be the set of initial nodes, \mathcal{F}_I the set of feasible neighboring nodes to node I . Let \mathcal{D} be the set of destination nodes.

The method is given in Procedure 1.

Procedure 1 Random entanglement throughput tree construction

Step 1. Initialize $\mathcal{G}_{et} = \emptyset$, $S' = \emptyset$. Select a node I of set \mathcal{I} and determine \mathcal{F}_I .

Step 2. If $\mathcal{F}_I = \emptyset$, then remove node I from \mathcal{I} , as $\mathcal{I} = \mathcal{I} - I$, otherwise compute probability $\Pr(I, J)$ via (5.5) for each node J of \mathcal{F}_I .

Step 3. Define uniformly distributed variable $x \in (0, 1]$. If $x > 0.5$, select that node J from \mathcal{F}_I that has large $\Pr(I, J)$. If $x \leq 0.5$, choose J randomly.

Step 4. Update sets \mathcal{G}_{et} and \mathcal{I} as $\mathcal{G}_{et} = \mathcal{G}_{et} \cup (I, J)$, $\mathcal{I} = \mathcal{I} \cup J$. If node J is a destination node, $J \in \mathcal{D}$, then update set S' as $S' = S' \cup J$.

Step 5. Update $\lambda'_{E_{L_i}(I,J)}$ as $\lambda'_{E_{L_i}(I,J)} = (1 - \varphi) \lambda'_{E_{L_i}(I,J)} + \varphi \lambda_{E_{L_i}(I,J)}$, where φ is an evolution parameter, $\varphi \in [0, 1]$, and $\lambda_{E_{L_i}(I,J)}$ is the initial value of entanglement utility. Merge nodes of \mathcal{G}_{et} that duplicate entangled connections, and check the reachability of the nodes of \mathcal{D} .

Step 6. Repeat steps 2–5 until $\mathcal{I} \neq \emptyset$ or $S' \neq \emptyset$. Remove unused entangled connections from \mathcal{G}_{et} and output \mathcal{G}_{et} .

The proof is concluded here. ■

The structure of a \mathcal{G}_{et} entanglement throughput tree is illustrated in Fig. 5-3.

5.2.3 Entanglement Assignment Cycle

In this section, we propose a solution for an optimal assignment (scheduling) of stored entanglement called the entanglement assignment cycle, $\alpha_{\mathcal{G}_{et}}$. The goal of $\alpha_{\mathcal{G}_{et}}$ is to achieve a minimal overall storage time $t_s^*(\mathcal{G}_{et})$ at a given \mathcal{G}_{et} entanglement throughput tree.

Lemma 3.1 *An entanglement assignment cycle can be determined by a weighted graph coloring method.*

Proof. To determine the minimal overall storage time for a \mathcal{G}_{et} entanglement throughput tree, the $\mathcal{C}_{\mathcal{G}_{et}}$ conflict graph of that \mathcal{G}_{et} is constructed first. In the $\mathcal{C}_{\mathcal{G}_{et}}$ graph, each

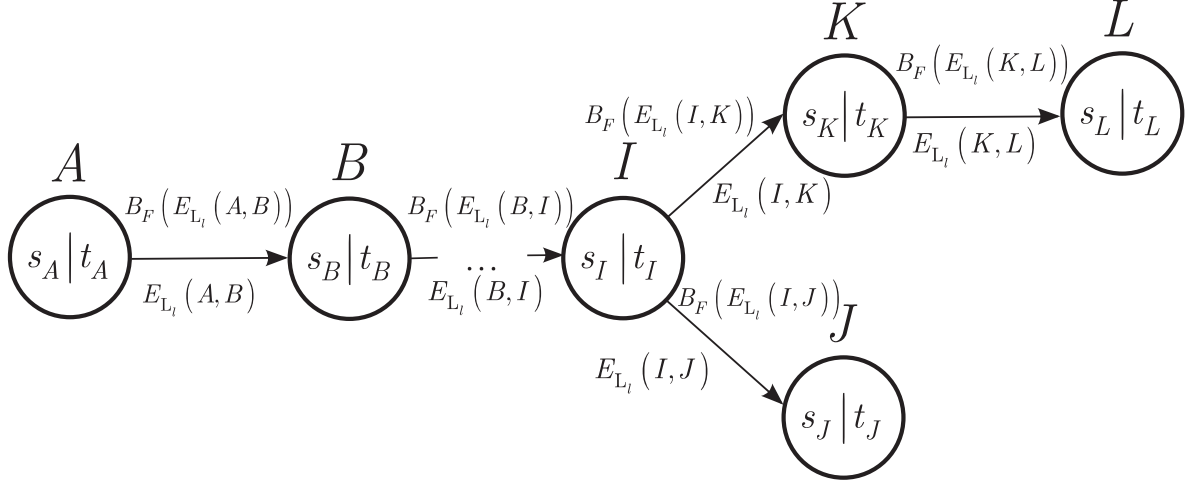


Figure 5-3: The structure of a \mathcal{G}_{et} entanglement throughput tree. A quantum node has an ID identifier tag, $ID = \{A, B, \dots, L\}$, and all incoming and outgoing entangled connections are identified by the s_{ID} source neighbor node and the t_{ID} target neighbor node. Node A represents a source, while the destination nodes are J, K, L . The $B_F(E_{L_i}(x, y))$ entanglement throughput of all (x, y) node pairs are depicted above the directed lines; the link identifier $E_{L_i}(x, y)$ is depicted under the links.

vertex corresponds to a directed link of \mathcal{G}_{et} (an entangled connection). An edge exists between two vertices of $\mathcal{C}_{\mathcal{G}_{et}}$, if only the vertices (entangled connections) have a conflict. A conflict occurs if two (stored) entangled connects are associated to the same physical link. The problem is therefore to associate each link of \mathcal{G}_{et} a $\alpha_{\mathcal{G}_{et}}$ storage schedule (optimal assignment of stored entanglement), which includes the list of time slots when a given link can transmit the stored entangled states such that $\alpha_{\mathcal{G}_{et}}$ total number of time units is minimized. Therefore, our goal is to determine what entangled connects of the given \mathcal{G}_{et} should be scheduled in which time unit, such that the total storage time is minimal in $\alpha_{\mathcal{G}_{et}}$.

Let $\tau_{n,t} \in \{0, 1\}$ be an indicator variable, defined as

$$\tau_{n,t} = \begin{cases} 1, & \text{if } n \text{ is associated at } t \\ 0, & \text{otherwise.} \end{cases} \quad (5.6)$$

For a periodic scheduling,

$$\tau_{n,t} = \tau_{n,t+iT}, \quad (5.7)$$

where T is a period and i is a constant.

For an entangled connection n , let us define $\wedge(n)$ as the set of entangled connects n' that are scheduled in the same time unit t , but the physical link can transmit only n or n' . As follows, for any $n' \in \wedge(n)$,

$$\tau_{n,t} + \tau_{n',t} \leq 1. \quad (5.8)$$

As it can be concluded, this problem is analogous to the coloring of the conflict graph $\mathcal{C}_{\mathcal{G}_{et}}$.

Then, let us assume that each entangled connection (entangled connection) has a weight $w(n)$, which is defined as

$$w(n) = \begin{cases} 1, & \text{if } F_i = F_{max} \\ \left\lceil \frac{F_{max}}{F_i} \right\rceil, & \text{if } F_i < F_{max} \end{cases}, \quad (5.9)$$

where F_i is the fidelity of entangled connection i and F_{max} is the largest fidelity available. As follows, for a lower-fidelity entangled connection, the transmission of a given amount of information requires more time units.

As the weights are determined, the problem is analogous to a weighted graph coloring of the conflict graph $\mathcal{C}_{\mathcal{G}_{et}}$, which is the assignment of at least $w(n)$ distinct colors to each entangled connection n such that no two entangled connections sharing the same color interfere with each other on the physical link. For this purpose, a simple distributed weighted coloring algorithm [126] can be straightforwardly applied.

The method for the $\mathcal{W}(\mathcal{C}_{\mathcal{G}_{et}})$ weighted coloring of conflict graph $\mathcal{C}_{\mathcal{G}_{et}}$ is summarized in Procedure 2.

After an entanglement assignment cycle has been determined by the weighted graph coloring method, in the next step the $\Delta(\mathcal{W}(\mathcal{C}_{\mathcal{G}_{et}}))$ time intervals between each time unit

Procedure 2 Weighted coloring of a conflict graph

Step 1. Determine conflict graph $\mathcal{C}_{\mathcal{G}_{et}}$ of \mathcal{G}_{et} , and compute weights $w(n)$ for all n . Assign weight $w(n)$ to vertex $n \in \mathcal{C}_{\mathcal{G}_{et}}$.

Step 2. Construct a new conflict graph $\mathcal{C}'_{\mathcal{G}_{et}}$ from $\mathcal{C}_{\mathcal{G}_{et}}$: for each vertex n with weight $w(n)$, create $w(n)$ vertices, $\{n_1, \dots, n_{w(n)}\}$, and add to $\mathcal{C}'_{\mathcal{G}_{et}}$.

Step 3. Add to $\mathcal{C}'_{\mathcal{G}_{et}}$ the edges connecting n_a and n_b , where $1 \leq a < b \leq w(n)$.

Step 4. Add to $\mathcal{C}'_{\mathcal{G}_{et}}$ the edge between i_a and j_b only if there is an edge between entangled connects i and j in $\mathcal{C}_{\mathcal{G}_{et}}$. Apply the unweighted vertex coloring algorithm [126] on $\mathcal{C}'_{\mathcal{G}_{et}}$.

Step 5. Assign n all the colors that are used by n_k , for $1 \leq k \leq w(n)$ in graph $\mathcal{C}'_{\mathcal{G}_{et}}$.

Step 6. Output the $\mathcal{W}(\mathcal{C}_{\mathcal{G}_{et}})$ weighted coloring of conflict graph $\mathcal{C}_{\mathcal{G}_{et}}$.

of a given cycle is computed. For this purpose, a linear programming method [51] can be applied. ■

5.3 Quantum Layer Optimization

In this section, we define the multi-objective optimization for the quantum layer. The multi-objective function covers a parallel optimization of quantum memory usage and entanglement throughput for a shortest path.

Thesis 3.2 (Quantum layer optimization) *At a given \mathcal{G}_m , the quantum layer of an entangled quantum network N can be optimized by a procedure \mathcal{P}_Q that achieves a parallel minimization of the quantum memory usage time t_s , the maximization of entanglement throughput B_F , and the minimization of the number $|\mathcal{P}|$ of entangled connections between two arbitrary quantum nodes.*

Proof. The aim of the procedure is to find an optimal entanglement throughput tree \mathcal{G}_{et}^* for which the $t_s(\mathcal{G}_{et}^*)$ overall storage time is minimal, that is,

$$t_s(\mathcal{G}_{et}^*) = t_s^*(\mathcal{G}_{et}^*); \quad (5.10)$$

the $B_F(\mathcal{G}_{et}^*)$ entanglement throughput for all links is maximal,

$$B_F(\mathcal{G}_{et}^*) = B_F^*(\mathcal{G}_{et}^*); \quad (5.11)$$

and the $|\mathcal{P}(\mathcal{G}_{et}^*)|$ number of entangled connections of a path is minimal, thus

$$|\mathcal{P}(\mathcal{G}_{et}^*)| = |\mathcal{P}^*(\mathcal{G}_{et}^*)|, \quad (5.12)$$

where \mathcal{P}^* is the shortest path.

The procedure is based on the fact that for a given \mathcal{G}_{et}^* with conflict graph $\mathcal{C}_{\mathcal{G}_{et}^*}$, from the knowledge of $\mathcal{W}(\mathcal{C}_{\mathcal{G}_{et}^*})$ weighted coloring of conflict graph $\mathcal{C}_{\mathcal{G}_{et}^*}$, $\Delta(\mathcal{W}(\mathcal{C}_{\mathcal{G}_{et}^*}))$ time intervals between each time unit of a given cycle, the required objective values of (5.10), (5.11), and (5.12) can be determined.

Let $\mathcal{S}_{\mathcal{G}_{et}^*}$ be the set of optimal \mathcal{G}_{et}^* entanglement throughput trees. Then the aim of the procedure is to determine $\mathcal{S}_{\mathcal{G}_{et}^*}$.

The problem can be rewritten via a solution set X with decision variables [51]

$$X = \{x_1, \dots, x_n\}, \quad (5.13)$$

where n is the number of all links in a given quantum memory utilization graph \mathcal{G}_m , and $x_i \in \{0, 1\}$ is defined as

$$x_i = \begin{cases} 1, & \text{if link } i \text{ of } \mathcal{G}_m \text{ is selected by } \mathcal{M} \\ 0, & \text{otherwise.} \end{cases} \quad (5.14)$$

Let $X_{\mathcal{G}_{et},i}$ be a solution i from solution set $X_{\mathcal{G}_{et}}$. Let $X_{\mathcal{G}_{et},j} \angle X_{\mathcal{G}_{et},i}$ refer to solution $X_{\mathcal{G}_{et},i}$ dominating solution $X_{\mathcal{G}_{et},j}$, which is

$$\begin{aligned} X_{\mathcal{G}_{et},j} \angle X_{\mathcal{G}_{et},i} : \{ & t_s^*(\mathcal{G}_{et}, i) \leq t_s^*(\mathcal{G}_{et}, j), \\ & B_F^*(\mathcal{G}_{et}, i) \geq B_F^*(\mathcal{G}_{et}, j), \\ & |\mathcal{P}^*(\mathcal{G}_{et}, i)| \leq |\mathcal{P}^*(\mathcal{G}_{et}, j)| \}, \end{aligned} \quad (5.15)$$

and for these relations, there is at least strict inequality [51]. If $X_{\mathcal{G}_{et},i}$ dominates all other possible solutions, then $X_{\mathcal{G}_{et},i}$ is a set of nondominated solutions.

For each set X , let κ refer to the set that contains the best nondominated solutions that have been found at a particular iteration. If κ changes, then the entanglement utilities of the links are updated. If κ is stationary, then the elements of set κ are used to update the entanglement utilities. The former serves as an improvement in the exploration process whereas the latter aims to yield more information via the best solutions [51].

At a given graph \mathcal{G}_m of quantum memory utilization, the procedure \mathcal{P}_Q for the optimization of the quantum layer is defined as follows. The output of \mathcal{P}_Q is an optimal set $\mathcal{S}_{\mathcal{G}_{et}}^*$ of entanglement throughput trees that realize the conditions of the multi-objective optimization function. The steps of the quantum layer optimization are summarized in Algorithm 1.

Note if there are no nondominated solutions, then the values of the weighting coefficients ρ , ς , and Υ in Step 5 of Algorithm 1 can be selected according to the actual trade-off requirements. ■

5.4 Classical Layer Optimization

In this section we characterize the classical layer optimization procedure.

Thesis 3.3 (Classical layer optimization) *The cost function of classical communications in a quantum Internet setting can be minimized by a procedure \mathcal{P}_C .*

Algorithm 1 Quantum layer optimization

Step 1. Set $\mathcal{S}_{\mathcal{G}_{et}}^* = \emptyset$, and for all entangled connects, initialize $\lambda'_{E_{L_l}(I,J)}$ as

$$\lambda'_{E_{L_l}(I,J)} = \lambda_{E_{L_l}(I,J)}.$$

Step 2. Determine X , and apply method \mathcal{M} for building an \mathcal{G}_{et} entanglement throughput tree as $\mathcal{M}(X) = \mathcal{G}_{et}^X$. For a given \mathcal{G}_{et}^X , determine the $\alpha_{\mathcal{G}_{et}}$ optimal assignment of stored entanglement, the t_s^* overall minimal storage time, the B_F^* maximal entanglement throughput, and the $|\mathcal{P}^*|$ minimal number of entangled connections, where \mathcal{P}^* is a shortest path.

Step 3. If X is not dominated by any $X_{\mathcal{G}_{et}} \in \kappa$, that is, $X_{\mathcal{G}_{et}} \angle X$ for any $X_{\mathcal{G}_{et}}$, then update κ as

$$\kappa = \kappa \cup X - \{X_{\mathcal{G}_{et}} | X_{\mathcal{G}_{et}} \angle X\}.$$

Step 4. If κ has been updated to κ' , then update the entanglement utility as $\lambda'_{E_{L_l}(I,J)} = \lambda_{E_{L_l}(I,J)}$ for all entangled connects of \mathcal{G}_m .

Step 5. If κ has not been updated, then for all $X_{\mathcal{G}_{et}} \in \kappa$ compute

$$\Pi = \rho t_s(\mathcal{G}_{et}^X) + \varsigma B_F^*(\mathcal{G}_{et}^X) + \Upsilon |\mathcal{P}^*(\mathcal{G}_{et}^X)|,$$

where $t_s(\mathcal{G}_{et}^X)$ is the storage time associated to tree \mathcal{G}_{et}^X , $B_F^*(\mathcal{G}_{et}^X)$ is the maximal entanglement throughput associated to tree \mathcal{G}_{et}^X , $|\mathcal{P}^*(\mathcal{G}_{et}^X)|$ is the number of entangled connections of the $\mathcal{P}^*(\mathcal{G}_{et}^X)$ shortest path of \mathcal{G}_{et}^X , while ρ , ς , and Υ are weighting coefficients. For all entangled connections of graph \mathcal{G}_m , update $\lambda'_{E_{L_l}(I,J)}$ as

$$\lambda'_{E_{L_l}(I,J)} = (1 - \Pr(I, J)) \lambda'_{E_{L_l}(I,J)} + \Pr(I, J) \Pi.$$

Step 6. Output optimal entanglement throughput tree set $\mathcal{S}_{\mathcal{G}_{et}}^*$.

Proof. Let

$$\begin{aligned}
& f_{t_s^*, B_F^*, |\mathcal{P}^*|}(\Theta_i) \\
&= \left(\sum_{g=1}^{N_{t_s^*}} S_{t_s^*, g}(i) + c_{N_{t_s^*}, g}^L(i) \right) + \left(\sum_{g=1}^{N_{B_F^*}} S_{B_F^*, g}(i) + c_{N_{B_F^*}, g}^L(i) \right) + \left(\sum_{g=1}^{N_{|\mathcal{P}^*|}} S_{|\mathcal{P}^*|, g}(i) + c_{N_{|\mathcal{P}^*|}, g}^L(i) \right)
\end{aligned} \tag{5.16}$$

be the cost function of classical communication of the multilayer optimization procedure, where $\Theta_i \in \mathbb{R}^p$ is a p -dimensional real vector of an i -th system state of the quantum network, $N_{t_s^*}$, $N_{B_F^*}$, $N_{|\mathcal{P}^*|}$ are the number of nodes that require the determination of optimal t_s^* , B_F^* and $|\mathcal{P}^*|$, $S_{t_s^*, g}(i)$, $S_{B_F^*, g}(i)$, $S_{|\mathcal{P}^*|, g}(i)$ refer to the number of classical steps required to find t_s^* , B_F^* and $|\mathcal{P}^*|$ for a particular node g of network N , while $c_{N_{t_s^*}, g}^L(i)$, $c_{N_{B_F^*}, g}^L(i)$, and $c_{N_{|\mathcal{P}^*|}, g}^L(i)$ are the costs of classical link L used for the determination of t_s^* , B_F^* and $|\mathcal{P}^*|$ for a given g .

Then, let introduce indices for Θ_i as

$$\Theta_i(j, k, l), \tag{5.17}$$

where j is the index of a desired optimal system state, k is the index of an optimal system state reproduction step, l is the index of a non-optimal system state event [98].

Let assume that there is a set of S sub-states $\{\Theta_1, \dots, \Theta_S\}$ in the network, then the T total network state is evaluated as

$$T(j, k, l) = \{\Theta_i(j, k, l) | i = 1, \dots, S\}. \tag{5.18}$$

Let $f_{t_s^*, B_F^*, |\mathcal{P}^*|}(\Theta_i(j, k, l))$ be the cost function of classical communication at a given $\Theta_i(j, k, l)$. Then, if

$$f_{t_s^*, B_F^*, |\mathcal{P}^*|}(\Theta_i(j+1, k, l)) < f_{t_s^*, B_F^*, |\mathcal{P}^*|}(\Theta_i(j, k, l)), \tag{5.19}$$

then the system state evolves from j to $j + 1$ as

$$\Theta_i(j + 1, k, l) = \Theta_i(j, k, l) + c(i) u(j), \quad (5.20)$$

where $c(i)$ is the number of random system states, while $u(j)$ quantifies a unit cost of system change [68, 98].

Therefore, for a set of S sub-states $\{\Theta_1, \dots, \Theta_S\}$ and current vector $\Theta \in \mathbb{R}^p$, the C_N total cost of classical communication is yielded as

$$C_N(\Theta, \Theta_i(j, k, l)) = \sum_{i=1}^S f_{t_s^*, B_F^*, |\mathcal{P}^*|}(\Theta_i(j, k, l)), i = 1, \dots, S, \quad (5.21)$$

which can be rewritten [98] as

$$\begin{aligned} & C_N(\Theta, T(j, k, l)) \\ &= \sum_{i=1}^S \left(-A e^{-R_A} \sum_{m=1}^p \left(\Theta^{(m)} - \Theta_i^{(m)} \right)^2 \right) + \sum_{i=1}^S \left(\nu e^{-R_\nu} \sum_{m=1}^p \left(\Theta^{(m)} - \Theta_i^{(m)} \right)^2 \right), \end{aligned} \quad (5.22)$$

where A is the distribution-entity of a current system state, R_A is the information transmission rate of A , ν is the distribution-entity of a system state, R_ν is the information transmission rate of ν , while $\Theta^{(m)}$ is the m -th element of a current network state vector Θ , and $\Theta_i^{(m)}$ is the m -th element of Θ_i .

Using $C_N(\Theta, T(j, k, l))$ (see (5.22)), an environment-dependent cost function C_e is defined as

$$C_e = C_N(\Theta, T(j, k, l)) e^{(M - f_{t_s^*, B_F^*, |\mathcal{P}^*|})(\Theta_i(j, k, l))}, \quad (5.23)$$

where M is a tuning parameter [98].

From (5.23), the F_{cost}^i cost function at a given $\Theta_i(j, k, l)$ is defined as

$$F_{cost}^i = f_{t_s^*, B_F^*, |\mathcal{P}^*|}(\Theta_i(j, k, l)) + C_e(\Theta_i(j, k, l)). \quad (5.24)$$

Using the proposed basic model, we define an optimization procedure \mathcal{P}_C of the classical layer to achieve a $C_N(\Theta, T(j, k, l))$ minimized cost function. The method is summarized in Algorithm 2.

These results conclude the proof. ■

5.4.1 Large-Constrained Optimization

The optimization efficiency can be further improved for a large constrained network scenario. This step can be replayed by a different approach, which allows an optimization of the classical layer for an arbitrary constrained setting. The solution is based on the idea of system state merging.

Lemma 3.2 *The optimization of the classical layer can be extended to a large-constrained optimization by state merging.*

Proof. An extended model of the classical layer optimization is as follows.

Let $N_{t_s^*}$, $N_{B_F^*}$, $N_{|\mathcal{P}^*|}$ be the number of nodes that require the determination of optimal t_s^* , B_F^* and $|\mathcal{P}^*|$. Then, let J be the objective function [78], as

$$J = \min \sum_{t=1}^T (\alpha_{t_s^*}(t) + \alpha_{B_F^*}(t) + \alpha_{|\mathcal{P}^*|}(t)), \quad (5.25)$$

where

$$\alpha_{t_s^*}(t) = \sum_{g=1}^{N_{t_s^*}} S_{t_s^*,g}(t) + c_{N_{t_s^*},g}^L(t), \quad (5.26)$$

$$\alpha_{B_F^*}(t) = \sum_{g=1}^{N_{B_F^*}} S_{B_F^*,g}(t) + c_{N_{B_F^*},g}^L(t), \quad (5.27)$$

and

$$\alpha_{|\mathcal{P}^*|}(t) = \sum_{g=1}^{N_{|\mathcal{P}^*|}} S_{|\mathcal{P}^*|,g}(t) + c_{N_{|\mathcal{P}^*|},g}^L(t), \quad (5.28)$$

Algorithm 2 Classical layer optimization

Step 1. For an i -th system state $\Theta_i(j, k, l)$ initialize cost function

$$f_{t_s^*, B_F^*, |\mathcal{P}^*|}(\Theta_i(j, k, l)) = f_{t_s^*, B_F^*, |\mathcal{P}^*|}(\Theta_i(j, k, l)) + C_N(\Theta_i(j, k, l), T(j, k, l)).$$

Define a random network state vector $\partial(i) \in \mathbb{R}^p$, where the $\partial_m(i)$ m -th element of $\partial(i)$ is a uniformly distributed number from the range of $[-1, 1]$.

Step 2. From $\Theta_i(j, k, l)$, define $\Theta_i(j+1, k, l)$ as

$$\Theta_i(j+1, k, l) = \Theta_i(j, k, l) + c(i) \frac{\partial(i)}{\sqrt{(\partial(i))^T \partial(i)}},$$

where $c(i)$ is the number of random system states.

Step 3. Using $f_{t_s^*, B_F^*, |\mathcal{P}^*|}(\Theta_i(j, k, l))$, determine $f_{t_s^*, B_F^*, |\mathcal{P}^*|}(\Theta_i(j+1, k, l))$ as $f_{t_s^*, B_F^*, |\mathcal{P}^*|}(\Theta_i(j+1, k, l)) = f_{t_s^*, B_F^*, |\mathcal{P}^*|}(\Theta_i(j, k, l)) + C_N(\Theta_i(j+1, k, l), T(j+1, k, l))$. If

$$f_{t_s^*, B_F^*, |\mathcal{P}^*|}(\Theta_i(j+1, k, l)) < f_{t_s^*, B_F^*, |\mathcal{P}^*|}(\Theta_i(j, k, l)),$$

update $f_{t_s^*, B_F^*, |\mathcal{P}^*|}(\Theta_i(j, k, l))$ as

$$f_{t_s^*, B_F^*, |\mathcal{P}^*|}(\Theta_i(j, k, l)) = f_{t_s^*, B_F^*, |\mathcal{P}^*|}(\Theta_i(j+1, k, l)).$$

Update $\Theta_i(j+1, k, l)$ as

$$\Theta_i(j+1, k, l) = \Theta_i(j, k, l) + c(i) \frac{\partial(i)}{\sqrt{(\partial(i))^T \partial(i)}},$$

and compute $f_{t_s^*, B_F^*, |\mathcal{P}^*|}(\Theta_i(j+1, k, l))$.

Step 4. Increase i , $i = i + 1$. If $i < S$, apply steps 1-3 for the current network sub-state. If $j < n_{G(\tilde{\Theta})}$, where $n_{G(\tilde{\Theta})}$ is the total number of iteration steps on j to reach an optimal global state $G(\tilde{\Theta})$, then increase j , $j = j + 1$.

Step 5. For all i , determine

$$F_{cost}^i = \sum_{j=1}^{n_{G(\tilde{\Theta})}+1} f_{t_s^*, B_F^*, |\mathcal{P}^*|}(\Theta_i(j, k, l)) + C_e(\Theta_i(j, k, l)).$$

Remove system states for which $F_{cost}^i \geq \chi_C$, where χ_C is a threshold on F_{cost}^i to get the minimized cost F_{cost}^{\min} as

$$F_{cost}^{\min} = \sum_{i=1}^{S-\varphi} F_{cost}^i,$$

where φ is the total number of removed system states. For a given E_k and E_l expected values of k and l , if $k < E_k$ then increase k , $k = k + 1$, and if $l < E_l$ increase l , $l = l + 1$.

where the coefficients $S_{t_s^*,g}(t)$, $S_{B_F^*,g}(t)$, $S_{|\mathcal{P}^*|,g}(t)$ refer to the number of classical steps required to find t_s^* , B_F^* and $|\mathcal{P}^*|$ at a particular network node g and time t , $t = 1, \dots, T$, while $c_{N_{t_s^*,g}}^L(t)$, $c_{N_{B_F^*,g}}^L(t)$, $c_{N_{|\mathcal{P}^*|,g}}^L(t)$ are the costs of classical link L at a particular g and t . Let assume that $\Theta_a(j, k, l)$, $\Theta_b(j, k, l)$ and $\Theta_c(j, k, l)$ are some system states of the classical layer subject of state merging. From these sub-states, the $\Theta_M(j, k, l)$ merged system is defined as

$$\Theta_M(j, k, l) = \Theta_a(j, k, l) + \Phi(\Theta_b(j, k, l) - \Theta_c(j, k, l)), \quad (5.29)$$

where Φ is a merging factor, $\Phi \in [0, 1]$.

Using (5.29), an i -th system state $\Theta_i(j, k, l)$ is updated as

$$\Theta_i(j, k, l) = \left(\tilde{\Theta}_i^a(j, k, l), \tilde{\Theta}_i^b(j, k, l), \tilde{\Theta}_i^c(j, k, l) \right)^T, \quad (5.30)$$

where

$$\tilde{\Theta}_i^a(j, k, l) = \begin{cases} \Theta_i(j, k, l), & \text{if } x_a > u \\ \Theta_M(j, k, l), & \text{otherwise} \end{cases}, \quad (5.31)$$

$$\tilde{\Theta}_i^b(j, k, l) = \begin{cases} \Theta_i(j, k, l), & \text{if } x_b > u \\ \Theta^*(j, k, l), & \text{otherwise} \end{cases}, \quad (5.32)$$

and

$$\tilde{\Theta}_i^c(j, k, l) = \begin{cases} \Theta^*(j, k, l), & \text{if } x_c > u \\ \Theta_M(j, k, l), & \text{otherwise} \end{cases}, \quad (5.33)$$

where u is a uniform random number, x_a, x_b and x_c are random numbers, $x_a, x_b, x_c \in [0, 1]$, $\Theta^*(j, k, l)$ is a system state that minimizes the objective function J . Then for $Q \in (a, b, c)$, the objective function value $J(\tilde{\Theta}_i^Q(j, k, l))$ is compared with the objective function $J(\Theta_i(j, k, l))$ of $\Theta_i(j, k, l)$, and $\tilde{\Theta}_i^Q(j, k, l)$ is updated by the following rule:

$$\tilde{\Theta}_i^Q(j, k, l) = \begin{cases} \Theta_i(j, k, l), & \text{if } J(\tilde{\Theta}_i^Q(j, k, l)) < J(\Theta_i(j, k, l)) \\ \tilde{\Theta}_i^Q(j, k, l), & \text{otherwise.} \end{cases} \quad (5.34)$$

The proof is concluded here. ■

5.5 Numerical Analysis

In this section, we study the performance of the proposed quantum layer and classical layer optimization methods.

5.5.1 Quantum Layer Optimization

To study the convergence of the quantum layer optimization, we characterize the $D(\cdot)$ closeness function of the elements of the solution set from an optimal Pareto front, and the $\zeta(\cdot)$ ratio of optimal solutions in the solution set.

Let $X_{\mathcal{G}_{et},i} = \{t_s^*(\mathcal{G}_{et}, i), B_F^*(\mathcal{G}_{et}, i), |\mathcal{P}^*(\mathcal{G}_{et}, i)|\}$ be an i -th solution from the solution set $X_{\mathcal{G}_{et}}(N_{it})$ found at a N_{it} finite number of iterations, and let

$$X_{\mathcal{G}_{et}}^\infty = \{t_s^*(\mathcal{G}_{et}, z), B_F^*(\mathcal{G}_{et}, z), |\mathcal{P}^*(\mathcal{G}_{et}, z)|\} \quad (5.35)$$

refer to a solution z from $X_{\mathcal{G}_{et}}(N_{it} \rightarrow \infty)$ at $N_{it} \rightarrow \infty$. Then, let $D(X_{\mathcal{G}_{et},i}, X_{\mathcal{G}_{et}}^\infty)$ be the distance on the Pareto front [51, 90, 126] between $X_{\mathcal{G}_{et},i}$ and $X_{\mathcal{G}_{et}}^\infty$, defined as

$$D(X_{\mathcal{G}_{et},i}, X_{\mathcal{G}_{et}}^\infty) = \frac{1}{\chi} (A + B + C), \quad (5.36)$$

with $D(X_{\mathcal{G}_{et},i}, X_{\mathcal{G}_{et}}^\infty) \in [0, 1]$, and where

$$A = \frac{|t_s^*(\mathcal{G}_{et}, z) - t_s^*(\mathcal{G}_{et}, i)|}{t_s^*(\mathcal{G}_{et}, z)}, \quad (5.37)$$

$$B = \frac{|B_F^*(\mathcal{G}_{et}, z) - B_F^*(\mathcal{G}_{et}, i)|}{B_F^*(\mathcal{G}_{et}, z)}, \quad (5.38)$$

and

$$C = \frac{||\mathcal{P}^*(\mathcal{G}_{et}, z)| - |\mathcal{P}^*(\mathcal{G}_{et}, i)||}{|\mathcal{P}^*(\mathcal{G}_{et}, z)|}, \quad (5.39)$$

while χ is a control parameter, $\chi > 0$.

Then, let $\zeta (X_{\mathcal{G}_{et}} (N_{it}), X_{\mathcal{G}_{et}} (N_{it} \rightarrow \infty))$ be a ratio of the solution sets $X_{\mathcal{G}_{et}} (N_{it})$ and $X_{\mathcal{G}_{et}} (N_{it} \rightarrow \infty)$ found at finite N_{it} and $N_{it} \rightarrow \infty$ as

$$\zeta (X_{\mathcal{G}_{et}} (N_{it}), X_{\mathcal{G}_{et}} (N_{it} \rightarrow \infty)) = \frac{\text{card}(X_{\mathcal{G}_{et}}(N_{it}) \wedge X_{\mathcal{G}_{et}}(N_{it} \rightarrow \infty))}{\text{card}(X_{\mathcal{G}_{et}}(N_{it}))}, \quad (5.40)$$

where $\text{card}(X_{\mathcal{G}_{et}} (N_{it}))$ is the cardinality of set $X_{\mathcal{G}_{et}} (N_{it})$, while $X_{\mathcal{G}_{et}} (N_{it}) \wedge X_{\mathcal{G}_{et}} (N_{it} \rightarrow \infty)$ is the intersection of solution sets $X_{\mathcal{G}_{et}} (N_{it})$ and $X_{\mathcal{G}_{et}} (N_{it} \rightarrow \infty)$ (solutions included by both solution sets). Note, since the χ control parameter in (5.36) determines the D distance from the optimal set, χ also affects the ratio of the solution sets (5.40). If the value of χ is high, the D distance in (5.36) is low, that results in a high cardinality of the intersection set in (5.40). If χ is low, the D distance in (5.36) is high, therefore the cardinality of the intersection set is small.

The quantity of (5.36) for various N_{it} and χ are depicted in Fig. 5-4. From the results it can be concluded that as N_{it} increases, the $D (X_{\mathcal{G}_{et},i}, X_{\mathcal{G}_{et}}^{\infty})$ distance significantly decreases, while the speed of convergence is controllable by χ . It also can be verified that the χ control parameter has a significant impact on $D (X_{\mathcal{G}_{et},i}, X_{\mathcal{G}_{et}}^{\infty})$, and the $D (X_{\mathcal{G}_{et},i}, X_{\mathcal{G}_{et}}^{\infty})$ distance can be made arbitrarily small via a moderate value for N_{it} .

In Fig. 5-5, the quantity of (5.40) is illustrated for different values of N_{it} . As N_{it} increases the $\zeta (X_{\mathcal{G}_{et}} (N_{it}), X_{\mathcal{G}_{et}} (N_{it} \rightarrow \infty))$ ratio increases significantly, while the χ control parameter has a moderate effect on the ratio of (5.40). The ratio exceeds 0.5 at $N_{it} \approx 0.5 \cdot 10^3$, and can be increased to arbitrarily high via a moderate increment in N_{it} .

The performance of the quantum layer optimization method is therefore approachable via the distance function (5.36) and ratio (5.40). The analysis revealed that at moderate N_{it} values, the precision of the optimization method can be arbitrary high via the selection of the χ control parameter. It also has been concluded, that a high ratio of the solutions at a finite and moderate N_{it} , are identical to the solutions at the limit case of $N_{it} \rightarrow \infty$.

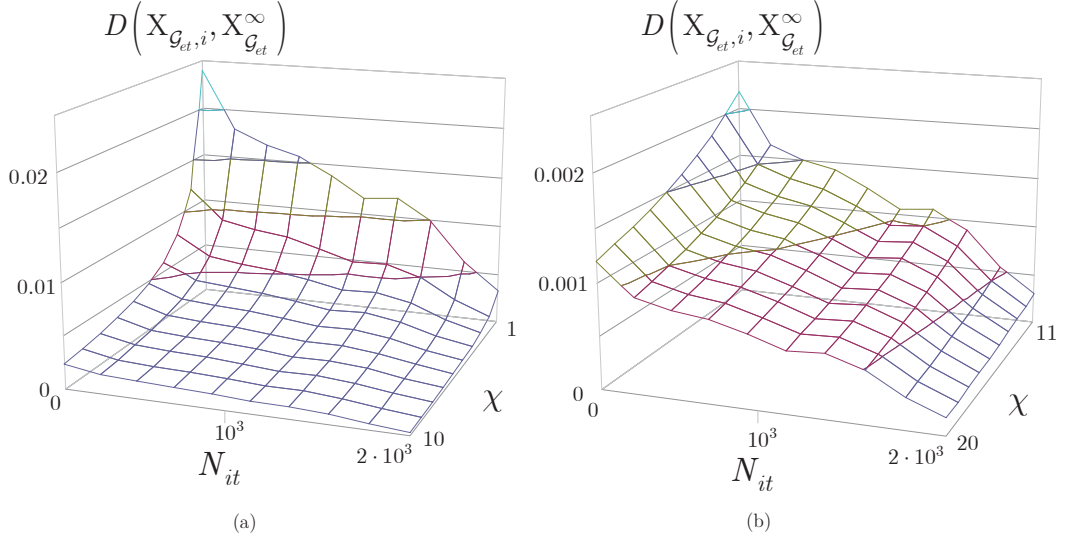


Figure 5-4: The $D(X_{g_{et},i}, X_{g_{et}}^\infty)$ distance in function of N_{it} and χ . (a) The values of $D(X_{g_{et},i}, X_{g_{et}}^\infty)$ for $0 < N_{it} \leq 2 \cdot 10^3$ and $1 \leq \chi \leq 10$. (b) The values of $D(X_{g_{et},i}, X_{g_{et}}^\infty)$ for $0 < N_{it} \leq 2 \cdot 10^3$ and $11 \leq \chi \leq 20$.

5.5.2 Classical Layer Optimization

Let $\phi_s(i)$ be the step-size function defined for an i -th state as

$$\phi_s(i) = \phi_{\max} - \Delta(\phi) \cdot \exp\left(\frac{-f(i,j,k,l)}{j}\right), \quad (5.41)$$

where

$$\Delta(\phi) = (\phi_{\max} - \phi_{\min}), \quad (5.42)$$

where ϕ_{\min} and ϕ_{\max} are some lower and upper bounds, $\phi_s(i) \in [\phi_{\min}, \phi_{\max}]$, while $f(i, j, k, l)$ is defined as

$$f(i, j, k, l) = \omega \frac{J^*}{J_P}, \quad (5.43)$$

where ω is a constant (restriction factor [66, 84, 132]), J^* is the minimal cost function (for J , see (5.25)) at a particular parameter setting (i, j, k, l) , J_P is the minimal cost function associated to the population.

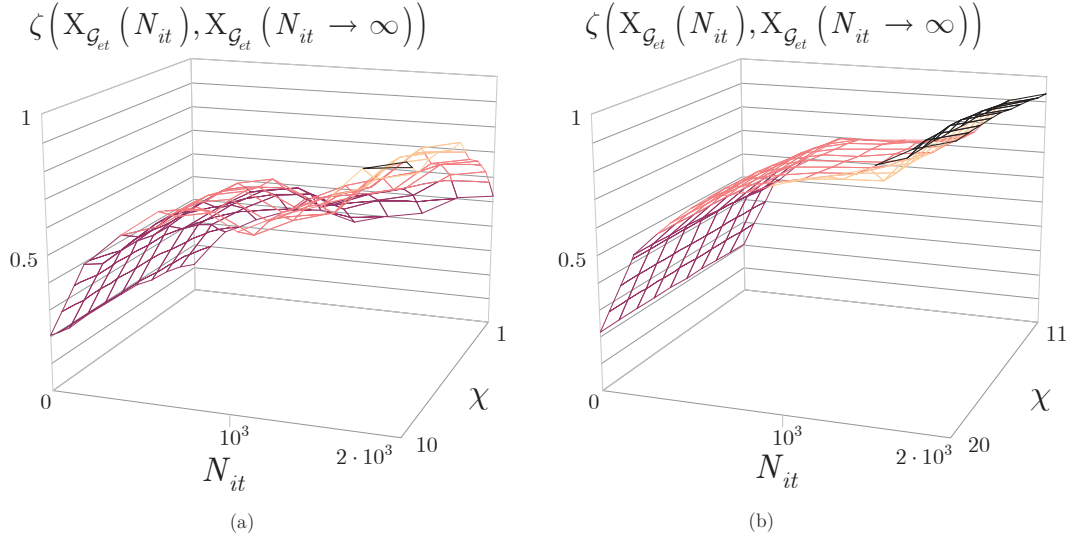


Figure 5-5: The ratio $\zeta(X_{G_{et}}(N_{it}), X_{G_{et}}(N_{it} \rightarrow \infty))$ in function of N_{it} and χ . (a) The values of $\zeta(X_{G_{et}}(N_{it}), X_{G_{et}}(N_{it} \rightarrow \infty))$ for $0 < N_{it} \leq 2 \cdot 10^3$ and $1 \leq \chi \leq 10$. (b) The values of $\zeta(X_{G_{et}}(N_{it}), X_{G_{et}}(N_{it} \rightarrow \infty))$ for $0 < N_{it} \leq 2 \cdot 10^3$ and $11 \leq \chi \leq 20$.

Then, at an iteration number j let $\kappa(j)$ be a ratio as

$$\kappa(j) = \frac{f(i,j,k,l)}{j}. \quad (5.44)$$

The step-size (5.41) in function of ϕ_{\min} and $\kappa(j)$ is depicted in Fig. 5-6.

From (5.41) and (5.43), the optimal cost function J^* at a particular setting of (i, j, k, l) is yielded as

$$J^* = -\frac{\ln\left(\frac{\phi_{\max} - \phi_s(i)}{\Delta(\phi)}\right)j}{\omega} J_P. \quad (5.45)$$

Then, let

$$\kappa(j) = x, \quad (5.46)$$

from which the iteration number can be rewritten as

$$j = \frac{f(i,j,k,l)}{x}, \quad (5.47)$$

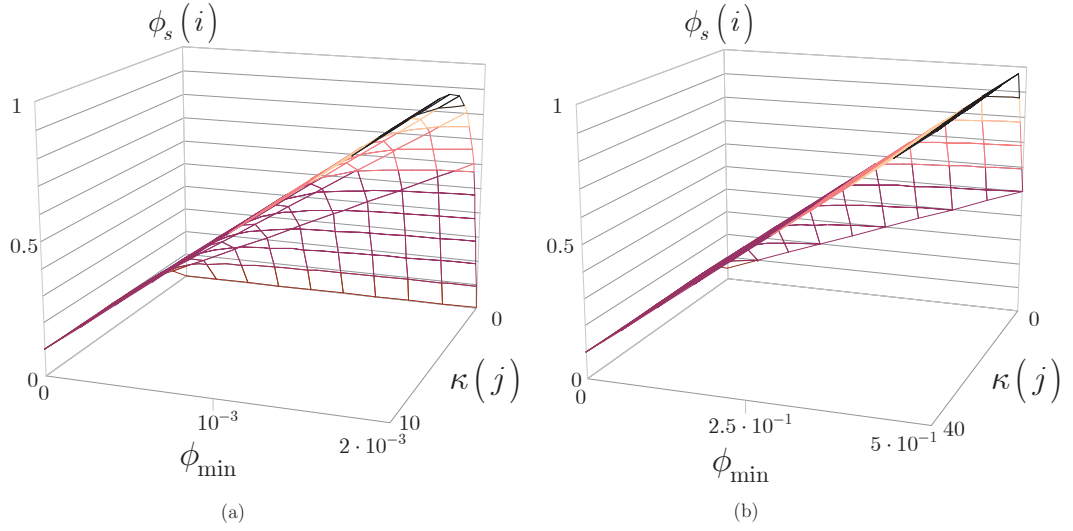


Figure 5-6: (a) The $\phi_s(i)$ step-size function for $\phi_{\min} \in [0, 2 \cdot 10^{-3}]$, $\phi_{\max} = 500\phi_{\min}$ and $\kappa(j) \in [0, 10]$. (b) The $\phi_s(i)$ step-size function for $\phi_{\min} \in [0, 5 \cdot 10^{-1}]$, $\phi_{\max} = 2\phi_{\min}$ and $\kappa(j) \in [0, 40]$.

and also fix $f(i, j, k, l)$ as

$$f(i, j, k, l) = x^2. \quad (5.48)$$

Then, from (5.46) and (5.48), J^* can be evaluated at a given x in function J_P and ω , as

$$J^* = \frac{x^2 J_P}{\omega}. \quad (5.49)$$

From (5.47) and (5.48), the function in (5.45) can be rewritten as

$$\begin{aligned} J^* &= -\frac{\ln\left(\frac{\phi_{\max} - \phi_s(i)}{\Delta(\phi)}\right) f(i, j, k, l)}{\omega x} J_P \\ &= -\frac{\ln\left(\frac{\phi_{\max} - \phi_s(i)}{\Delta(\phi)}\right) x}{\omega} J_P, \end{aligned} \quad (5.50)$$

therefore the cost function J^* at a particular (5.46) and (5.48) can also be evaluated in function of the step size (5.41).

The J^* cost function values associated to the $\phi_s(i)$ step size function values of Fig. 5-6 at $J_P = 1$ and $J_P = 1$ and $\omega = 100$ are depicted in Fig. 5-7.

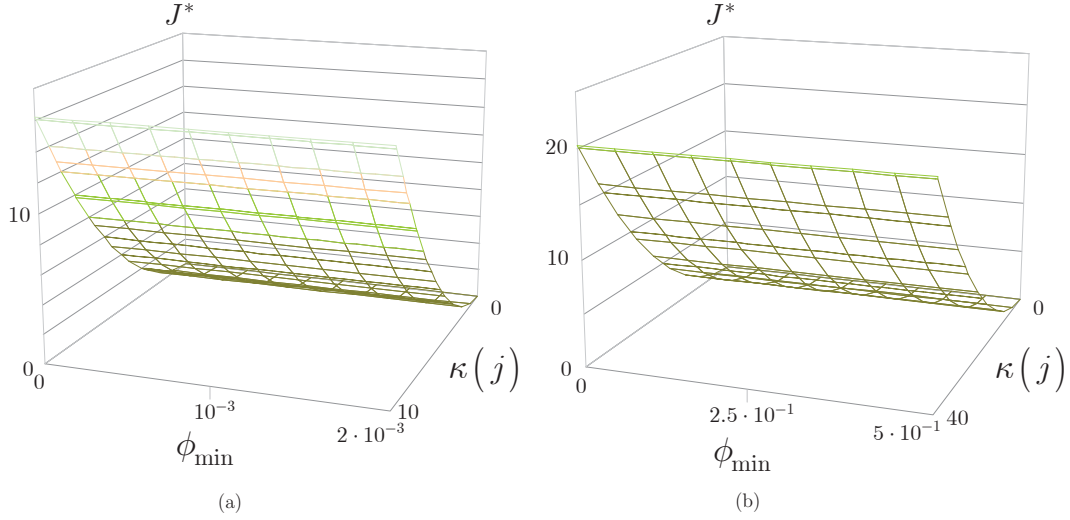


Figure 5-7: The J^* cost function values associated to the $\phi_s(i)$ step size function value, (a) $J_P = 1$ and $\omega = 1$, (b) $J_P = 1$ and $\omega = 100$.

The analysis is therefore revealed that for any $\phi_s(i)$, the cost function J^* increases with the $\kappa(j)$ ratio, and the values of J^* are tunable via the control parameter ω for arbitrary J_P and $\kappa(j)$ values. The proposed classical layer optimization model is therefore flexible, and allows a dynamics adaption for diverse environmental settings. As future work, our aim is to provide a transmission analysis and comparisons with other schemes.

5.6 Conclusions

This chapter conceived a multilayer optimization method for the quantum Internet. Multilayer optimization defines separate procedures for the optimization of the quantum layer and the classical layer. Quantum layer optimization defines a multi-objective function by minimizing the total usage of quantum memories in the quantum nodes, maximizing the entanglement throughput over all entangled connections, and reducing the number of entangled connections between the arbitrary source and target quantum nodes. We defined the structure of the quantum memory utilization graph and entanglement throughput tree. The classical layer optimization utilizes the fundamentals of swarm intelligence for the

minimization of the cost function. Since the proposed multilayer optimization method has no physical layer requirements, it can serve as a useful tool for quantum network communications and future quantum Internet.

Chapter 6

Discussion

This dissertation described services for the quantum Internet. Quantum Internet is an adequate answer for the computational power that became available as quantum computers became publicly available. The structure of the quantum Internet keeps the data of users safe for future networking. However, the commercial quantum computers are currently under development and represent tomorrow's problems, the engineering of high-performance and well-designed services and protocols for the quantum Internet is today's tasks. As quantum computers are built and become available, the structure of the quantum Internet also has to be ready to provide a seamless transition from the traditional Internet to the quantum Internet. This dissertation is aimed at this purpose through the definition of novel and efficient services for our future quantum networking.

6.1 Future Work

Future research should define further services and protocols for the quantum Internet. An important subject to explore is the organization and engineering of the standards for the quantum Internet. Similar to traditional networking, the standardization of the protocols of the quantum Internet helps to define a uniform platform to create a global quantum network. The standardization will also serve as an evolving framework to reflect

the dynamically changing requirements of the quantum Internet. As a first promising approach to address these important problems, the Quantum Internet Research Group (QIRG) [95] has already been formed with an international support and researcher collaboration. The QIRG also defined a technical roadmap [127] of capability milestones for the development of the experimental quantum Internet. The aim of the proposal is to find solutions for the future engineering problems brought up by the quantum Internet, such as the definition of a standardized architectural framework (interoperability, connection establishment, node roles, network coding, multiparty state transfer) and an application programming interface (API) design and the definition of the application level of the quantum Internet.

Bibliography

- [1] Aaronson, S. and Chen, L. Complexity-theoretic foundations of quantum supremacy experiments. *Proceedings of the 32nd Computational Complexity Conference, CCC '17*, pages 22:1-22:67 (2017).
- [2] Bacsardi, L. On the Way to Quantum-Based Satellite Communication, *IEEE Comm. Mag.* 51:(08) pp. 50-55. (2013).
- [3] Barends, R. et al. Superconducting quantum circuits at the surface code threshold for fault tolerance. *Nature* 508, 500-503 (2014).
- [4] Biamonte, J. et al. Quantum Machine Learning. *Nature*, 549, 195-202 (2017).
- [5] Bisztray, T. and Bacsardi, L. The Evolution of Free-Space Quantum Key Distribution, *InfoComm. Journal X*:(1) pp. 22-30. (2018).
- [6] Briegel, H. J., Dur, W., Cirac, J. I. and Zoller, P. Quantum repeaters: the role of imperfect local operations in quantum communication. *Phys. Rev. Lett.* 81, 5932-5935 (1998).
- [7] Cacciapuoti, A. S., Caleffi, M., Tafuri, F., Cataliotti, F. S., Gherardini, S. and Bianchi, G. Quantum Internet: Networking Challenges in Distributed Quantum Computing, *arXiv:1810.08421* (2018).
- [8] Caleffi, M. End-to-End Entanglement Rate: Toward a Quantum Route Metric, *2017 IEEE Globecom*, DOI: 10.1109/GLOCOMW.2017.8269080 (2018).

- [9] Caleffi, M. Optimal Routing for Quantum Networks, *IEEE Access*, Vol 5, DOI: 10.1109/ACCESS.2017.2763325 (2017).
- [10] Caleffi, M., Cacciapuoti, A. S. and Bianchi, G. Quantum Internet: from Communication to Distributed Computing, *arXiv:1805.04360* (2018).
- [11] Castelvecchi, D. The quantum internet has arrived, *Nature*, News and Comment, <https://www.nature.com/articles/d41586-018-01835-3> (2018).
- [12] Chen, L. and Hayashi, M. Multicopy and stochastic transformation of multipartite pure states, *Physical Review A*, Vol.83, No.2, 022331 (2011).
- [13] Chou, C., Laurat, J., Deng, H., Choi, K. S., de Riedmatten, H., Felinto, D. and Kimble, H. J. Functional quantum nodes for entanglement distribution over scalable quantum networks. *Science*, 316(5829):1316-1320 (2007).
- [14] Chuan, T. K., Maillard, J., Modi, K., Paterek, T., Paternostro, M. and Piani, M. Quantum discord bounds the amount of distributed entanglement, *arXiv:1203.1268v3*, *Phys. Rev. Lett.* 109, 070501 (2012).
- [15] Cubitt, T. S., Verstraete, F., Dur, W. and Cirac, J. I. Separable States Can Be Used To Distribute Entanglement, *Phys. Rev. Lett.* 91, 037902 (2003).
- [16] Debnath, S. et al. Demonstration of a small programmable quantum computer with atomic qubits. *Nature* 536, 63-66 (2016).
- [17] DiCarlo, L. et al. Demonstration of two-qubit algorithms with a superconducting quantum processor. *Nature* 460, 240-244 (2009).
- [18] Di Caro, F. D. G., Gambardella, L. M. Swarm intelligence for routing in mobile ad hoc networks. *IEEE Swarm Intelligence Symposium*, pages 76-83 (2005).
- [19] Dijkstra, E. W. A note on two problems in connexion with graphs. *Numerische Mathematik*, 1(1): 269-271 (1959).

- [20] Duan, L. M., Lukin, M. D., Cirac, J. I. and Zoller, P. Long-distance quantum communication with atomic ensembles and linear optics. *Nature*, 414, 413-418 (2001).
- [21] Dur, W. and Briegel, H. J. Entanglement purification and quantum error correction. *Rep. Prog. Phys*, 70, 1381-1424 (2007).
- [22] Dur, W., Briegel, H. J., Cirac, J. I. and Zoller, P. Quantum repeaters based on entanglement purification. *Phys. Rev. A*, 59, 169-181 (1999).
- [23] Enk, S. J., Cirac, J. I. and Zoller, P. Photonic channels for quantum communication. *Science*, 279, 205-208 (1998).
- [24] Evans, N., Dickey, C. G. and Grothoff, C. Routing in the Dark: Pitch Black, *Twenty-Third Annual Computer Security Applications Conference (ACSAC 2007)*, ISSN: 1063-9527, Miami Beach, FL, USA (2007).
- [25] Farooq, M. and Di Caro, G. A. Routing protocols for next generation networks inspired by collective behaviors of insect societies: an overview. *Swarm Intelligence, Natural Computing Series*, pages 101-160 (2008).
- [26] Fedrizzi, A., Ursin, R., Herbst, T., Nespoli, M., Prevedel, R., Scheidl, T., Tiefenbacher, F., Jennewein, T. and Zeilinger, A. High-fidelity transmission of entanglement over a high-loss free-space channel, *Nature Physics*, 5(6):389–392 (2009).
- [27] Franceschetti, M. and Meester, R. *Random Networks for Communication*, 212 pages, ISBN-10: 0521854423, ISBN-13: 978-0521854429, Cambridge University Press (2008).
- [28] Gisin, N. and Thew, R. Quantum Communication. *Nature Photon.* 1, 165-171 (2007).
- [29] Goebel, A. M., Wagenknecht, G., Zhang, Q., Chen, Y., Chen, K., Schmiedmayer, J. and Pan, J. W. Multistage Entanglement Swapping. *Phys. Rev. Lett.* 101, 080403 (2008).

- [30] Gulde, S. et al. Implementation of the Deutsch-Jozsa algorithm on an ion-trap quantum computer. *Nature* 421, 48-50 (2003).
- [31] Gyongyosi, L. and Imre, S. A Survey on Quantum Computing Technology, *Computer Science Review*, Elsevier, DOI: 10.1016/j.cosrev.2018.11.002, ISSN: 1574-0137 (2018).
- [32] Gyongyosi, L. and Imre, S. Adaptive Routing for Quantum Memory Failures in the Quantum Internet, *Quantum Information Processing*, Springer Nature, DOI: 10.1007/s11128-018-2153-x (2018).
- [33] Gyongyosi, L. and Imre, S. Decentralized Base-Graph Routing for the Quantum Internet, *Phys. Rev. A*, American Physical Society, DOI: 10.1103/PhysRevA.98.022310 (2018).
- [34] Gyongyosi, L. and Imre, S. Dynamic topology resilience for quantum networks, *Proc. SPIE 10547*, Advances in Photonics of Quantum Computing, Memory, and Communication XI, 105470Z; doi: 10.1117/12.2288707 (2018).
- [35] Gyongyosi, L. and Imre, S. Entanglement Availability Differentiation Service for the Quantum Internet, *Sci. Rep.*, Nature, DOI:10.1038/s41598-018-28801-3 (2018).
- [36] Gyongyosi, L. and Imre, S. Entanglement-Gradient Routing for Quantum Networks, *Sci. Rep.*, Nature, DOI:10.1038/s41598-017-14394-w (2017).
- [37] Gyongyosi, L. and Imre, S. Multilayer Optimization for the Quantum Internet, *Sci. Rep.*, DOI:10.1038/s41598-018-30957-x, Nature (2018).
- [38] Gyongyosi, L. and Imre, S. Topology Adaption for the Quantum Internet, *Quantum Information Processing*, Springer Nature, DOI: 10.1007/s11128-018-2064-x (2018).
- [39] Gyongyosi, L., Imre, S. and Nguyen, H. V. A Survey on Quantum Channel Capacities, *IEEE Communications Surveys and Tutorials* **99**, 1, doi: 10.1109/COMST.2017.2786748 (2018).

- [40] Harrow, A. W. and Montanaro, A. Quantum Computational Supremacy, *Nature*, vol 549, pages 203-209 (2017).
- [41] Hayashi, M. Prior entanglement between senders enables perfect quantum network coding with modification, *Physical Review A*, Vol.76, 040301(R) (2007).
- [42] Hayashi, M., Iwama, K., Nishimura, H., Raymond, R. and Yamashita, S. Quantum network coding, *Lecture Notes in Computer Science* (STACS 2007 SE52 vol. 4393) ed Thomas, W. and Weil, P. (Berlin Heidelberg: Springer) (2007).
- [43] Hensen, B. et al., Loophole-free Bell inequality violation using electron spins separated by 1.3 kilometres, *Nature* 526 (2015).
- [44] Higgins, B. L., Berry, D. W., Bartlett, S. D., Wiseman, H. M. and Pryde, G. J. Entanglement-free Heisenberg-limited phase estimation. *Nature* 450, 393-396 (2007).
- [45] Hucul, D. et al., Modular entanglement of atomic qubits using photons and phonons, *Nature Physics* 11(1) (2015).
- [46] Humphreys, P. et al., Deterministic delivery of remote entanglement on a quantum network, *Nature* 558 (2018).
- [47] IBM. *A new way of thinking: The IBM quantum experience*. URL: <http://www.research.ibm.com/quantum>. (2017).
- [48] Imre, S. and Balazs, F. *Quantum Computing and Communications – An Engineering Approach*, John Wiley and Sons Ltd, ISBN 0-470-86902-X (2005).
- [49] Imre, S. and Gyongyosi, L. *Advanced Quantum Communications – An Engineering Approach*. 488 pages, ISBN-10: 1118002369, ISBN-13: 978-11180023, Wiley-IEEE Press (New Jersey, USA) (2013).
- [50] Jiang, L., Taylor, J. M., Nemoto, K., Munro, W. J., Van Meter, R. and Lukin, M. D. Quantum repeater with encoding. *Phys. Rev. A*, 79:032325 (2009).

- [51] Jie, Y. and Kamal, A. E. Multi-Objective Multicast Routing Optimization in Cognitive Radio Networks, *IEEE Wireless Communications and Networking Conference (IEEE WCNC)* (2014).
- [52] Jozsa, R. Fidelity for Mixed Quantum States, *J. Mod. Optics* 41, pp. 2315-2323 (1995).
- [53] Kak, A. Small-World Peer-to-Peer Networks and Their Security Issues, *Lecture Notes on Computer and Network Security*, Purdue University (2016).
- [54] Kay, A. Resources for Entanglement Distribution via the Transmission of Separable States, arXiv:1204.0366v4, *Phys. Rev. Lett.* 109, 080503 (2012).
- [55] Kimble, H. J. The quantum Internet. *Nature*, 453:1023-1030 (2008).
- [56] Kleinberg, J. The Small-World Phenomenon: An Algorithmic Perspective, *Proceedings of the 32nd Annual ACM Symposium on Theory of Computing (STOC'00)* (2000).
- [57] Kobayashi, H., Le Gall, F., Nishimura, H. and Rotteler, M. General scheme for perfect quantum network coding with free classical communication, *Lecture Notes in Computer Science* SE-52 vol. 5555, Springer) pp 622-633 (2009).
- [58] Kobayashi, H., Le Gall, F., Nishimura, H. and Rotteler, M. Perfect quantum network communication protocol based on classical network coding, *Proceedings of 2010 IEEE International Symposium on Information Theory (ISIT)* pp 2686-90. (2010).
- [59] Kok, P., Munro, W. J., Nemoto, K., Ralph, T. C., Dowling, J. P. and Milburn, G. J. Linear optical quantum computing with photonic qubits. *Rev. Mod. Phys.* 79, 135-174 (2007).
- [60] Krisnanda, T., Zuppardo, M., Paternostro, M. and Paterek, T. Revealing non-classicality of unmeasured objects, *Phys. Rev. Lett.*, 119, 120402 (2017).

- [61] Lang, M. D. and Caves, C. M. Quantum Discord and the Geometry of Bell-Diagonal States, *Phys. Rev. Lett.* 105, 150501 (2010).
- [62] Laurenza, R. and Pirandola, S. General bounds for sender-receiver capacities in multipoint quantum communications, *Phys. Rev. A* 96, 032318 (2017).
- [63] Leepila, R., Oki, E. and Kishi, N. Scheme to Find k Disjoint Paths in Multi-Cost Networks, *IEEE International Conference on Communications (ICC) 2011*, Kyoto, Japan, DOI: 10.1109/icc.2011.5962477 (2011).
- [64] Leepila, R. *Routing Schemes for Survivable and Energy-Efficient Networks*, PhD Thesis, Department of Information and Communication Engineering, The University of Electro-Communications (2014).
- [65] Leung, D., Oppenheim, J. and Winter, A. Quantum network communication; the butterfly and beyond, *IEEE Trans. Inf. Theory* 56, 3478-90. (2010).
- [66] Li, M. S., Ji, T. Y., Tang, W. J., Wu, Q. H. and Saunders, J. R. Bacterial foraging algorithm with varying population, *Biosystems* 100(3), 185-197 (2010).
- [67] Liao, S.-K. et al. Satellite-to-ground quantum key distribution, *Nature* 549, pages 43–47 (2017).
- [68] Liu, Y., Passino, K. M. Biomimicry of Social Foraging Bacteria for Distributed Optimization: Models, Principles, and Emergent Behaviors, *Journal of Optimization Theory and Applications* Vol. 115, No. 3, pp. 603–628 (2002).
- [69] Lloyd, S. and Weedbrook, C. Quantum generative adversarial learning. *Phys. Rev. Lett.*, 121, arXiv:1804.09139 (2018).
- [70] Lloyd, S. Capacity of the noisy quantum channel. *Physical Rev. A*, 55:1613–1622 (1997).

- [71] Lloyd, S. The Universe as Quantum Computer, *A Computable Universe: Understanding and exploring Nature as computation*, H. Zenil ed., World Scientific, Singapore, *arXiv:1312.4455v1* (2013).
- [72] Lloyd, S., Mohseni, M. and Rebentrost, P. Quantum algorithms for supervised and unsupervised machine learning. *arXiv:1307.0411* (2013).
- [73] Lloyd, S., Mohseni, M. and Rebentrost, P. Quantum principal component analysis. *Nature Physics*, 10, 631 (2014).
- [74] Lloyd, S., Shapiro, J. H., Wong, F. N. C., Kumar, P., Shahriar, S. M. and Yuen, H. P. Infrastructure for the quantum Internet, *ACM SIGCOMM Computer Communication Review*, 34(5):9–20 (2004).
- [75] Matsuo, T., Satoh, T., Nagayama, S. and Van Meter, R. Analysis of Measurement-based Quantum Network Coding over Repeater Networks under Noisy Conditions, *Phys. Rev. A* 97, 062328 (2018).
- [76] Monz, T. et al. Realization of a scalable Shor algorithm. *Science* 351, 1068-1070 (2016).
- [77] Moore, G. E. Cramming more components onto integrated circuits. *Electronics*, vol. 38, 8, pp.114 (1965).
- [78] Motevasel, M., Bazyari, S. Probabilistic Energy Management of micro-grids with respect to Economic and Environmental Criteria, *Science Journal (CSJ)*, Vol. 36, No: 3 Special Issue, ISSN: 1300-1949 (2015).
- [79] Munro, W. J., Stephens, A. M., Devitt, S. J., Harrison, K. A. and Nemoto, K. Quantum communication without the necessity of quantum memories, *Nature Photonics* 6, 777- 781 (2012).

- [80] Muralidharan, S., Kim, J., Lutkenhaus, N., Lukin, M. D. and Jiang, L. Ultrafast and Fault-Tolerant Quantum Communication across Long Distances, *Phys. Rev. Lett.* 112, 250501 (2014).
- [81] Neumann, F. and Witt, C. Bioinspired computation in combinatorial optimization algorithms and their computational complexity. *Natural Computing Series* (2010).
- [82] Newman, M., Watts, D. and Barabasi, A. L. *The Structure and Dynamics of Networks*, Princeton University Press (2006).
- [83] Nielsen, M. A. The entanglement fidelity and quantum error correction, *arXiv:quant-ph/9606012* (1996).
- [84] Niu, B., Fan, Y., Xiao, H. and Bing, X. Bacterial foraging based approaches to portfolio optimization with liquidity risk, *Neurocomputing* 98, 90-100 (2012).
- [85] Noelleke, C. et al, Efficient Teleportation Between Remote Single-Atom Quantum Memories, *Physical Review Letters* 110, 140403 (2013).
- [86] Ofek, N. et al. Extending the lifetime of a quantum bit with error correction in superconducting circuits. *Nature* 536, 441-445 (2016).
- [87] Pant, M., Krovi, H., Towsley, D., Tassiulas, L., Jiang, L., Basu, P., Englund, D. and Guha, S. Routing entanglement in the quantum internet, *arXiv:1708.07142* (2017).
- [88] Park, J., Lee, S. Separable states to distribute entanglement, *arXiv:1012.5162v2*, *Int. J. Theor. Phys.* 51 (2012) 1100-1110 (2010).
- [89] Petz, D. *Quantum Information Theory and Quantum Statistics*, Springer-Verlag, Heidelberg, Hiv: 6. (2008).
- [90] Pinto, D., Baran, B. Solving multiobjective multicast routing problem with a new ant colony optimization approach. *Proceedings of ACM, International IFIP/ACM Latin American Conference on Networking* (2005).

- [91] Pirandola, S. Capacities of repeater-assisted quantum communications, *arXiv:1601.00966* (2016).
- [92] Pirandola, S., Braunstein, S. L., Laurenza, R., Ottaviani, C., Cope, T. P. W., Spedalieri, G. and Banchi, L. Theory of channel simulation and bounds for private communication, *Quantum Sci. Technol.* 3, 035009 (2018).
- [93] Pirandola, S., Laurenza, R., Ottaviani, C. and Banchi, L. Fundamental limits of repeaterless quantum communications, *Nature Communications*, 15043, doi:10.1038/ncomms15043 (2017).
- [94] Preskill, J. Quantum Computing in the NISQ era and beyond, *Quantum* 2, 79 (2018).
- [95] Quantum Internet Research Group (QIRG), web: <https://datatracker.ietf.org/rg/qirg/about/> (2018).
- [96] Rak, J. *Resilient Routing in Communication Networks*, Springer (2015).
- [97] Rak, J. k-penalty: A Novel Approach to Find k-Disjoint Paths with Differentiated Path Costs, *IEEE Commun. Lett.*, vol. 14, no. 4, pp. 354-356 (2010).
- [98] Rani, B. S., Kumar, C. A. A Comprehensive Review on Bacteria Foraging Optimization Technique, *Multi-objective Swarm Intelligence*, Theoretical Advances and Applications, Studies in Computational Intelligence, Volume 592, Springer (2015).
- [99] Ren, J.-G. et al. Ground-to-satellite quantum teleportation, *Nature* 549, pages 70–73 (2017).
- [100] Rozpedek, F., Schiet, T., Thinh, L., Elkouss, D., Doherty, A., and S. Wehner, Optimizing practical entanglement distillation, *Phys. Rev. A* 97, 062333 (2018).
- [101] Saleem, G. A. D. C. M., Farooq, M. Swarm intelligence based routing protocol for wireless sensor networks: survey and future directions. *Information Sciences*, 181(20):4597-4624 (2011).

- [102] Sandberg, O. Distributed Routing in Small-World Networks, *ALLENEX* (2006).
- [103] Sangouard, N., Dubessy, R. and Simon, C. Quantum repeaters based on single trapped ions. *Phys. Rev. A*, 79, 042340 (2009).
- [104] Sangouard, N. et al., Quantum repeaters based on atomic ensembles and linear optics, *Reviews of Modern Physics* 83, 33 (2011).
- [105] Schoute, E., Mancinska, L., Islam, T., Kerenidis, I. and Wehner, S. Shortcuts to quantum network routing, *arXiv:1610.05238* (2016).
- [106] Schumacher, B. Sending quantum entanglement through noisy channels, *Phys Rev A*. 54(4), 2614-2628 (1996).
- [107] Sheng, Y. B., Zhou, L. Distributed secure quantum machine learning. *Science Bulletin*, 62, 1025-2019 (2017).
- [108] Shor, P. W. Algorithms for quantum computation: Discrete logarithms and factoring. In *Proc. 35th Symposium on Foundations of Computer Science*, 124–134, Los Alamitos, CA, IEEE Computer Society Press (1994).
- [109] Shor, P. W. Fault-tolerant quantum computation, *37th Symposium on Foundations of Computing*, IEEE Computer Society Press, pp. 56-65 (1996).
- [110] Shor, P. W. Scheme for reducing decoherence in quantum computer memory. *Phys. Rev. A*, 52, R2493-R2496 (1995).
- [111] Simon, C., de Riedmatten, H., Afzelius, M., Sangouard, N., Zbinden, H. and Gisin N. Quantum Repeaters with Photon Pair Sources and Multimode Memories. *Phys. Rev. Lett.* 98, 190503 (2007).
- [112] Streltsov, A., Kampermann, H. and Bruss, D. Quantum cost for sending entanglement, *Phys. Rev. Lett.* 108, 250501 (2012).

- [113] Taherkhani, M. A., Navi, K. and Van Meter, R. Resource-aware System Architecture Model for Implementation of Quantum aided Byzantine Agreement on Quantum Repeater Networks, *arXiv:1701.04588* (2017).
- [114] Tittel, W., Afzelius, M., Chaneliere, T., Cone, R. L., Kroll, S., Moiseev, S. A. and Sellars, M. Photon-echo quantum memory in solid state systems. *Laser Photon. Rev.* 4, 244-267 (2009).
- [115] Vandersypen, L. M. K. et al. Experimental realization of Shor's quantum factoring algorithm using nuclear magnetic resonance. *Nature* 414, 883-887 (2001).
- [116] Van Loock, P., Ladd, T. D., Sanaka, K., Yamaguchi, F., Nemoto, K., Munro, W. J. and Yamamoto, Y. Hybrid quantum repeater using bright coherent light. *Phys. Rev. Lett.* 96, 240501 (2006).
- [117] Van Meter, R. *Architecture of a Quantum Multicomputer Optimized for Shor's Factoring Algorithm*, PhD Dissertation, Keio University (2006).
- [118] Van Meter, R. *Quantum Networking*, John Wiley and Sons Ltd, ISBN 1118648927, 9781118648926 (2014).
- [119] Van Meter, R. and Devitt, S. J. Local and Distributed Quantum Computation, *IEEE Computer* 49(9), 31-42 (2016).
- [120] Van Meter, R., Ladd, T. D., Munro, W. J. and Nemoto, K. System Design for a Long-Line Quantum Repeater, *IEEE/ACM Transactions on Networking* 17(3), 1002-1013 (2009).
- [121] Van Meter, R., Satoh, T., Ladd, T. D., Munro, W. J. and Nemoto, K. Path Selection for Quantum Repeater Networks, *Networking Science*, Vol. 3, Issue 1-4, pp 82-95 (2013).
- [122] Van Meter, R., Satoh, T., Nagayama, S., Matsuo, T. and Suzuki, S. Optimizing Timing of High-Success-Probability Quantum Repeaters, *arXiv:1701.04586* (2017).

- [123] Vedral, V. and Plenio, M. B. Entanglement measures and purification procedures, *Phys. Rev. A* 57, 1619–1633 (1998).
- [124] Vedral, V. The role of relative entropy in quantum information theory, *Rev. Mod. Phys.* 74, 197–234 (2002).
- [125] Vedral, V., Plenio, M. B., Rippin, M. A. and Knight, P. L. Quantifying Entanglement, *Phys. Rev. Lett.* 78, 2275–2279 (1997).
- [126] Wang, W. et al. Efficient interference-aware TDMA link scheduling for static wireless networks. *Proceedings of ACM, International Conference on Mobile Computing and Networking* (2006).
- [127] Wehner, S., Elkouss, D., and R. Hanson. Quantum internet: A vision for the road ahead, *Science* 362, 6412 (2018).
- [128] Wootters, W. and Zurek, W. H. A single quantum cannot be cloned. *Nature*, 299:802–803, doi:10.1038/299802a0. (1982).
- [129] Xiao, Y. F., Gong, Q. Optical microcavity: from fundamental physics to functional photonics devices. *Science Bulletin*, 61, 185–186 (2016).
- [130] Yuan, Z., Chen, Y., Zhao, B., Chen, S., Schmiedmayer, J. and Pan, J. W. *Nature* 454, 1098–1101 (2008).
- [131] Zhang, W. et al. Quantum Secure Direct Communication with Quantum Memory. *Phys. Rev. Lett.* 118, 220501 (2017).
- [132] Zhang, Y., Zhou, W. and Yi, J. A Novel Adaptive Chaotic Bacterial Foraging Optimization Algorithm, *2016 International Conference on Computational Modeling, Simulation and Applied Mathematics* (2016).
- [133] Zhao, B., Chen, Z. B., Chen, Y. A., Schmiedmayer, J. and Pan, J. W. Robust creation of entanglement between remote memory qubits. *Phys. Rev. Lett.* 98, 240502 (2007).

Appendix A

List of Papers

A.1 Peer-Reviewed Journals

- [1] Gyongyosi, L. and Imre, S. A Poisson Model for Entanglement Optimization in the Quantum Internet, *Quantum Information Processing*, Springer Nature, DOI: 10.1007/s11128-019-2335-1 (2019).
- [2] Gyongyosi, L. and Imre, S. Quantum Circuit Design for Objective Function Maximization in Gate-Model Quantum Computers, *Quantum Information Processing*, Springer Nature, DOI: 10.1007/s11128-019-2326-2 (2019).
- [3] Gyongyosi, L. and Imre, S. Entanglement Access Control for the Quantum Internet, *Quantum Information Processing*, Springer Nature, DOI: 10.1007/s11128-019-2226-5 (2019).
- [4] Gyongyosi, L. and Imre, S. Opportunistic Entanglement Distribution for the Quantum Internet, *Scientific Reports*, Nature, DOI:10.1038/s41598-019-38495-w (2019).
- [5] Gyongyosi, L. and Imre, S. Adaptive Routing for Quantum Memory Failures in the Quantum Internet, *Quantum Information Processing*, Springer Nature, DOI: 10.1007/s11128-018-2153-x (2018).

- [6] Gyongyosi, L. and Imre, S. Dense Quantum Measurement Theory, *Scientific Reports*, Nature, DOI: 10.1038/s41598-019-43250-2 (2019).
- [7] Gyongyosi, L. and Imre, S. Diversity Space of Multicarrier Continuous-Variable Quantum Key Distribution, *Int. J. Commun. Syst.* (Wiley) (2019).
- [8] Gyongyosi, L. and Imre, S. A Survey on Quantum Computing Technology, *Computer Science Review*, Elsevier, DOI: 10.1016/j.cosrev.2018.11.002, ISSN: 1574-0137 (2018).
- [9] Gyongyosi, L. and Imre, S. Gaussian Quadrature Inference for Multicarrier Continuous-Variable Quantum Key Distribution, *Quantum Studies: Mathematics and Foundations*, Springer Nature, DOI: 10.1007/s40509-019-00183-9 (2019).
- [10] Gyongyosi, L. and Imre, S. Secret Key Rate Proof of Multicarrier Continuous-Variable Quantum Key Distribution, *Int. J. Commun. Syst.* (Wiley), DOI: 10.1002/dac.3865, ISSN: 1099-1131 (2018).
- [11] Gyongyosi, L. and Imre, S. Reconciliation Optimization for Continuous-Variable Quantum Key Distribution, *SPIE Photonics West OPTO 2019 Proceedings* (2019).
- [12] Gyongyosi, L. and Imre, S. Topology Adaption for the Quantum Internet, *Quantum Information Processing*, Springer Nature, DOI:10.1038/s41598-018-30957-x, ISSN: 1570-0755, 1573-1332 (2018).
- [13] Gyongyosi, L. and Imre, S. Multilayer Optimization for the Quantum Internet, *Scientific Reports*, Nature, DOI:10.1038/s41598-018-30957-x (2018).
- [14] Gyongyosi, L. and Imre, S. Decentralized Base-Graph Routing for the Quantum Internet, *Physical Review A*, American Physical Society DOI: 10.1103/PhysRevA.98.022310 (2018).

- [15] Gyongyosi, L. and Imre, S. Entanglement Availability Differentiation Service for the Quantum Internet, *Scientific Reports*, Nature, DOI:10.1038/s41598-018-28801-3 (2018).
- [16] Gyongyosi, L. and Imre, S. Multiple Access Multicarrier Continuous-Variable Quantum Key Distribution, *Chaos, Solitons and Fractals*, Elsevier DOI: 10.1016/j.chaos.2018.07.006, ISSN: 0960-0779 (2018).
- [17] Gyongyosi, L., Imre, S. and Nguyen, H. V. A Survey on Quantum Channel Capacities, *IEEE Communications Surveys and Tutorials*, IEEE DOI: 10.1109/COMST.2017.2786748 (2018).
- [18] Gyongyosi, L. and Imre, S. Low-Dimensional Reconciliation for Continuous-Variable Quantum Key Distribution, *Appl. Sci.*, DOI: 10.3390/app8010087, ISSN 2076-3417 (2018).
- [19] Gyongyosi, L. and Imre, S. A Poisson Model for Entanglement Optimization in the Quantum Internet, *2018 SPIE Quantum Information Science, Sensing, and Computation Proceedings* (2018).
- [20] Gyongyosi, L. and Imre, S. Dynamic Topology Resilience for Quantum Networks, *2018 SPIE Photonics West OPTO Proceedings* (2018).
- [21] Gyongyosi, L. and Imre, S. Entanglement-Gradient Routing for Quantum Networks, *Scientific Reports*, Nature, DOI:10.1038/s41598-017-14394-w (2017).
- [22] Gyongyosi, L. Quantum Imaging of High-Dimensional Hilbert Spaces with Radon Transform, *International Journal of Circuit Theory and Applications (IJCTA)*, *Special Issue on Quantum Circuits* (Wiley) (2017).
- [23] Mraz, A., Kis, Zs., Bacsardi, L. and Gyongyosi, L. Quantum Circuit-based Modeling of Continuous-Variable Quantum Key Distribution System, *International Journal*

- of Circuit Theory and Applications (IJCTA), Special Issue on Quantum Circuits* (Wiley) (2017).
- [24] Gyongyosi, L. and Imre, S. Statistical Quadrature Evolution by Inference for Continuous-Variable Quantum Key Distribution, *SPIE Photonics West OPTO 2017 Proceedings, "Advances in Photonics of Quantum Computing, Memory, and Communication X"* (2016).
- [25] Gyongyosi, L. and Imre, S. Gaussian Quadrature Inference for Continuous-Variable Quantum Key Distribution, *Proceedings of SPIE Quantum Information and Computation IX* (2016).
- [26] Gyongyosi, L. and Imre, S. Adaptive Gaussian Quadrature Detection for Continuous-Variable Quantum Key Distribution, *SPIE Photonics West OPTO 2016 Proceedings, "Advances in Photonics of Quantum Computing, Memory, and Communication IX"* (2015).
- [27] Gyongyosi, L. and Imre, S. Multidimensional Manifold Extraction for Multicarrier Continuous-Variable Quantum Key Distribution, *Proceedings of SPIE Quantum Information and Computation XIII* (2015).
- [28] Gyongyosi, L. A Statistical Model of Information Evaporation of Perfectly Reflecting Black Holes, *International Journal of Quantum Information (IJQI)*, ISSN 0219-7499 (print), 1793-6918 (online) (2014).
- [29] Gyongyosi, L. The Private Classical Capacity of a Partially Degradable Quantum Channel, *Physica Scripta - Special Issue on Quantum Information*, Institute of Physics (IOP), Online ISSN: 1402-4896 Print ISSN: 0031-8949 (2014).
- [30] Gyongyosi, L. and Imre, S. Eigenchannel Decomposition for Continuous-Variable Quantum Key Distribution, *SPIE Photonics West OPTO 2015 Proceedings, "Advances in Photonics of Quantum Computing, Memory, and Communication VIII"*, (2015).

- [31] Gyongyosi, L. The Structure and Quantum Capacity of a Partially Degradable Quantum Channel, *IEEE Access*, ISSN: 2169-3536 (2014).
- [32] Gyongyosi, L. and Imre, S. Geometrical Analysis of Physically Allowed Quantum Cloning Transformations for Quantum Cryptography, *Information Sciences*, ELSEVIER, ISSN: 0020-0255; (2014).
- [33] Gyongyosi, L. Quantum Information Transmission over a Partially Degradable Channel, *IEEE Access*, ISSN: 2169-3536 (2014).
- [34] Gyongyosi, L. The Correlation Conversion Property of Quantum Channels, *Quantum Information Processing*, Springer, ISSN: 1570-0755 (print version), ISSN: 1573-1332 (electronic version). (2013).
- [35] Gyongyosi, L. and Imre, S. Adaptive Multicarrier Quadrature Division Modulation for Continuous-Variable Quantum Key Distribution, *Proceedings of SPIE Quantum Information and Computation XII* (2014).
- [36] Gyongyosi, L. and Imre, S. Long-distance Continuous-Variable Quantum Key Distribution with Advanced Reconciliation of a Gaussian Modulation, *Proceedings of SPIE Photonics West OPTO 2013, „Advances in Photonics of Quantum Computing, Memory, and Communication VII”* (2014).

A.2 Conference Papers

- [1] Gyongyosi, L. and Imre, S. Dense Measurements for Gate-Model Quantum Computers, *Bulletin of the American Physical Society*, APS March Meeting 2018, Session on General Quantum Information and Quantum Computation, March 4–8, 2019; Boston, Massachusetts, USA.
- [2] Gyongyosi, L. and Imre, S. Time Complexity Reduction for Gate-Model Quantum

- Computers, *Proceedings of SPIE Quantum Information Science, Sensing, and Computation XI*, 14 - 18 April 2019, Baltimore, Maryland, USA.
- [3] Gyongyosi, L. and Imre, S. Dense Measurements for Quantum Computations, *Proceedings of Quantum Information and Measurement (QIM) V: Quantum Technologies*, OSA (The Optical Society of America), 04 April 2019 – 06 April 2019, University of Rome La Sapienza, Rome, Italy.
- [4] Gyongyosi, L. and Imre, S. A Universal Quantum Algorithm for Time Complexity Reduction of Quantum Computers, *Proceedings of Quantum Information Processing 2019 (QIP 2019)*, January 14-18, 2019, University of Colorado Boulder, USA.
- [5] Gyongyosi, L. and Imre, S. Improved Reconciliation for Continuous-Variable Quantum Key Distribution, *Proceedings of Advances in Photonics of Quantum Computing, Memory, and Communication XII*, SPIE OPTO 2019, 7 - 2 February 2019, San Francisco, California, USA.
- [6] Gyongyosi, L. and Imre, S. Problem Solving Optimization by Machine Learning for Gate-Model Quantum Computers, *Proceedings of Quantum Techniques in Machine Learning (QTML2018)*, 12-16 Nov. 2018, Durban, South Africa.
- [7] Gyongyosi, L. and Imre, S. Unsupervised Machine Learning Control of Quantum Gates in Gate-Model Quantum Computers, *Proceedings of the Frontiers in Optics 2018 (FiO 2018)*, Optical Society of America (OSA), 16-20 Sept. 2018, Washington, D.C., USA.
- [8] Gyongyosi, L. and Imre, S. Entanglement Concentration Service for the Quantum Internet, *Proceedings of the Frontiers in Optics 2018 (FiO 2018)*, Optical Society of America (OSA), 16-20 Sept. 2018, Washington, D.C., USA.
- [9] Gyongyosi, L. and Imre, S. Post-Processing Optimization for Continuous-Variable Quantum Key Distribution, *Proceedings of QCrypt 2018, 8th International Conference on Quantum Cryptography*, 27–31 August 2018, Shanghai, China.

- [10] Gyongyosi, L. and Imre, S. Layout Generation with Decoherence Estimation for Gate-Model Quantum Computer Architectures, *Bulletin of the American Physical Society*, APS DAMOP, 49th Annual Meeting of the APS Division of Atomic, Molecular and Optical Physics APS Meeting, Session on Quantum Information Science, May 28–June 1 2018; Ft. Lauderdale, Florida, USA.
- [11] Gyongyosi, L. Quantum Circuit Design Automation for Quantum Computers, *Proceedings of the 2018 International Conference on Quantum Communication, Measurement and Computing (QCMC 2018)*, March 12-16, 2018, Louisiana State University, Baton Rouge, USA.
- [12] Gyongyosi, L. and Imre, S. A Poisson Model for Entanglement Optimization in the Quantum Internet, *Proceedings of SPIE Quantum Information Science, Sensing, and Computation X*, 15 - 19 April 2018, Orlando, Florida, USA.
- [13] Gyongyosi, L. and Imre, S. Quantum Circuit Designs for Gate Model Quantum Computers, *Bulletin of the American Physical Society*, APS March Meeting 2018, APS Division of Quantum Information (DQI) Session, March 5–9, 2018; Los Angeles, California, USA.
- [14] Gyongyosi, L. and Imre, S. Dynamic Topology Resilience for Quantum Networks, *Advances in Photonics of Quantum Computing, Memory, and Communication XI*, SPIE OPTO 2018, 27 January - 1 February 2018, San Francisco, California, USA.
- [15] Gyongyosi, L. Entanglement Distribution and Routing in Quantum Communication Networks, *Quantum Summit 2017*, 11-17 Oct 2017, Chengdu, China.
- [16] Gyongyosi, L. Efficient Decentralized Routing in Quantum Networks, *QCrypt 2017, 7th International Conference on Quantum Cryptography*, 18-22 Sept 2017, University of Cambridge, Cambridge, United Kingdom.
- [17] Gyongyosi, L. Multicarrier Continuous-Variable Quantum Key Distribution, *QCrypt*

2017, *7th International Conference on Quantum Cryptography*, 18-22 Sept 2017, University of Cambridge, Cambridge, United Kingdom.

- [18] Gyongyosi, L. and Imre, S. Hamiltonian Dynamics for Entanglement Distribution in Quantum Networks, *SPIE Quantum Communications and Quantum Imaging XV*, 6 - 10 August 2017, San Diego, California, USA.
- [19] Gyongyosi, L. and Imre, S. Decentralized Routing and Diameter Bounds in Entangled Quantum Networks, *APS DAMOP 2017*, 48th Annual Meeting of the APS Division of Atomic, Molecular and Optical Physics, Session on Quantum Networks and Photon Sources, Bulletin of the American Physical Society, The American Physical Society, June 5–9, 2017; Sacramento, California, USA.
- [20] Gyongyosi, L. and Imre, S. Fast Entanglement Establishment via Local Dynamics for Quantum Repeater Networks, *APS March Meeting 2017*, Session on Entanglement in Open Quantum Systems, Bulletin of the American Physical Society, The American Physical Society, March 13–17, 2017; New Orleans, Louisiana, USA.
- [21] Gyongyosi, L. and Imre, S. Statistical Quadrature Evolution by Inference for Continuous-Variable Quantum Key Distribution, *SPIE Photonics West OPTO 2017*, “*Advances in Photonics of Quantum Computing, Memory, and Communication X*”, 28 Jan - 2 Feb 2017, San Francisco, California, USA.
- [22] Gyongyosi, L. and Imre, S. Statistical Quadrature Evolution for Continuous-Variable Quantum Key Distribution, *APS DAMOP 2016*, *47th Annual Meeting of the APS Division of Atomic, Molecular, and Optical Physics*, Section on Quantum Information Theory, Bulletin of the American Physical Society, The American Physical Society, Volume 61, Number 7, May 23–27, 2016; Providence, Rhode Island, USA.
- [23] Gyongyosi, L. and Imre, S. Diversity Extraction for Multicarrier Continuous-Variable Quantum Key Distribution, *IEEE Signal Processing Conference Proceedings*, 2016

- 24th European Signal Processing Conference (EUSIPCO 2016), Section on Quantum Communications, Budapest, 29 Aug - 2 Sept (2016).
- [24] Mraz, A., Gyongyosi, L. and Imre, S. Performance Evaluation of Scalar Reconciliation for Continuous-Variable Quantum Key Distribution, *IEEE Signal Processing Conference Proceedings*, 2016 24th European Signal Processing Conference (EUSIPCO 2016), Section on Quantum Communications, Budapest, 29 Aug - 2 Sept (2016).
- [25] Gyongyosi, L. and Imre, S. Gaussian Quadrature Inference for Continuous-Variable Quantum Key Distribution, *SPIE Quantum Information and Computation IX*, 17 - 21 Apr 2016, Baltimore, Maryland, USA (2016).
- [26] Gyongyosi, L. and Imre, S. Adaptive Gaussian Quadrature Detection for Continuous-Variable Quantum Key Distribution, *SPIE Photonics West OPTO 2016, "Advances in Photonics of Quantum Computing, Memory, and Communication IX"*, 13-18 Feb 2016, San Francisco, California, USA.
- [27] Gyongyosi, L. Entropy Transfer of Quantum Gravity Information Processing, *APS DAMOP 2015, 46th Annual Meeting of the APS Division of Atomic, Molecular, and Optical Physics*, Bulletin of the American Physical Society, The American Physical Society, Volume 60, Number 7, June 8–12, 2015; Columbus, Ohio, USA.
- [28] Gyongyosi, L. and Imre, S. Multidimensional Manifold Extraction for Multicarrier Continuous-Variable Quantum Key Distribution, *SPIE Quantum Information and Computation XIII*, 20 - 24 Apr 2015, Baltimore, Maryland, USA (2015).
- [29] Gyongyosi, L. and Imre, S. Adaptive Quadrature Detection for Multicarrier Continuous-Variable Quantum Key Distribution, *APS March Meeting 2015*, Session on Quantum Foundations and Technologies, Bulletin of the American Physical Society, March 2–6, 2015; San Antonio, Texas, USA.

- [30] Gyongyosi, L. and Imre, S. Eigenchannel Decomposition for Continuous-Variable Quantum Key Distribution, *SPIE Photonics West OPTO 2015*, “*Advances in Photonics of Quantum Computing, Memory, and Communication VIII*”, 7-12 Feb 2015, San Francisco, California, USA.
- [31] Gyongyosi, L. Singular Layer Transmission for Continuous-Variable Quantum Key Distribution, *2014 IEEE Photonics Conference*, 12 - 16 October 2014, San Diego, California USA.
- [32] Gyongyosi, L. and Imre, S. Quantum Imaging of High-Dimensional Hilbert Spaces with Radon Transform, *2014 Frontiers in Optics/Laser Science XXX (FiO/LS)*, 19-23 October 2014, Tucson, Arizona, USA.
- [33] Gyongyosi, L. and Imre, S. Information Processing with Quantum Gravity, *Photon14 Conference*, Quantum Electronics and Photonics 2014, Section on Quantum Information, Institute of Physics (IOP), Imperial College London, London, UK.
- [34] Gyongyosi, L. Information Processing Structure of Quantum Gravity, *Gordon Research Conference on Quantum Science: Simulation, Verification, and Control of Complex Quantum Many-Body Systems*, July 27 - August 1, Stonehill College, Easton, MA, USA (2014).
- [35] Gyongyosi, L. Multiuser Quadrature Allocation for Continuous-Variable Quantum Key Distribution, *Quantum Theory from Problems to Advances (QTPA)*, International Centre for Mathematical Modeling in physics, engineering and cognitive sciences (ICMM), June 9-12, 2014, Linnaeus University, Växjö, Sweden.
- [36] Gyongyosi, L. Quantum Imaging of High-Dimensional Hilbert Spaces with Radon Transform, *Quantum Theory from Problems to Advances (QTPA)*, International Centre for Mathematical Modeling in physics, engineering and cognitive sciences (ICMM), June 9-12, 2014, Linnaeus University, Växjö, Sweden.

- [37] Gyongyosi, L. and Imre, S. Information Processing with Quantum Gravity Environment, *Quantum Theory from Problems to Advances (QTPA)*, International Centre for Mathematical Modeling in physics, engineering and cognitive sciences (ICMM), June 9-12, 2014, Linnaeus University, Växjö, Sweden.
- [38] Gyongyosi, L. and Imre, S. Information Processing Structure of Quantum Gravity, *APS DAMOP 2014*, 45th Annual Meeting of the APS Division of Atomic, Molecular and Optical Physics, *Session on Quantum Information Theory*, The American Physical Society, Volume 59, Number 8, June 2–6, 2014; Madison, Wisconsin, USA.
- [39] Gyongyosi, L. and Imre, S. Adaptive Multicarrier Quadrature Division Modulation for Continuous-Variable Quantum Key Distribution, *SPIE Quantum Information and Computation XII*, 8 - 9 May 2014, Baltimore, Maryland, USA (2014).
- [40] Gyongyosi, L. and Imre, S. Long-Distance Continuous-Variable Quantum Key Distribution with Scalar Reconciliation and Gaussian Adaptive Multicarrier Quadrature Division, *APS March Meeting 2014*, Session on Quantum Communication, Decoherence, and Cryptography, Bulletin of the American Physical Society, Volume 59, Number 1, March 3–7, 2014; Denver, Colorado, USA.
- [41] Gyongyosi, L. and Imre, S. Long-distance two-way continuous variable quantum key distribution over optical fiber with Gaussian modulation, *SPIE Photonics West OPTO 2014*, „*Advances in Photonics of Quantum Computing, Memory, and Communication VII*”, Session: Quantum Communication and Quantum Computing with Photons II, 1-6 Feb 2014, San Francisco, California, USA.
- [42] Gyongyosi, L. Long-Distance Two-way Continuous-Variable Quantum Key Distribution with a Gaussian Modulation, *Single Photon Workshop 2013 (SPW 2013)*, Oak Ridge National Laboratory, Quantum Information Science Group, Oct. 15-18, 2013, Oak Ridge, USA.

- [43] Gyongyosi, L. Improved Long-Distance Two-way Continuous Variable Quantum Key Distribution over Optical Fiber, Session on Quantum Communications, *2013 Frontiers in Optics/Laser Science XXIX (FiO/LS)*, 6-10 October 2013, Orlando, Florida, USA.
- [44] Gyongyosi, L. and Imre, S. Entanglement Sharing without Entanglement Transmission, Session on Quantum Communications, *2013 Frontiers in Optics/Laser Science XXIX (FiO/LS)*, 6-10 October 2013, Orlando, Florida, USA.
- [45] Gyongyosi, L. and Imre, S. Quantum Communication over Partially Degradable Quantum Channels, Session on Optics and Photonics of Disordered Systems, *2013 Frontiers in Optics/Laser Science XXIX (FiO/LS)*, 6-10 October 2013, Orlando, Florida, USA.
- [46] Gyongyosi, L. and Imre, S. Long-Distance Two-way Continuous Variable Quantum Key Distribution over Optical Fiber with Gaussian Modulation, *IONS-NA 7, 7th North American IONS conference*, 2-4 Oct 2013, Center for Optoelectronics and Optical Communications, The University of North Carolina at Charlotte (UNCC), USA.
- [47] Gyongyosi, L. The Correlation Conversion Property of Quantum Channels, *Quantum Foundations and Quantum Information (QFQI)*, International Centre for Mathematical Modeling in physics, engineering and cognitive sciences (ICMM), June 10-13, 2013, Linnaeus University, Växjö, Sweden.
- [48] Gyongyosi, L. and Imre, S. The Quantum Capacity of a Partially Degradable Quantum Channel, *Quantum Foundations and Quantum Information (QFQI)*, International Centre for Mathematical Modeling in physics, engineering and cognitive sciences (ICMM), June 10-13, 2013, Linnaeus University, Växjö, Sweden.
- [49] Gyongyosi, L. and Imre, S. Polar Codes for Partially Degradable Quantum Channels, *Quantum Foundations and Quantum Information (QFQI)*, International Cen-

tre for Mathematical Modeling in physics, engineering and cognitive sciences (ICMM), June 10-13, 2013, Linnaeus University, Växjö, Sweden.

- [50] Gyongyosi, L. and Imre, S. Quantum Channels that cannot Transmit Quantum Correlations can Generate Quantum Entanglement from Classical Correlation, *APS DAMOP 2013*, The 44th Annual DAMOP Meeting of the APS Division of Atomic, Molecular, and Optical Physics (American Physical Society), Section on Quantum Information and Communication, Jun. 2013, Quebec City, Quebec, Canada.
- [51] Gyongyosi, L. Polaractivation of Hidden Private Classical Capacity Region of Quantum Channels, *IEEE Symposium on Quantum Computing and Computational Intelligence 2013 (IEEE QCCI 2013)*, IEEE Symposium Series on Computational Intelligence (IEEE SSCI 2013), 16-19 Apr 2013, Singapore.
- [52] Gyongyosi, L. and Imre, S. Pilot Quantum Error Correction for Global-Scale Quantum Communications, *IEEE Symposium on Quantum Computing and Computational Intelligence 2013 (IEEE QCCI 2013)*, IEEE Symposium Series on Computational Intelligence (IEEE SSCI 2013), 16-19 Apr 2013, Singapore.
- [53] Gyongyosi, L. and Imre, S. The Correlation Conversion Property of Quantum Channels, *SPIE Quantum Information and Computation XI*, Session on Quantum Entanglement, 29 April - 3 May 2013, Baltimore, Maryland, USA.

Appendix B

Extended Routing Services for the Quantum Internet

This appendix proposes an extended application [32] of the routing service [33] of Chapter 3.

B.1 Introduction

Here we define an adaptive routing method for the management of quantum memory failures in the quantum Internet. In the quantum Internet, the entangled quantum states are stored in the local quantum memories of the quantum nodes. A quantum memory failure in a particular quantum node can destroy several entangled connections in the entangled network. A quantum memory failure event makes the immediate and efficient determination of shortest replacement paths an emerging issue in a quantum Internet scenario. The replacement paths omit those nodes that are affected by the quantum memory failure to provide a seamless network transmission. In the proposed solution, the shortest paths are determined by the routing service of Chapter 3.

B.1.1 Results

The novel contributions of this chapter are as follows:

1. *We define a dynamic adaptive routing method for the management of quantum memory failures in the quantum Internet.*
2. *The proposed algorithm determines shortest node-disjoint replacement paths in the entangled network structure of the quantum Internet, and minimizes the number of losable entangled contacts in a main-path.*
3. *The shortest node-disjoint replacement paths in the entangled quantum network are determined in a decentralized manner with high computational efficiency.*

This appendix is organized as follows. In Section B.2, we characterize the problem and the impacts of a quantum memory failure scenario in an entangled quantum network. In Section B.3, we discuss the determination of shortest node-disjoint replacement paths and evaluate the complexity of the method. A performance evaluation is included in Section B.4.

B.2 System Model

Let us assume that an overlay entangled quantum network N is given, where the set \mathcal{S}^* of entangled connections is determined in the base-graph G^k [33] such that $\Pr_{L_l}(x, y) \geq \Pr_{L_l}^*$, where $\Pr_{L_l}^*$ is a threshold probability of an L_l -level entangled connection E_h .

A repeater node is referred to as a high-degree node, $\tilde{\phi}(R_i)$, if $\deg(\tilde{\phi}(R_i)) > \deg'(V)$, $\tilde{\phi}(R_i) \in G^k$, where $\deg'(V)$ is the threshold degree of node set V determined for the given entangled overlay quantum network N .

In our network model, the high-degree nodes are omitted from the shortest main path \mathcal{P} . The explanation of this phenomenon is as follows. Since a $\tilde{\phi}(R_i)$ high-degree node stores the highest number of entangled quantum systems in its local quantum memory, a

quantum memory failure in $\tilde{\phi}(R_i)$ will result in the loss of the highest number of entangled connections in the quantum network. A rational decision is therefore explained as follows. Use only the standard (non-high-degree nodes) in \mathcal{P} , since if a quantum memory failure occurs in a standard node $\phi(R_i) \in G^k$ of \mathcal{P} , the high-degree nodes still can participate in a shortest replacement path \mathcal{P}' . It is because a replacement path is used for only a short time while the re-establishment of the destroyed entangled contacts of $\phi(R_i)$ in \mathcal{P} is in progress. As the entangled connections of $\phi(R_i)$ are restored after the memory failure, the transmission continues on the main path \mathcal{P} .

Because the main path \mathcal{P} omits high-degree nodes, the average length (number of nodes) of the path increases with respect to the shortest path in \mathcal{S}^* , but the risk that a high number of entangled connections will vanish during a quantum memory failure is therefore reduced to a minimum. The length of the replacement path \mathcal{P}' will be shorter than \mathcal{P} , for \mathcal{P}' can contain the high-degree nodes.

Without loss of generality, in a quantum communication scenario, a quantum path with highest number of entangled connections usually means high communication efficiency and stability. It is also the situation for the shortest path \mathcal{P} determined by our method, however, these attributes are achieved through the application of an increased number of non high-degree nodes, instead of the use of some high-degree nodes. In the proposed model, a high number of the non-high-degree nodes in the quantum network also yields a high number of entangled connections for the paths; therefore the shortest path will have a high efficiency, reliability and stability.

A quantum memory failure situation in an overlay quantum repeater network N is illustrated Fig. B.1. The actual shortest path \mathcal{P} contains no high-degree repeater nodes, for a memory failure would destroy a high number of entangled contacts in the network (Fig. B.1(a)). A quantum memory failure in an intermediate (non-high-degree) quantum repeater node R_{q-2} requires the immediate establishment of a replacement shortest path \mathcal{P}' in the base-graph. The new shortest path \mathcal{P}' contains the high-degree repeater nodes $\tilde{R}_{q'-2}$ and $\tilde{R}_{q'-1}$, for \mathcal{P}' is used only while the re-establishment of the entangled contacts

of R_{q-2} is not completed (Fig. B.1(b)).

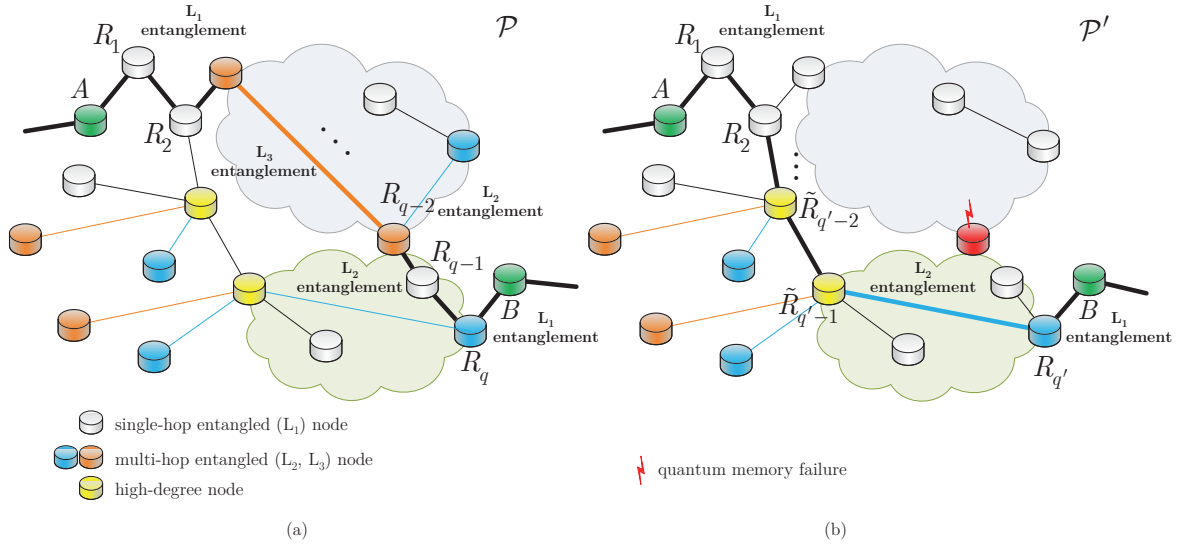


Figure B.1: A scenario of a quantum memory failure in an entangled overlay quantum network N . (a) The main path \mathcal{P} consists of a source node A and target node B , with several quantum repeater nodes R_i , $i = 1, \dots, q$ connected through multi-level entangled connections. The quantum nodes are referred to as single-hop entangled (L_1 -level, depicted by gray nodes) and multi-hop entangled (L_2 - and L_3 -level, depicted by blue and orange nodes). The actual shortest main path \mathcal{P} determined in the base-graph is depicted by the bold lines. The high-degree nodes (depicted by yellow) store the highest number of entangled states in their quantum memories and are not included in \mathcal{P} . (b) A quantum memory failure in repeater node R_{q-2} (depicted by red) destroys all entangled contacts of the given node. For seamless transmission, a node-disjoint shortest replacement path \mathcal{P}' is needed between source node R_2 and target node R_q , through high-degree repeater nodes $\tilde{R}_{q'-2}$ and $\tilde{R}_{q'-1}$. Path \mathcal{P}' between $\phi(R_2) \in G^k$ and $\phi(R_q) \in G^k$ is determined by a decentralized routing \mathcal{A} in the base-graph G^k .

B.2.1 Quantum Memory Failures

The proposed method utilizes different coefficients for the entangled connections of a shortest main path \mathcal{P} and shortest replacement path \mathcal{P}' , which distinction defines the problem of finding node-disjoint paths of a multi-level entangled quantum network. Particularly, this problem is analogous to a min-sum (minimize the sum of costs of connection

paths) problem [63, 64, 96, 97] in a multi-cost network, which is an NP-complete problem [63, 96]. Note that similar to the determination of a shortest main path \mathcal{P} , the replacement path \mathcal{P}' is also determined by our decentralized routing \mathcal{A} in a base-graph.

Shortest Paths at a Quantum Memory Failure

Using the decentralized routing \mathcal{A} (see Chapter 3) in G'^k , the shortest path with respect to the scaled coefficient $s(\zeta(\cdot))$ can be determined in at most $\mathcal{O}(\log n)^2$ steps, as follows.

Using the results of Chapter 3, the term $d((\phi(x), \phi(y)))^k$ can be expressed as

$$d((\phi(x), \phi(y)))^k = \frac{p(\phi(x), \phi(y))}{p(\phi(x), \phi(y)) H_n(p(\phi(x), \phi(y)) - c_{\phi(x), \phi(y)})}, \quad (\text{B.1})$$

thus at a given k , the $d((\phi(x), \phi(y)))$ distance function between $\phi(x), \phi(y)$ is as

$$d((\phi(x), \phi(y))) = \sqrt[k]{\frac{p(\phi(x), \phi(y))}{p(\phi(x), \phi(y)) H_n(p(\phi(x), \phi(y)) - c_{\phi(x), \phi(y)})}}. \quad (\text{B.2})$$

Using the $\phi(x), \phi(y)$ maps of the nodes and the scaled cost $s(\zeta(E(\phi(x), \phi(y)))) \in [0, 1]$, a base-graph G'^k is constructed with transformed node positions $\phi'(x), \phi'(y)$ as follows.

The aim is then to find $\phi'(x), \phi'(y)$ at a given $s(\zeta(E(\phi(x), \phi(y))))$, via a target distance $d((\phi'(x), \phi'(y)))$.

To determine the $\phi'(\cdot)$ scaled positions, we first identify $s(\zeta(E(\phi(x), \phi(y))))$ by $p(\phi(x), \phi(y))$ as

$$p(\phi(x), \phi(y)) = s(\zeta(E(\phi(x), \phi(y)))) , \quad (\text{B.3})$$

from which the target distance $d((\phi'(x), \phi'(y)))$ between $\phi'(x), \phi'(y) \in G'^k$ is as

$$d((\phi'(x), \phi'(y))) = \sqrt[k]{\frac{s(\zeta(E(\phi(x), \phi(y))))}{s(\zeta(E(\phi(x), \phi(y)))) H_n(s(\zeta(E(\phi(x), \phi(y)))) - c_{\phi(x), \phi(y)})}}. \quad (\text{B.4})$$

The distance function in (B.4) is therefore results of the scaled positions $\phi'(x), \phi'(y)$ in G'^k at a given reference position.

Specifically, to establish a given shortest main path \mathcal{P} between a source node $\phi(s)$ and target node $\phi(t)$ such that \mathcal{P} contains no high-degree repeater node $\tilde{\phi}(R_i)$, a given entangled connection $E_h(\phi(x), \phi(y))$, $E_h \in \mathcal{P}$ between nodes $\phi(x), \phi(y) \in G^k$ in the main path \mathcal{P} is weighted by the coefficient $\gamma(E_h)$:

$$\gamma(E_h) = \frac{\beta(\phi(x)) + \beta(\phi(y))}{2}, \quad (\text{B.5})$$

where $\beta(\phi(n))$ is defined as a normalization, precisely

$$\beta(\phi(n)) = \frac{\chi(\phi(n))}{\max_i \chi(\phi(i))}, \quad (\text{B.6})$$

where

$$\chi(\phi(n)) = \sum_{\phi(p) \neq \phi(q)} s \frac{|\mathcal{P}_{\phi(n)}(\phi(p), \phi(q))|}{|\mathcal{P}(\phi(p), \phi(q))|}, \quad (\text{B.7})$$

where $|\mathcal{P}_{\phi(n)}(\phi(p), \phi(q))|$ is the number of shortest paths (of the same minimal length) between nodes $\phi(p), \phi(q) \in G^k$ and traversing node $\phi(n)$, and where $|\mathcal{P}(\phi(p), \phi(q))|$ is the number of shortest paths (of the same minimal length) between nodes $\phi(p), \phi(q) \in G^k$.

Let us assume that in an intermediate repeater node $\phi(R_i)$, a quantum memory failure occurs on the main path $\mathcal{P}(\phi(A), \phi(B))$, which destroys all entangled contacts of that node. For seamless communication, an immediate shortest replacement path $\mathcal{P}'(\phi(s), \phi(r))$ has to be established between nodes $\phi(s), \phi(r) \in G^k$. The replacement shortest path, however, can contain the high-degree nodes $\tilde{\phi}(R_i)$, which have been removed from the main path $\mathcal{P}(\phi(A), \phi(B))$. The replacement shortest path $\mathcal{P}'(\phi(s), \phi(r))$ is aimed to serve as only a temporary path. It replaces the main path $\mathcal{P}(\phi(A), \phi(B))$ while the entangled contacts of $\phi(R_i)$ have not been completely re-established.

For a given connection E_h of the replacement shortest path $\mathcal{P}'(\phi(s), \phi(r))$, the con-

nection coefficient (B.5) is redefined as

$$\tau(E_h) = \frac{\gamma(E_h)}{\max_i \gamma(E_i)}, \quad (\text{B.8})$$

which provides a normalized metric for E_h in $\mathcal{P}'(\phi(s), \phi(r))$.

Using coefficients (B.5) and (B.8), the optimization problem formulates a minimization, without loss of generality as

$$\Phi(C) = \min \left(\sum_{k \in K} \sum_{h \in E} \gamma(E_h) C_{k,h} + \sum_{k \in K} \sum_{h \in E} \tau(E_h) Z_{k,h} \right), \quad (\text{B.9})$$

where K is the set of users, k is the index of a given user U_k , E is a set of entangled (directed) connections, h is the index of a given connection E_h , $C_{k,h}$ is a variable that equals 1 if the entangled connection E_h is used by the main path \mathcal{P} associated with user U_k (0 otherwise), and $Z_{k,h}$ is a variable that equals 1 if the entangled connection E_h is used by the replacement path \mathcal{P}' associated with user U_k .

The optimization in (B.9) is therefore a minimization of the overall cost coefficient of the flows by means of main path \mathcal{P} and replacement path \mathcal{P}' , subject to some constraints. These constraints are described next.

Particularly, for the main path \mathcal{P} , a flow conservation rule [63, 96] leads to precisely

$$\Delta(C_{k,h}) = \sum_{\mathcal{X}_{h,j}} C_{k,h} - \sum_{\mathcal{X}_{h,i}} C_{k,h}, \quad (\text{B.10})$$

where

$$\begin{aligned} \mathcal{X}_{h,j} = h \in \left\{ h : E_h \left(\phi(x_w)_{U_k}, \phi(x_j)_{U_k} \right) \in E; \right. \\ \left. \phi(x_j)_{U_k} \in V; \right. \\ \left. \phi(x_j)_{U_k} \neq \phi(x_w)_{U_k} \right\}, \end{aligned} \quad (\text{B.11})$$

where $\phi(x_w)_{U_k} \in G^k$ is a node associated with the demand of user $k \in K$, where $E_h \left(\phi(x_w)_{U_k}, \phi(x_j)_{U_k} \right)$ is an egress connection incident associated with node $\phi(x_w)_{U_k} \in$

G^k , where $E_h(\phi(x_i)_{U_k}, \phi(x_w)_{U_k})$ is an ingress connection incident associated with node $\phi(x_w)_{U_k} \in G^k$, and where

$$\begin{aligned} \mathcal{X}_{h,i} = h \in \{ & h : E_h(\phi(x_i)_{U_k}, \phi(x_w)_{U_k}) \in E; \\ & \phi(x_i)_{U_k} \in V; \\ & \phi(x_i)_{U_k} \neq \phi(x_w)_{U_k} \}. \end{aligned} \quad (\text{B.12})$$

Using (B.11) and (B.12), $\Delta(C_{k,h})$ can be evaluated as

$$\Delta(C_{k,h}) = \begin{cases} 1, & \text{if } \phi(x_w)_{U_k} = \phi(A)_{U_k} \\ -1, & \text{if } \phi(x_w)_{U_k} = \phi(B)_{U_k} \\ 0, & \text{otherwise} \end{cases} . \quad (\text{B.13})$$

Similarly, for the replacement path \mathcal{P}' , the following constraint is defined via (B.11) and (B.12):

$$\Delta(Z_{k,h}) = \sum_{\mathcal{X}_{h,j}} Z_{k,h} - \sum_{\mathcal{X}_{h,i}} Z_{k,h} = \begin{cases} 1, & \text{if } \phi(x_w)_{U_k} = \phi(A)_{U_k} \\ -1, & \text{if } \phi(x_w)_{U_k} = \phi(B)_{U_k} \\ 0, & \text{otherwise} \end{cases} . \quad (\text{B.14})$$

For a given entangled connection E_h , the following relation states that the requested number of entangled states of a particular fidelity F on the main path \mathcal{P} and replacement path \mathcal{P}' is bounded as:

$$\varphi(E_h) = \sum_{k \in K} (C_{k,h} Q^{(F)}(U_k) + Z_{k,h} Q^{(F)}(U_k)) \leq Q^{(F)}(E_h), \quad (\text{B.15})$$

where $Q^{(F)}(E_h)$ refers to the number of d -dimensional maximally entangled states per second of a particular fidelity F available through the entangled connection E_h (entanglement throughput), and where $Q^{(F)}(U_k)$ is the demand of U_k associated with the entangled connection E_h with respect to the number of d -dimensional maximally entangled states

per second of a particular fidelity F .

Because \mathcal{P} and \mathcal{P}' are node-disjoint paths in our model, the following constraint holds for a given E_h and U_k :

$$C_{k,h} + Z_{k,h} \leq 1. \quad (\text{B.16})$$

B.3 Shortest Replacement Paths in the Entangled Network

Here we discuss a heuristic to solve (B.9) via the determination of a set of z node-disjoint replacement paths $S^{(z)}(\mathcal{P}') = \{\mathcal{P}'_1, \dots, \mathcal{P}'_z\}$ in the base-graph G^k of an entangled quantum repeater network N . The algorithm focuses on a given demand ρ of a user U_k , with a source node $\phi(s)_{U_k,\rho} \in G^k$ and target node $\phi(t)_{U_k,\rho} \in G^k$.

Let $\delta(\cdot)$ identify the cost function of the algorithm such that if a given connection E_h belongs to the main path \mathcal{P} , then $\delta(E_h) = \gamma(E_h)$ (B.5), whereas if E_h belongs to a replacement path \mathcal{P}' , then $\delta(E_h) = \tau(E_h)$ (B.8). Thus,

$$\delta(E_h) = \begin{cases} \gamma(E_h), & \text{if } E_h \in \mathcal{P} \\ \tau(E_h), & \text{if } E_h \in \mathcal{P}' \end{cases}. \quad (\text{B.17})$$

Utilizing the notations of the frameworks KPA [96, 97] and KPI [63, 64], some preliminaries for our scheme are as follows. Let set $S^{(j-1)}(\mathcal{P}') = \{\mathcal{P}'_1, \dots, \mathcal{P}'_{j-1}\}$ refer to the previously discovered $j-1$ node-disjoint paths, where \mathcal{P}'_1 refers to the main path, i.e., $\mathcal{P}'_1 = \mathcal{P}$. Specifically, for each node-disjoint path \mathcal{P}_p , $p = 1, \dots, z$, a cost matrix $C_{U_k,\rho}^{(p)}$ is defined, which is a matrix of connection costs $\delta^{(p)}(E_h)$, where $\delta^{(p)}(E_h)$ is an auxiliary cost of entangled connection E_h of the p -th path. The $C_{U_k,\rho}^{(p)}$ matrix is used to calculate the concurring path cost such that the cost of the concurring entangled connections is increasing by a given value.

Particularly, for a given set $S^{(j-1)}(\mathcal{P}')$ of already discovered $j-1$ paths, a j -th path identifies a current (candidate) path \mathcal{P}'_j to be discovered. A given entangled connection

E_h of a path \mathcal{P}'_i is identified as a prohibited entangled connection $\mathcal{F}^{(\mathcal{P}'_i)}(E_h)$ with respect to \mathcal{P}'_i if E_h is incident to any transit quantum node of path \mathcal{P}'_i [63, 96].

A given E_h is referred to as a concurring entangled connection $\mathcal{C}^{(\mathcal{P}'_j)}(E_h)$ with respect to a given path \mathcal{P}'_j if E_h is incident to any common transit quantum node of \mathcal{P}'_j also used by any other of the paths from the set $S^{(j-1)}(\mathcal{P}')$ of the previously discovered $j - 1$ paths. Without loss of generality, the initial matrix $C_{U_k, \rho}^{(p)}$ provides the initial path cost $c^{(j)} = \sum_{E_h \in \mathcal{P}'_j} \delta_c^{(j)}(E_h)$ for a given path \mathcal{P}'_j to increase the cost of each concurring entangled connection of \mathcal{P}'_j , where $\delta_c^{(j)}(E_h)$ is an initial cost of entangled connection E_h and where $E_h \in \mathcal{P}'_j$ is an entangled connection on path \mathcal{P}'_j .

Let $M_{U_k, \rho}^{\delta^{(j)}(E_h)}$ be the matrix of replacement path coefficients, with $\delta^{(j)}(E_h)$ for all entangled connections of a current path \mathcal{P}'_j associated with a user U_k . For a given matrix $M_{U_k, \rho}^{\delta^{(j)}(E_h)}$, let $\Omega^{(j)}(\delta)$ refer to the total cost of a path \mathcal{P}'_j .

For a current path index j , let $M_{U_k, \rho}^{(\zeta)}$ refer to a matrix of coefficients $\zeta(E_h) = \delta^{(j)}(E_h)$ of entangled connection E_h , where $\zeta(E_h)$ is an auxiliary cost of E_h .

The steps of the method are summarized in Algorithm B.1. The algorithm determines z node-disjoint paths for a demand of a user. The main path \mathcal{P} is identified first and followed by the $z - 1$ replacement paths. For a given j -th path, the cost of any prohibited entangled connection is increased by the cost of all previously discovered $j - 1$ paths of demand for which the given entangled connection is prohibited [63, 96]. Traversing the prohibited entangled connections with respect to a given j -th path therefore results in an increased coefficient. The cost of concurring entangled connections increases if a given j -th path has common entangled connections with the $j - 1$ paths.

B.3.1 Discussion

A brief description of the algorithm follows.

In Step 1, some initialization steps are made and an actual shortest main path $\mathcal{P}'_1 = \mathcal{P}$ is determined for the next calculations.

In Step 2, some steps for the next (j -th) node-disjoint path (candidate path) are

Algorithm B.1 Node-disjoint replacement paths in an entangled network

Step 1. Let $\delta^{(j)}(E_h)$ be the cost coefficient of E_h on a j -th path $j = 1 \dots z$, where j indexes a current path. Let $j = 1$ for the main path $\mathcal{P}'_{j=1} = \mathcal{P}$, and for all entangled connections E_h of N , let $\zeta(E_h) = \delta^{(j)}(E_h)$, where $\zeta(E_h)$ is an auxiliary cost of E_h .

Step 2. For $j > 1$, let us assume that a set $S^{(j-1)}(\mathcal{P}')$ of $j - 1$ node-disjoint shortest paths is already discovered: $S^{(j-1)}(\mathcal{P}') = \{\mathcal{P}'_1, \dots, \mathcal{P}'_{j-1}\}$. Let i refer to a path from $S^{(j-1)}(\mathcal{P}')$. For each already discovered node-disjoint path \mathcal{P}'_i from $S^{(j-1)}(\mathcal{P}')$ and for each $\mathcal{F}^{(\mathcal{P}'_i)}(E_h)$, increase the cost of the entangled connection $\zeta(E_h)$ by $\Omega^{(i)}$, where $\Omega^{(i)}$ is the total cost of \mathcal{P}'_i in $M_{U_k, \rho}^{\delta^{(i)}(E_h)}$ and where $M_{U_k, \rho}^{\delta^{(i)}(E_h)}$ is a matrix such that $\delta^{(i)}(E_h)$ is the cost of an entangled connection E_h on the i -th path. Thus,

$$\zeta(E_h) = \zeta(E_h) + \Omega^{(i)},$$

where $\Omega^{(i)}$ is the path cost of \mathcal{P}'_i (a sum of $\delta^{(i)}(E_h)$ for a traversed entangled connection E_h):

$$\Omega^{(i)} = \sum_{E_h \in \mathcal{P}'_i} \delta^{(i)}(E_h), i = 1, \dots, j - 1,$$

where $E_h \in \mathcal{P}'_i$ refers to E_h on path \mathcal{P}'_i .

Step 3. Define $M_{U_k, \rho}^{(\zeta)} = M_{U_k, \rho}^{\delta^{(j)}(E_h)}$, where $M_{U_k, \rho}^{(\zeta)}$ is a matrix of coefficients $\zeta(E_h)$ of entangled connection E_h initialized in Step 1. Using the k -dimensional n -size base-graph G'^k , determine the j -th node-disjoint path \mathcal{P}'_j using the scaled coefficient $s(\zeta(E_h)) \in [0, 1]$ for a given $M_{U_k, \rho}^{(\zeta)}$.

Step 4. If \mathcal{P}'_j is not node-disjoint with the paths of $S^{(j-1)}(\mathcal{P}')$, then increase the costs $\delta^{(1)}(E_h), \dots, \delta^{(k)}(E_h)$ of each concurring entangled connection $\mathcal{C}^{(\mathcal{P}'_j)}(E_h)$ of \mathcal{P}'_j by the path cost $c^{(j)} \in C_{U_k, \rho}^{(j)}$ of \mathcal{P}'_j with cost matrix $C_{U_k, \rho}^{(j)}$. Thus, the cost of entangled connection E_h of the p -th path is

$$\delta^{(p)}(E_h) = \delta^{(p)}(E_h) + c^{(j)}, p = 1, \dots, z,$$

where path cost $c^{(j)}$ is

$$c^{(j)} = \sum_{E_h \in \mathcal{P}'_j} \delta_c^{(j)}(E_h).$$

Remove the discovered $j - 1$ paths from $S^{(j-1)}(\mathcal{P}')$, and register the concurring entangled connection $\mathcal{C}^{(\mathcal{P}'_j)}(E_h)$ via variable $\kappa := \kappa + 1$, where κ is initialized as $\kappa = 1$. If $\kappa > \partial$, where ∂ is the maximum allowable number of concurrences, then terminate the procedure; otherwise, repeat the process from Step 1 with $j = 1$.

Algorithm B.1 Node-disjoint replacement paths in an entangled network (cont.)

Step 5. If \mathcal{P}'_j is node-disjoint with the paths of $S^{(j-1)}(\mathcal{P}')$, then increase j :
 $j := j + 1$. If $j > z$, stop the process and return $S^{(z)}(\mathcal{P}')$; otherwise, go to Step 1 with the current j .

Step 6. For a given main path $\mathcal{P}'_1 = \mathcal{P}$, output the Ψ total path cost of $z - 1$ node-disjoint replacement paths between $\phi(s)_{U_k, \rho}$ and $\phi(t)_{U_k, \rho}$ of ρ :

$$\Psi(S^{(z-1)}(\mathcal{P}')) = \sum_{p=2}^z \sum_{E_h \in \mathcal{P}'_p} \delta^{(p)}(E_h),$$

where $S^{(z-1)}(\mathcal{P}') = \{\mathcal{P}'_2, \dots, \mathcal{P}'_z\}$, E_h is an entangled connection on path \mathcal{P}'_p , and $\delta^{(p)}(E_h)$ is the cost of the entangled connection E_h of the p -th path.

performed. In particular, the coefficients of the prohibited entangled connections that are traversed by the actual main path are increased by a given quantity. This step aims to avoid a situation in which the establishment of the next node-disjoint path of a given user fails. Some calculations are performed for the j -th path using the already determined set of $j - 1$ node-disjoint paths $S^{(j-1)}(\mathcal{P}')$. The cost of any prohibited entangled connection is increased by the total cost of a given path \mathcal{P}'_i .

In Step 3, the j -th disjoint (shortest) path \mathcal{P}'_j is determined by the decentralized algorithm \mathcal{A} in the base-graph G'^k , which contains the scaled $\phi'(x), \phi'(y) \in G'^k$ of the nodes of $\phi(x), \phi(y) \in G^k$. The base-graph G'^k is evaluated from G^k , and it contains the ϕ' scaled maps of the nodes of the entangled overlay quantum network N and the scaled coefficients of the entangled connection, $s(\zeta(E_h))$ using $M_{U_k, \rho}^{(\zeta)}$.

In G'^k , a given contact between two nodes $\phi'(x), \phi'(y)$ is characterized by the scaled coefficient $s(\zeta(E(\phi(x), \phi(y)))) \in [0, 1]$, where $\zeta(E(\phi(x), \phi(y)))$ is the cost of an entangled connection E_h in G^k . Particularly, G'^k is constructed such that the distribution of the scaled coefficients follows an inverse k -power distribution, and the decentralized routing scheme \mathcal{A} can determine the shortest path in G'^k in at most (3.25) steps [33].

Step 4 deals with the situation when the j -th path \mathcal{P}'_j is not node-disjoint with the paths of $S^{(j-1)}(\mathcal{P}')$. If more than one already discovered path from $S^{(j-1)}(\mathcal{P}')$ traverses

a given entangled connection, then the cost of the concurring entangled connection is increased by the total cost of path \mathcal{P}'_j . Step 4 is completed by the incrementing and checking of a κ concurrence counter.

Step 5 handles the case when a j -th path \mathcal{P}'_j is node-disjoint with the paths of $S^{(j-1)}(\mathcal{P}')$. In this situation, j is incremented: $j := j + 1$; if $j > z$, the iteration stops and returns the $z - 1$ node-disjoint shortest replacement paths $S^{(z-1)}(\mathcal{P}') = \{\mathcal{P}'_2, \dots, \mathcal{P}'_z\}$ for a given main path $\mathcal{P}'_1 = \mathcal{P}'$; otherwise, the algorithm jumps back to Step 1 with the actual value of j .

In Step 6, after set $S^{(z-1)}(\mathcal{P}')$ is determined, the Ψ total cost of the $z - 1$ replacement paths of demand ρ of U_k is precisely as follows:

$$\Psi(S^{(z-1)}(\mathcal{P}')) = \sum_{p=2}^z \sum_{E_h \in \mathcal{P}'_p} \delta^{(p)}(E_h), \quad (\text{B.18})$$

where E_h is an entangled connection on path \mathcal{P}'_p . The Ψ total cost for the set $S^{(z)}(\mathcal{P}')$ of the z node-disjoint paths is therefore

$$\Psi(S^{(z)}(\mathcal{P}')) = \sum_{p=1}^z \sum_{E_h \in \mathcal{P}'_p} \delta^{(p)}(E_h). \quad (\text{B.19})$$

The base-graphs G^k and G'^k of a given overlay quantum repeater network N are illustrated in Fig. B.2.

B.3.2 Computational Complexity

In particular, each of the shortest paths is determined by a decentralized routing algorithm \mathcal{A} in a k -dimensional n -size base-graph, therefore the overall complexity the proposed method is bounded from above by

$$\mathcal{O}(\partial \log n)^2, \quad (\text{B.20})$$

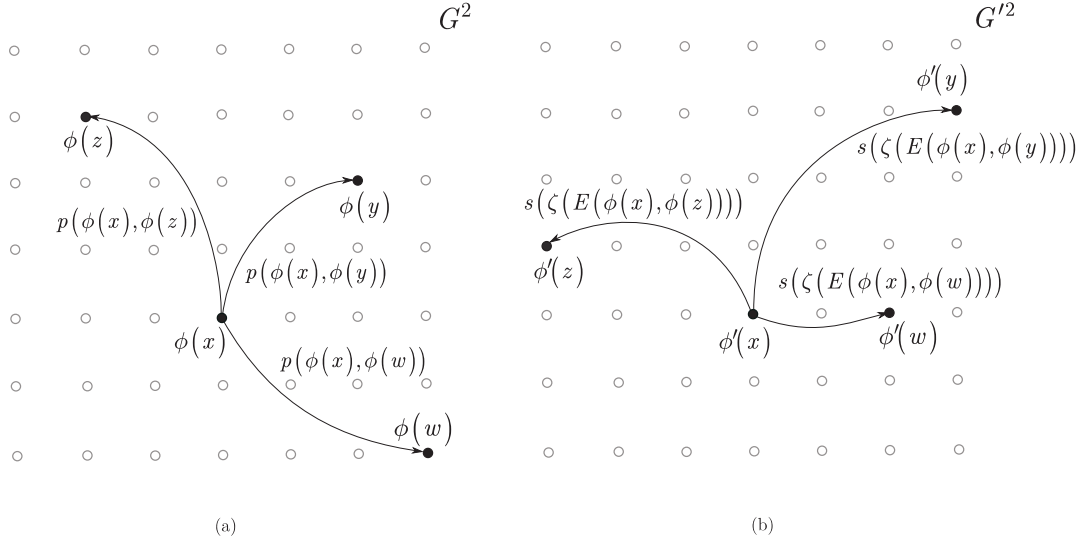


Figure B.2: A $k = 2$ -dimensional base-graph G^2 of the overlay quantum repeater network N . (a) A reference source node $\phi(x)$ has entangled connections with $\phi(y)$, $\phi(z)$, and $\phi(w)$. Each entangled connection is characterized by a given probability $p(\cdot)$ that depends on the level of entanglement. (b) Determination of a node-disjoint path \mathcal{P}'_j between a reference source node $\phi'(x)$ and the scaled positions $\phi'(y)$, $\phi'(z)$, and $\phi'(w)$ for a given $M_{U_{k,\rho}}^{(\zeta)}$ in base-graph G'^2 , where $s(\zeta(E(\cdot))) \in [0, 1]$ is a scaled cost of the entangled connection.

for a given maximum allowable number ∂ of concurring entangled connections.

B.4 Performance Evaluation

In this section, we compare the performance of our scheme with the KPA, KPI, and the k -successively shortest link-disjoint paths (KSP) [64] algorithms.

The KPA and KPI algorithms are based on Dijkstra's shortest path [19] algorithm. As follows, at a particular ∂ , the computational complexity of these schemes is $\mathcal{O}(\partial n^2)$ [63, 64, 97].

The worst-case complexity of the KSP algorithm can be evaluated in function of the number z of disjoint paths, as $\mathcal{O}(zn \log n)$ [64].

Fig. 3. illustrates the performance comparisons, and N_O refers to the number of operations. The performance of our scheme is depicted Fig. B.3(a). In Fig. B.2(b) the

performance of the KPA, KPI algorithms is depicted. In Fig. B.3(c) the performance of the KSP algorithm is shown.

For the analyzed parameter ranges, in our algorithm N_O is maximized as $N_O = 400$, while for the compared methods the resulting quantities are $N_O(\text{KPA}, \text{KPI}) = 10^5$, and $N_O(\text{KSP}) = 2 \cdot 10^3$, respectively.

As a conclusion, in comparison with the KPA, KPI and KSP methods, our solution provides a moderate complexity solution to determine the connection-disjoint paths in the quantum network, for an arbitrary number of n and ∂ .

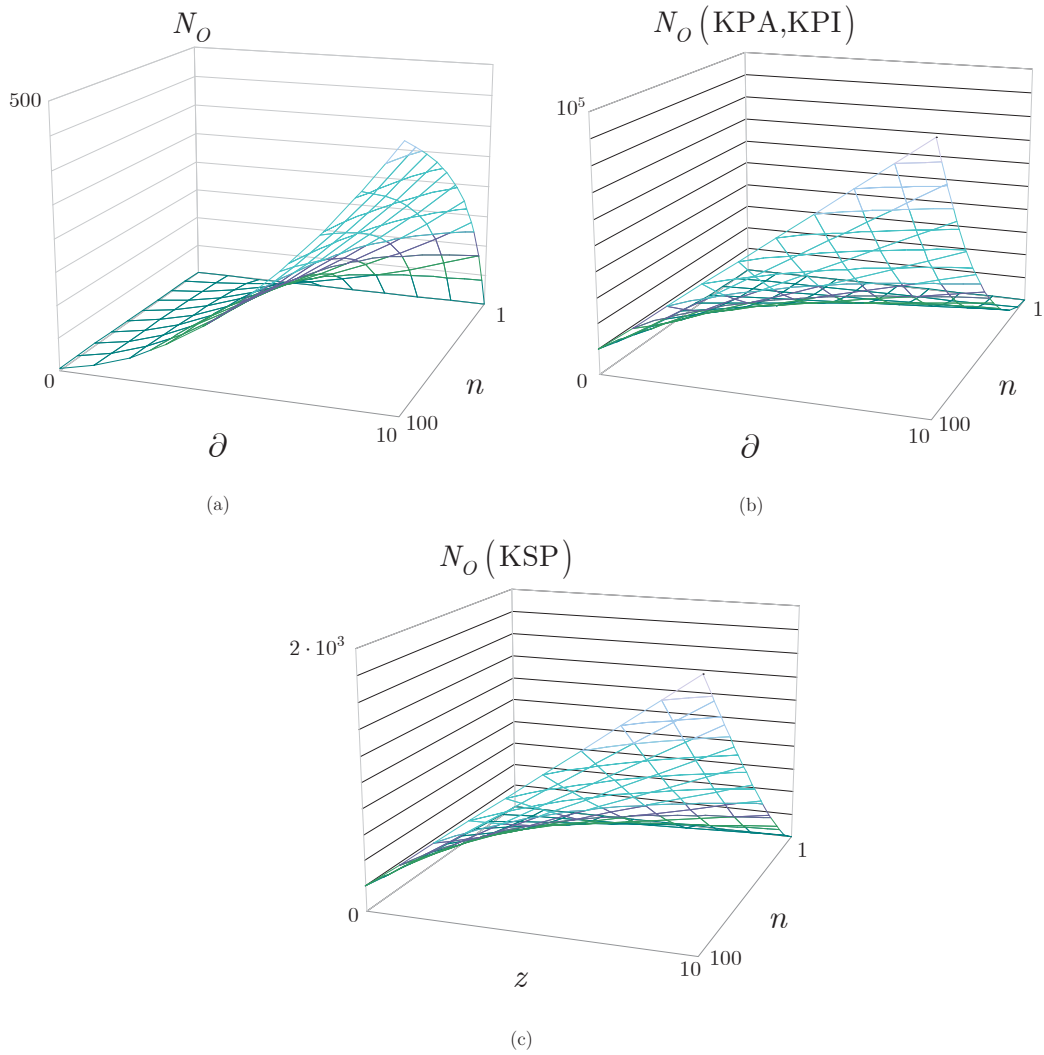


Figure B.3: (a) The computational complexity (N_O refers to the number of operations) of the proposed method in function of ∂ and n , $\partial \in [0, 10]$, $n \in [0, 100]$ (b) The computational complexity of the KPI and KPA methods in function of ∂ and n , $\partial \in [0, 10]$, $n \in [0, 100]$. (c) The computational complexity of the KSP method in function of z and n , $z \in [0, 10]$, $n \in [0, 100]$.

Appendix C

EAD Service

C.1 Classical Correlations

The classical correlation is transmitted subsystem B of (4.1) in Step 1 is as follows. Since ρ_{AB} is a Bell-diagonal state [61] of two qubits A and B it can be written as

$$\rho_{AB} = \frac{1}{4} \left(I + \sum_{j=1}^3 c_j \sigma_j^A \otimes \sigma_j^B \right) = \sum_{a,b} \lambda_{ab} |\beta_{ab}\rangle \langle \beta_{ab}|, \quad (\text{C.1})$$

where terms σ_j refer to the Pauli operators, while $|\beta_{ab}\rangle$ is a Bell-state

$$|\beta_{ab}\rangle = \frac{1}{\sqrt{2}} (|0, b\rangle + (-1)^a |1, 1 \oplus b\rangle), \quad (\text{C.2})$$

while λ_{ab} are the eigenvalues as

$$\lambda_{ab} = \frac{1}{4} \left(1 + (-1)^a c_1 - (-1)^{a+b} c_2 + (-1)^b c_3 \right). \quad (\text{C.3})$$

The \mathcal{I} quantum mutual information of Bell diagonal state ρ_{AB} quantifies the total correlations in the joint system ρ_{AB} as

$$\begin{aligned}
\mathcal{I} &= S(\rho_A) + S(\rho_B) - S(\rho_{AB}) \\
&= S(\rho_B) - S(B|A) \\
&= 2 - S(\rho_{AB}) \\
&= \sum_{a,b} \lambda_{ab} \log_2(4\lambda_{ab}),
\end{aligned} \tag{C.4}$$

where $S(\rho) = -\text{Tr}(\rho \log_2 \rho)$ is the von Neumann entropy of ρ , and $S(B|A) = S(\rho_{AB}) - S(\rho_A)$ is the conditional quantum entropy.

The $\mathcal{C}(\rho_{AB})$ classical correlation function measures the purely classical correlation in the joint state ρ_{AB} . The amount of purely classical correlation $\mathcal{C}(\rho_{AB})$ in ρ_{AB} can be expressed as follows [61]:

$$\begin{aligned}
\mathcal{C}(\rho_{AB}) &= S(\rho_B) - \tilde{S}(B|A) \\
&= S(\rho_B) - \min_{E_k} \sum_k p_k S(\rho_{B|k}) \\
&= 1 - H\left(\frac{1+c}{2}\right) \\
&= \frac{1+c}{2} \log_2(1+c) + \frac{1-c}{2} \log_2(1-c),
\end{aligned} \tag{C.5}$$

where

$$\rho_{B|k} = \frac{\langle k|\rho_{AB}|k\rangle}{\langle k|\rho_A|k\rangle} \tag{C.6}$$

is the post-measurement state of ρ_B , the probability of result k is

$$p_k = Dq_k \langle k|\rho_A|k\rangle, \tag{C.7}$$

while d is the dimension of system ρ_A and the q_k make up a normalized probability distribution, $E_k = Dq_k |k\rangle \langle k|$ are rank-one POVM (positive-operator valued mea-

sure) elements of the POVM measurement operator E_k [61], while $H(p) = -p \log_2 p - (1-p) \log_2 (1-p)$ is the binary entropy function, and

$$c = \max |c_j|. \quad (\text{C.8})$$

For the transmission of B the subsystem ρ_{AB} is expressed as given by (4.1), thus the classical correlation during the transmission is

$$\mathcal{C}(\rho_{AB}) = 1 - H\left(\frac{1+c}{2}\right) = 1, \quad (\text{C.9})$$

where $c = 1$.

Appendix D

Multilayer Optimization Service

D.1 Cost Uncertainty of Large-Scaled Optimization

The determination of the minimal cost function (5.25) is can be approached by an output variable $O_J = f(\psi_{in})$, where ψ_{in} is the set of input variables, and $f(\cdot)$ is a function that transfers the uncertainty from the independent input random variables ψ_{in} to the output variable O_J [78]. The output set O_J can be rewritten as

$$O_J = f(q, w_1, \dots, w_z), \quad (\text{D.1})$$

where q is the set of certain variables, while w_i is an input variable under certainty with probability function $\delta_{f_{w_i}}$.

Then, for a given variable w_i , two $pc(w_i)$ probability concentrations [78], $pc^{(1)}(w_i)$ and $pc^{(2)}(w_i)$ are defined as

$$pc^{(1)}(w_i) = (w_{i,1}, \zeta_{i,1}) \quad (\text{D.2})$$

and

$$pc^{(2)}(w_i) = (w_{i,2}, \zeta_{i,2}), \quad (\text{D.3})$$

where $w_{i,g}$, is the poth location of w_i [78], $g = 1, 2$, while $\zeta_{i,g}$ is a weighting factor.

Therefore, at a given (i, g) parameterization, where $i = 1, \dots, z$ and $g = 1, 2$, O_J is expressed by variable $O_J^{(i,g)}$ as

$$O_J^{(i,g)} = f(q, w_{i,g}, \mu_{w_1}, \mu_{w_2}, \dots, \mu_{w_z}), \quad (\text{D.4})$$

where μ_{w_i} is the mean of w_i , while $w_{i,1}$ and $w_{i,2}$ are the poth locations of w_i . Therefore, the problem is reduced to $2z$ deterministic equations [78], from which the mean and standard deviation of the output random variable $O_J^{(i,g)}$ can be computed.

Appendix E

Abbreviations

API Application Programming Interface

EAD Entanglement Availability Differentiation

IPSec Internet Protocol Security

POVM Positive-Operator Valued Measure

QIRG Quantum Internet Research Group

QKD Quantum Key Distribution

QLAN Quantum Local Area Network

QMAN Quantum Metropolitan Area Network

QWAN Quantum Wide Area Network

TLS Transport Layer Security

Appendix F

Notations

The notations of the dissertation are summarized in Table F.1.

Table F.1: Summary of notations.

| <i>Notation</i> | <i>Description</i> |
|-----------------|--|
| L1 | Manhattan distance (L1 metric). |
| l | Level of entanglement. |
| F | Fidelity of entanglement. |
| L_l | An l -level entangled connection. For an L_l link, the hop-distance is 2^{l-1} . |
| $d(x, y)_{L_l}$ | Hop-distance of an l -level entangled connection between nodes x and y . |
| L_1 | L_1 -level (direct) entanglement, $d(x, y)_{L_1} = 2^0 = 1$. |
| L_2 | L_2 -level entanglement, $d(x, y)_{L_2} = 2^1 = 2$. |

| | |
|----------------------|--|
| L_3 | L_3 -level entanglement, $d(x, y)_{L_3} = 2^2 = 4$. |
| $E(x, y)$ | An edge between quantum nodes x and y , refers to an L_l -level entangled connection. |
| $\Pr_{L_l}(E(x, y))$ | Probability of existence of an entangled connection $E(x, y)$, $0 < \Pr_{L_l}(E(x, y)) \leq 1$. |
| N | Overlay quantum network, $N = (V, E)$, where V is the set of nodes, E is the set of edges. |
| V | Set of nodes of N . |
| E | Set of edges of N . |
| G^k | An n -size, k -dimensional base-graph. |
| n | Size of base-graph G^k . |
| k | Dimension of base-graph G^k . |
| A | Transmitter node, $A \in V$. |
| B | Receiver node, $B \in V$. |
| R_i | A repeater node in V , $R_i \in V$. |
| E_j | Identifies an L_l -level entanglement, $l = 1, \dots, r$, between quantum nodes x_j and y_j . |
| $E = \{E_j\}$ | Let $E = \{E_j\}$, $j = 1, \dots, m$ refer to a set of edges between the nodes of V . |

| | |
|---------------------------|---|
| $\phi(x)$ | Position assigned to an overlay quantum network node $x \in V$ in a k -dimensional, n -sized finite square-lattice base-graph G^k . |
| $\phi: V \rightarrow G^k$ | Mapping function that achieves the mapping from V onto G^k . |
| $d(\phi(x), \phi(y))$ | L1 distance between $\phi(x)$ and $\phi(y)$ in G^k . For $\phi(x) = (j, k)$, $\phi(y) = (m, o)$ evaluated as $d((j, k), (m, o)) = m - j + o - k $. |
| $p(\phi(x), \phi(y))$ | The probability that $\phi(x)$ and $\phi(y)$ are connected through an L_l -level entanglement in G^k . |
| H_n | Normalizing term, defined as $H_n = \sum_z d(\phi(x), \phi(z))$. |
| $c_{\phi(x), \phi(y)}$ | Constant, defined as $c_{\phi(x), \phi(y)} = \Pr_{L_l}(E(x, y)) - \frac{d(\phi(x), \phi(y))^{-k}}{H_n}$, where $\Pr_{L_l}(E(x, y))$ is the probability that nodes $x, y \in V$ are connected through an L_l -level entanglement in the overlay quantum network N . |
| $\Pr(E \phi)$ | Conditional probability between the $\phi(\cdot)$ configuration of positions of the quantum nodes in G^k and the set E of the m edges of the overlay network V . |
| $\Pr(\phi E)$ | Posteriori distribution of configuration ϕ at a given set E . |
| $\Pr(\phi)$ | Candidate distribution. |

| | |
|---|--|
| $q(r s)$ | Proposal density function to stabilize the Markov chain, proposes a next state s^* given a state s_i . |
| u_j | The j -th neighbor quantum node of x_i , $\{x_i, u_j\} \in E$ with base-graph position $\phi(u_j) \in G^k$. |
| v_j | The j -th neighbor quantum node of y_i , $\{y_i, v_j\} \in E$ with base-graph position $\phi(v_j) \in G^k$. |
| $ \phi(u_j)\rangle, \phi(v_j)\rangle$ | Quantum systems, prepared locally by all u_j and v_j neighbor nodes of x_i, y_i . |
| M | Local measurement, which yields $M \phi(u_j)\rangle = \phi(u_j)$ and $M \phi(v_j)\rangle = \phi(v_j)$. |
| $\zeta(x_i, y_i)$ | Parameter for the evaluation of the results of the local measurements of two nodes x_i and y_i . |
| $\Phi(x_i, y_i)$ | Parameter for the evaluation of the results of the local measurements of two nodes x_i and y_i . |
| swap | Swap operation. The x_i, y_i -swap of ϕ_1 , such that $\phi_1(x_i) = \phi_2(y_i)$, $\phi_1(y_i) = \phi_2(x_i)$, and $\phi_1(z_i) = \phi_2(z_i)$ for all $z_i \neq x_i, y_i$. |
| $p_{\text{swap}}(\phi(x_i), \phi(y_i))$ | Swapping probability. Nodes x_i, y_i swap their position information with this probability. |
| \mathcal{A} | Decentralized algorithm \mathcal{A} in the k -dimensional n -sized base-graph G^k . |

| | |
|--------------------------|---|
| $D(G^k)$ | Diameter of G^k . Refers to the maximum value of the shortest path (total number of edges on a path) between any pair of mapped nodes in G^k . |
| $D(\mathcal{A})$ | Minimal number of steps required by \mathcal{A} to find the shortest path. |
| B_n | Box of size $n \times n$. |
| S_i | Subsquare of B_n of side length n^γ , where $k/4 < \gamma < 1$. |
| S_{ik} | Sub-sub-squares of side length n^{γ^2} , yielded from the sub-division of a subsquare S_i into smaller units. |
| A_1 | Event that there exists at least two subsquares S_i and S_j in B_n such that there is no exists edge between them. |
| A_2 | Event that there exists at one S_i in B_n such that there are two sub-sub-squares S_{ik} in S_i which are not connected by edge. |
| $D_{max}(S_i)$ | Largest diameter of the S_i subsquares of side length n^γ . |
| $D_{max}(S_{ik})$ | The largest diameter of the S_{ik} sub-sub-squares of side length n^{γ^2} . |
| $T(\phi_1, \phi_2)$ | Transition matrix, where ϕ_2 is the x_i, y_i -swap of ϕ_1 , such that $\phi_1(x_i) = \phi_2(y_i)$, $\phi_1(y_i) = \phi_2(x_i)$, and $\phi_1(z_i) = \phi_2(z_i)$ for all $z_i \neq x_i, y_i$. |
| $\Omega(\phi_1, \phi_2)$ | Parameter for the definition of Markov chain. |

| | |
|-------------------------------|--|
| $\varepsilon(\phi_1, \phi_2)$ | Parameter for the definition of Markov chain. |
| $E(x \vee y)$ | Edges connected to $x \in V$ or $y \in V$. |
| m | Iteration step. Utilizing the tessellation of B_n for m times results in end squares with side length n^{γ^m} , for which situation m events, A_1, \dots, A_m exist. |
| C, Z | Constants, $C > 0, Z > 0$. |
| e_j | Event. |
| $\Pr(e_j)$ | Probability that an event e_j occurs. |
| X_j | Geometric random variable. |
| $E(X_j)$ | Mean $E(X_j)$ of an geometric random variable X_j , evaluated as $E(X_j) = \frac{1}{\Pr(e_j)} = \mathcal{O}(\log n)$, where n is the size of the k -dimensional base-graph G^k . |
| ρ_{ABC} | Initial system. |
| σ_{ABC} | Final system. |
| ρ_{AB}, ρ_C | Initial subsystems. |
| $ \delta_B\rangle^{(m,n)}$ | Subsystem B , $ \varphi_B\rangle = \alpha 0\rangle + \beta 1\rangle$, encoded via an (m, n) redundant quantum parity code as $ \delta_B\rangle^{(m,n)} = \alpha \chi_+\rangle_1^{(m)} \dots \chi_+\rangle_n^{(m)} + \beta \chi_-\rangle_1^{(m)} \dots \chi_-\rangle_n^{(m)}$, where $ \chi_{\pm}\rangle^{(m)} = 0\rangle^{\otimes m} \pm 1\rangle^{\otimes m}$. |
| T | Period time selected by Alice and Bob. |

| | |
|-----------------------------------|---|
| $\mathcal{N}_{1\dots n}$ | Intermediate quantum repeaters between Alice and Bob. |
| σ^x | Pauli X matrix. |
| H_{AC} | Hamiltonian, $H_{AC} = \sigma_A^x \sigma_C^x$. |
| E_{AC} | Energy of Hamiltonian H_{AC} . |
| U_{AC} | Unitary, applied by Alice on subsystem AC for a time t , $U_{AC} = \exp(-iH_{AC}t)$, where $H_{AC} = \sigma_A^x \sigma_C^x$ is a Hamiltonian, σ^x is the Pauli X matrix. |
| t | Application time of unitary U_{AC} , determined by Alice and Bob. |
| I | Identity operator. |
| \hbar | Reduced Planck constant. |
| $E(\cdot)$ | Relative entropy of entanglement. |
| T_π | Oscillation period, $T_\pi = 4t$, where π is the period. |
| $ \xi(\frac{\pi}{4})\rangle_{AB}$ | Output AB subsystem at time t , $ \xi(\frac{\pi}{4})\rangle_{AB} = \frac{1}{\sqrt{2}}(\psi_+\rangle - i \phi_+\rangle)$, where $ \psi_+\rangle = \frac{1}{\sqrt{2}}(01\rangle + 10\rangle)$, $ \phi_+\rangle = \frac{1}{\sqrt{2}}(00\rangle + 11\rangle)$ are maximally entangled states. |
| $\sigma_{AB}^{T_B}$ | Partial transpose of output AB subsystem σ_{AB} . |
| $N(\sigma_{AB}^{T_B})$ | Negativity for the $\sigma_{AB}^{T_B}$ partial transpose of σ_{AB} . |

| | |
|---------------------------|---|
| $\lambda_{E_{L_l}(x,y)}$ | Initial entanglement utility of link $E_{L_l}(x, y)$. |
| $\lambda'_{E_{L_l}(x,y)}$ | Updated entanglement utility of link $E_{L_l}(x, y)$. |
| $B_F(E_{L_l}(x, y))$ | Entanglement throughput of a given L_l -level entangled connection $E_{L_l}(x, y)$ between nodes (x, y) . |
| S | A quantum switcher node, switches between entangled connects using its local quantum memory, and applies entanglement swapping. |
| \mathcal{G}_m | Quantum memory utilization graph, directed graph mapped from the network model with abstracted nodes and links. |
| \mathcal{G}_{et} | Entanglement throughput tree is derived from a \mathcal{G}_m quantum memory utilization graph. |
| ID | Identifier of a node in \mathcal{G}_{et} , $ID = \{A, B, \dots\}$. |
| S_I | Set of unvisited neighbor nodes of a particular node I . |
| $\Omega(I, J)$ | Cost function between nodes (I, J) . |
| $C(E_{L_l}(I, J))$ | Cost of entangled connection $E_{L_l}(I, J)$. |
| ζ_J | Cost of quantum storage in node J . |
| $\Pr(I, J)$ | Probability that from node I a node J is selected. |
| χ, δ | Weighting coefficients in $\Pr(I, J)$. |

| | |
|----------------------------------|--|
| \mathcal{M} | Method of building an \mathcal{G}_{et} entanglement throughput tree. |
| S' | Set of already reached destination nodes. |
| \mathcal{I} | Set of initial nodes. |
| \mathcal{F}_I | Set of feasible neighboring nodes to node I . |
| \mathcal{D} | Set of destination nodes. |
| $\alpha_{\mathcal{G}_{et}}$ | Entanglement assignment cycle, an optimal assignment (scheduling) of stored entanglement. |
| $t_s^*(\mathcal{G}_{et})$ | Minimal overall storage time at a given \mathcal{G}_{et} . |
| $\mathcal{C}_{\mathcal{G}_{et}}$ | Conflict graph of \mathcal{G}_{et} . In the $\mathcal{C}_{\mathcal{G}_{et}}$ graph, each vertex corresponds to a directed link of \mathcal{G}_{et} (an entangled connection). There is an edge between two vertices of $\mathcal{C}_{\mathcal{G}_{et}}$, if only the vertices (entangled connections) has a conflict. |
| $\tau_{n,t}$ | Indicator variable, $\tau_{n,t} \in \{0, 1\}$, defined as $\tau_{n,t} = \begin{cases} 1, & \text{if } n \text{ is associated at time } t \\ 0, & \text{otherwise.} \end{cases}$ |
| $\wedge(n)$ | Set of entangled connects n' that are scheduled in the same time unit t , but the physical link can transmit only n or n' . |

| | |
|--|---|
| $w(n)$ | Weight of an entangled connection, defined as $w(n) = \begin{cases} 1, & \text{if } F_i = F_{\max} \\ \left\lceil \frac{F_{\max}}{F_i} \right\rceil, & \text{if } F_i < F_{\max} \end{cases},$ where F_i is the fidelity of entangled connection i , F_{\max} is the largest fidelity. |
| $\mathcal{W}(\mathcal{C}_{\mathcal{G}_{et}})$ | Weighted coloring of conflict graph $\mathcal{C}_{\mathcal{G}_{et}}$. |
| $\Delta(\mathcal{W}(\mathcal{C}_{\mathcal{G}_{et}}))$ | Time intervals between each time unit of a given cycle. |
| \mathcal{G}_{et}^* | Optimal entanglement throughput tree. |
| $t_s(\mathcal{G}_{et}^*)$ | Overall storage time at an optimal \mathcal{G}_{et}^* . |
| $B_F(\mathcal{G}_{et}^*)$ | Entanglement throughput at an optimal \mathcal{G}_{et}^* . |
| $ \mathcal{P}(\mathcal{G}_{et}^*) $ | Number of entangled connections at an optimal \mathcal{G}_{et}^* . |
| $\mathcal{S}_{\mathcal{G}_{et}}^*$ | Set of optimal \mathcal{G}_{et}^* entanglement throughput trees. |
| X | Solution set X with decision variables $X = \{x_1, \dots, x_n\}$, where n is the number of all links in a given quantum memory utilization graph \mathcal{G}_m , and $x_i \in \{0, 1\}$ is defined as $x_i = \begin{cases} 1, & \text{if link } i \text{ of } \mathcal{G}_m \text{ is selected by method } \mathcal{M} \\ 0, & \text{otherwise.} \end{cases}$ |
| $X_{\mathcal{G}_{et},j} \angle X_{\mathcal{G}_{et},i}$ | Set $X_{\mathcal{G}_{et},i}$ dominates $X_{\mathcal{G}_{et},j}$. |

| | |
|---|---|
| κ | Set that contains the best non-dominated solutions that have been found at a particular iteration. |
| $f_{t_s^*, B_F^*, \mathcal{P}^* }(\Theta_i)$ | Cost function of classical layer optimization, where $\Theta_i \in \mathbb{R}^p$ is a p -dimensional real vector of an i -th system state of the quantum network. |
| $\Theta_i \in \mathbb{R}^p$ | A p -dimensional real vector of an i -th system state of the quantum network. |
| $\Theta_i(j, k, l)$ | An i -th system state, where j is the index of a desired optimal system state, k is the index of an optimal system state reproduction step, l is the index of a non-optimal system state event. |
| T | Total network state, $T(j, k, l) = \{\Theta_i(j, k, l) i = 1, \dots, S\}$, at a set of S sub-states $\{\Theta_1, \dots, \Theta_S\}$. |
| $c(i)$ | Number of random system states. |
| $u(j)$ | A unit cost of system change. |
| C_N | Total cost of classical communication. |
| A | Distribution-entity of a current system state. |
| R_A | Information transmission rate of A . |
| ν | Distribution-entity of a system state. |
| R_ν | Information transmission rate of ν . |

| | |
|--|---|
| $\Theta^{(m)}$ | The m -th element of a current network state vector Θ . |
| $\Theta_i^{(m)}$ | The m -th element of Θ_i . |
| C_e | An environment-dependent cost function. |
| M | Tuning parameter. |
| F_{cost}^i | Cost function at a given $\Theta_i(j, k, l)$. |
| $N_{t_s^*}, N_{B_F^*}, N_{ \mathcal{P}^* }$ | The number of nodes that require the determination of optimal t_s^* , B_F^* and $ \mathcal{P}^* $. |
| $S_{t_s^*}(t), S_{B_F^*}(t), S_{ \mathcal{P}^* }(t)$ | The number of classical steps required to find t_s^* , B_F^* and $ \mathcal{P}^* $ at a particular network time t , $t = 1, \dots, T$. |
| J | Objective function. |
| $c_{N_{t_s^*}}^L(t), c_{N_{B_F^*}}^L(t), c_{N_{ \mathcal{P}^* }}^L(t)$ | Link cost of classical link L used for the determination of t_s^* , B_F^* and $ \mathcal{P}^* $ at a particular time t . |
| $\Theta_M(j, k, l)$ | Merged system state for the optimization of the classical layer. |
| Φ | Merging factor, $\Phi \in [0, 1]$. |
| u | Uniform random number. |
| x_a, x_b, x_c | Random numbers, $x_a, x_b, x_c \in [0, 1]$. |

| | |
|----------------------|--|
| $O_J = f(\psi_{in})$ | Output variable, where ψ_{in} is the set of input variables, and $f(\cdot)$ is a function that transfers the uncertainty from the independent input random variables ψ_{in} to the output variable O_J . |
| q | Set of certain variables. |
| w_i | An input variable under certainty with probability function $\delta_{f_{w_i}}$. |
| $pc(w_i)$ | Probability concentration of w_i . |
| $\zeta_{i,g}$ | Weighting factor. |
| $O_J^{(i,g)}$ | Output variable O_J at a given (i, g) . |
| μ_{w_i} | Mean of w_i . |
| $w_{i,1}, w_{i,2}$ | Both locations of w_i . |